International Journal of Hydrogen Energy 217 (2026) 153765

Contents lists available at ScienceDirect

International Journal of Hydrogen Energy

journal homepage: www.elsevier.com/locate/he

Energy resilience and decarbonization via hybrid renewable energy systems: A techno-economic study☆

Waqar Ali Khan [a,b], Ashkan Pakseresht [c], Caslon Chua [a], Ali Yavari [a,b,*]

[a] School of Science, Computing and Emerging Technologies, Swinburne University of Technology, Melbourne, Victoria 3122, Australia
[b] Hydrogen 4.0 Lab, Swinburne University of Technology, Melbourne, Victoria 3122, Australia
[c] Brunel Business School, Brunel University of London, Uxbridge UB8 3PH, United Kingdom

ARTICLE INFO

Keywords:
Hybrid renewable energy systems
Hydrogen storage
Techno-economic assessment
Rule-based dispatch algorithm
Levelized Cost of Energy (LCOE)
Levelized Cost of Hydrogen (LCOH)

ABSTRACT

Global energy systems remain dominated by fossil fuels, accounting for over 80% of primary supply and driving severe climate impacts through greenhouse gas emissions. The transition to renewable sources such as solar and wind is hindered by their intermittency — daily generation can fluctuate by more than 70%, with strong seasonal variability — leading to continued reliance on fossil-based backup generation. Achieving near-complete energy autonomy while maintaining economic viability therefore remains a major challenge. This study evaluates the techno-economic feasibility of hybrid solar–wind–battery–hydrogen systems across nine configurations using a Rule-Based Heuristic Dispatch Algorithm (RB-HDA). System performance was assessed through four key metrics: demand met, fossil-fuel reliance, and economic feasibility via Levelized Cost of Energy (LCOE) and Levelized Cost of Hydrogen (LCOH). Hybrid solar–wind–battery systems met 99.89% of demand with an LCOE of 0.39–2.32 AUD/kWh, but remained limited by seasonal deficits. Integrating hydrogen storage improved resilience to 99.999% demand met with only one fossil-fuel backup hour annually, achieving an LCOH of 0.04 AUD/kg while maintaining an LCOE of 2.32 AUD/kWh. The results demonstrate hydrogen's role as a pivotal enabler of long-term energy autonomy and a scalable, high-reliability alternative to fossil-based generation.

1. Introduction

In 2023, global primary energy consumption reached a record high, with fossil fuels including coal, oil, and natural gas contributing approximately 81.5% of the total energy supply [1]. This heavy dependence on fossil fuels has led to severe environmental impacts, including rising Greenhouse Gas (GHG) emissions and escalating climate instability [2]. According to the 2024 Global Carbon Budget report, Carbon-di-oxide (CO_2) emissions from fossil fuels and land-use change are projected to reach 41.6 gigatons of carbon dioxide ($GtCO_2$) in 2024, marking a 2% increase from 2023 [3]. The persistent upward trajectory of emissions, despite growing renewable capacity additions, underscores the inadequacy of current energy transition strategies and highlights the urgent need for integrated solutions that can effectively displace fossil-based generation. The urgency of transitioning to cleaner energy systems is particularly important in regions heavily reliant on fossil fuels, such as Victoria State in Australia. With its current energy mix, Victoria is projected to experience significant climate impacts, including a 2.4 °C increase in annual temperatures, a doubling in the number of very hot days, longer and more intense fire seasons, and an increase in extreme rainfall events [4]. The energy sector, particularly electricity generation, is a major contributor to these challenges, accounting for nearly 52% of Victoria's total GHG [5]. These trends highlight the critical need for a transition toward renewable energy systems that can not only reduce emissions but also enhance energy security and resilience in the face of increasing climate risks.

Renewable energy resources (Renewable Energy Resources (RERs)), particularly solar and wind, have emerged as key solutions due to their abundance, sustainability, and potential to decarbonize the global energy sector [6,7]. On a lifecycle basis, Photovoltaic (PV) emits approximately 20–50 gCO_2-eq/kWh, wind power emits around 10–20 gCO_2-eq/kWh, and green hydrogen — when produced via electrolysis using renewable energy — emits near-zero direct CO_2 emissions, making them significantly cleaner compared to fossil-based sources [8–10]. However, the inherent intermittency of these resources presents a major

☆ This article is part of a Special issue entitled: 'Green Cities (Ramadan)' published in International Journal of Hydrogen Energy.

* Corresponding author.
E-mail addresses: wkhan@swin.edu.au (W.A. Khan), ashkan.pakseresht@brunel.ac.uk (A. Pakseresht), cchua@swin.edu.au (C. Chua), mail@aliyavari.com (A. Yavari).

https://doi.org/10.1016/j.ijhydene.2026.153765
Received 22 September 2025; Received in revised form 24 January 2026; Accepted 27 January 2026
Available online 13 February 2026

challenge for large-scale deployment, with solar and wind generation fluctuating by over 70% within a single day and showing pronounced seasonal variability, particularly in temperate regions such as southern Australia [11]. This intermittency not only creates reliability concerns but also perpetuates dependence on fossil-fuel backup generation, thereby undermining decarbonization objectives. Hybrid Renewable Energy Systems (HRES), particularly those integrating solar and wind, offer a promising solution by leveraging resource complementarity to enhance energy reliability [12,13]. Moreover, incorporating energy storage technologies, such as batteries and hydrogen, can further mitigate supply fluctuations and ensure continuous, stable power generation [14]. Yet, despite growing interest in hybrid configurations, critical knowledge gaps remain regarding the optimal coordination of dual-storage systems (battery and hydrogen), their scale-dependent economics, and their effectiveness in addressing seasonal energy deficits — gaps that this study explicitly addresses. Understanding the techno-economic feasibility of these hybrid configurations is therefore essential for accelerating the transition toward a resilient, low-carbon energy future, as emphasized in recent studies focusing on storage-enabled hybrid systems and their role in sustainable electrification strategies [15–18].

Extensive research has explored the potential of HRES, particularly those combining solar and wind, to overcome the limitations of standalone RERs — that is, configurations relying on a single resource such as solar-only or wind-only — by leveraging resource complementarity [19–23]. For instance, [24] demonstrated that the temporal synergy between solar and wind generation enhances system resilience and reduces dependence on fossil-based backup energy supply. Building on this foundation, recent studies have further investigated resource complementarity patterns across diverse geographical contexts, confirming that solar–wind integration can reduce daily variability by 30%–50% compared to standalone systems [25–27]. However, due to the intermittent nature of renewable energy, especially under variable climatic conditions, standalone hybrid systems remain vulnerable to short-term and seasonal mismatches between supply and demand. Battery storage has been widely adopted to address short-term fluctuations, effectively balancing intraday supply–demand mismatches and enhancing grid stability [28–30]. Recent advances in battery technology, including improvements in energy density and cycle life, have further enhanced their viability for renewable integration, with lithium-ion and advanced lead–acid batteries now achieving roundtrip efficiencies exceeding 90% [31,32]. Nevertheless, battery storage is constrained by limited energy capacity and discharge duration, which restricts its ability to bridge extended periods of low renewable generation, particularly during seasonal deficits in winter months [33–35]. This limitation becomes especially pronounced in temperate climates where solar irradiance and wind speeds can decline simultaneously for weeks, creating energy shortfalls that battery systems alone cannot economically address.

Hydrogen, as an energy carrier, has gained increasing attention as a viable long-duration solution for maintaining energy sufficiency during prolonged periods of low renewable output [36,37]. Recent developments in electrolyzer technology, particularly Proton Exchange Membrane (PEM) systems, have demonstrated significant cost reductions and efficiency improvements, with stack costs declining by approximately 40% between 2020 and 2024 [38,39]. Unlike batteries, which are optimized for short-term storage (hours to days), hydrogen storage enables seasonal energy shifting by converting surplus renewable electricity into hydrogen via electrolysis and storing it for later conversion back to electricity through fuel cells [40,41]. This capability positions hydrogen as a critical enabler for achieving near-complete energy autonomy in hybrid systems, particularly in regions with pronounced seasonal renewable variability. Despite its promise, hydrogen storage introduces additional system complexity and capital costs, including the need for electrolyzers, storage tanks, and fuel cells [40]. Furthermore, the economic viability of hydrogen integration is highly scale-dependent. Smaller systems often produce insufficient surplus energy to justify the capital investment, whereas larger systems can achieve competitive Levelized Cost of Hydrogen (LCOH) through sustained electrolyzer operation [42,43].

Several recent studies have investigated HRES integrating both battery and hydrogen storage to address the limitations of single-storage configurations. For example, recent techno-economic studies [41,44,45], have demonstrated that dual-storage systems can achieve reliability levels exceeding 99% while maintaining Levelized Cost of Energy (LCOE) values competitive with conventional generation. However, these studies often focus on limited system configurations (typically 2–3 variants), provide insufficient analysis of seasonal deficit management, or employ simplified dispatch strategies that do not account for operational conflicts between competing storage technologies [46–48]. Moreover, existing literature rarely distinguishes between temporal fossil-fuel dependence (backup hours) and energy-based reliance (percentage of total energy from fossil sources), metrics that are critical for assessing true system autonomy. For example, [41] examined solar–wind–battery–hydrogen configurations but did not explicitly address the hierarchical coordination required to optimize battery and hydrogen utilization simultaneously, nor did they quantify the scale thresholds at which hydrogen becomes economically viable. Similarly, [49] explored hydrogen integration in HRES but focused primarily on steady-state performance metrics, overlooking dynamic dispatch challenges and seasonal variability impacts. Recent optimization studies have proposed advanced energy management strategies, including Model Predictive Control (MPC) and Machine Learning (ML)-based approaches. Yet these methods often require extensive computational resources and real-time data availability that may not be practical for all deployment contexts [50–52].

The LCOE and LCOH are widely recognized metrics for assessing the economic feasibility of energy systems [36,37]. LCOE represents the average cost per unit of electricity generated over the system lifetime, accounting for capital costs, operational expenses, and energy output, while LCOH quantifies the cost of hydrogen production per kilogram, incorporating electrolyzer efficiency, renewable surplus availability, and storage requirements. While LCOE provides a standardized basis for comparing different generation technologies. It does not capture the full complexity of hybrid systems with multiple storage components, where energy flows between generation, storage, and consumption create interdependencies that affect overall cost-effectiveness [53,54]. Recent studies [55–57], have highlighted that LCOE alone may underestimate the true value of hybrid systems by not accounting for reliability benefits, avoided fossil-fuel costs, and environmental externalities. Similarly, LCOH is sensitive to electrolyzer utilization rates, with low-capacity factors leading to disproportionately high unit costs due to underutilized capital assets [58]. This scale sensitivity underscores the importance of optimizing system sizing to ensure sufficient renewable surplus for sustained hydrogen production, a consideration that has received limited attention in prior techno-economic assessments.

Despite these advances, significant research gaps remain that limit the practical deployment of fully decarbonized hybrid renewable systems. First, there is a lack of comprehensive multi-configuration comparative frameworks that systematically evaluate the incremental benefits of adding each component (solar, wind, battery, hydrogen) to a hybrid system. Most existing studies compare only a few configurations, making it difficult for system designers and policymakers to identify optimal design pathways and understand trade-offs across reliability, cost, and sustainability dimensions [59,60]. Second, the coordinated dispatch of dual-storage systems (battery and hydrogen) remains underexplored, with limited guidance on how to resolve operational conflicts, prioritize charging/discharging sequences, and protect component lifetimes while maximizing system performance. Existing dispatch strategies often treat battery and hydrogen independently or apply simplified rule-based approaches that do not capture the temporal complementarity between short-term (battery) and long-term

(hydrogen) storage [40,41]. Third, the scale-dependent economics of hydrogen integration are poorly quantified, with insufficient understanding of minimum system sizes, renewable surplus requirements, and electrolyzer utilization thresholds necessary for cost-effective deployment. This knowledge gap hinders investment decisions and policy design, as stakeholders lack clear benchmarks for when hydrogen becomes economically competitive with fossil-based backup generation. Fourth, seasonal deficit management in temperate climates — where solar and wind generation can decline simultaneously for extended periods — has received inadequate attention, despite being a critical barrier to achieving year-round energy autonomy. Finally, holistic performance metrics that simultaneously capture reliability (demand coverage), sustainability (fossil-fuel dependence), and economic viability (LCOE and LCOH) are lacking, with most studies relying on LCOE alone and failing to distinguish between temporal and energy-based fossil-fuel reliance.

To address these gaps, this study evaluates the techno-economic feasibility of hybrid solar–wind–battery–hydrogen systems in Broadmeadows, a suburb of Victoria characterized by high residential energy demand, limited renewable penetration, and distinct seasonal variability. In this study, a system refers to the complete set of energy components — including generation, storage, and backup — working together to supply electricity. A configuration denotes a specific arrangement of these components, such as solar-only, wind-only, or combined solar–wind systems, each considered with or without battery and hydrogen storage. Broadmeadows was chosen as a representative urban–suburban setting to assess system scalability under real climatic and demographic conditions. This regional context is particularly relevant as Victoria's energy sector faces dual pressures of decarbonization mandates and reliability requirements, making it an ideal test case for evaluating advanced hybrid configurations that can inform policy and deployment strategies in similar temperate regions globally. Using a simulation-based approach, nine configurations are modeled and compared to quantify their influence on energy sufficiency, reduction in fossil-fuel backup hours, and cost-effectiveness through LCOE and LCOH metrics. Unlike previous studies that assume idealized energy conditions — such as constant generation profiles, unlimited storage, or uniform seasonal demand [40,41,61] — this study incorporates realistic temporal dynamics, including seasonal variability, fluctuating renewable output, and storage constraints, to provide a more practical assessment of hybrid system feasibility. Furthermore, this study develops and validates a Rule-Based Heuristic Dispatch Algorithm (RB-HDA) that explicitly coordinates battery and hydrogen storage in a hierarchical framework, prioritizing battery charging for short-term balancing before activating electrolyzers, and sequencing battery discharge, fuel-cell operation, and diesel backup during deficit periods to resolve operational conflicts and protect component lifetimes.

This study aims to answer three key research questions:

1. How does a solar–wind hybrid system (without storage) impact on fossil fuel energy dependence and energy resilience under varying seasonal conditions?
2. To what extent do battery and hydrogen storage reduce seasonal energy deficits and reliance on fossil-fuel operation in hybrid renewable systems?
3. How do different hybrid system configurations affect the LCOE and LCOH?

By systematically addressing these questions across nine distinct configurations, this study provides several novel contributions to the field. First, it presents a comprehensive comparative framework that spans from standalone systems (solar-only, wind-only) to fully integrated configurations (solar–wind–battery–hydrogen), enabling clear identification of incremental benefits and optimal design pathways. Second, it introduces a validated hierarchical dispatch algorithm that coordinates dual-storage systems with explicit conflict resolution, advancing beyond simplified approaches used in prior studies. Third, it quantifies the scale-dependent economics of hydrogen integration, demonstrating pathways to ultra-low LCOH through optimized electrolyzer utilization. Fourth, it explicitly addresses seasonal deficit management by demonstrating how hydrogen storage enables near-complete energy autonomy, overcoming the fundamental limitations of battery-only systems. Finally, it establishes a holistic four-metric evaluation framework (percentage of demand met, fossil-fuel energy hours, fossil-fuel reliance, and dual economic metrics LCOE/LCOH) that provides a more comprehensive assessment than traditional LCOE-focused analyses.

This study aims to provide data-driven insights that support energy planners, policymakers, and industry stakeholders in making informed decisions on system design and investment. In particular, the results clarify how different levels of storage integration (batteries for short-term balancing and hydrogen for long-term reserves) affect reliability, how system sizing of solar and wind capacities influences seasonal energy sufficiency, and how cost metrics such as LCOE and LCOH shape investment strategies. The findings therefore offer a comprehensive understanding of how hybrid configurations perform under seasonal constraints, ultimately guiding the transition toward sustainable, resilient, and economically viable renewable energy infrastructures. Moreover, by demonstrating specific thresholds for hydrogen viability and quantifying the trade-offs between reliability and cost across multiple configurations, this study provides actionable guidelines that can accelerate the practical deployment of decarbonized energy systems in temperate climate regions worldwide.

The rest of this paper is structured as following: Section 2 presents the geographical and meteorological characteristics of Broadmeadows, Victoria, providing an overview of local wind and solar resources along with the methodology used to develop a representative electricity demand profile for the study area. Section 3 outlines the system configurations analyzed in this study, detailing the solar, wind, battery, and hydrogen components considered in the hybrid energy models. Section 4 presents the results, focusing on energy sufficiency, fossil-fuel operation hours, fossil-fuel energy use, and cost-effectiveness across the different hybrid configurations. Section 5 discusses the key findings, addressing fossil fuel energy use, storage impacts, and economic feasibility while highlighting deployment challenges. Section 6 concludes the paper, summarizing the key insights and outlining future research directions.

2. Geographical location and meteorological data

The study focuses on Broadmeadows, a suburban region situated at 37.6859° S, 144.9247° E, in Melbourne, Victoria, Australia, approximately 15 km north of Melbourne's Central Business District (CBD). Broadmeadow is characterized by a temperate oceanic climate with distinct seasonal variations in solar irradiance, wind speeds, and energy demand. Given its geographical location, the area exhibits strong solar potential in summer and variable wind speeds throughout the year, making it a suitable case for evaluating hybrid solar–wind energy systems.

2.1. Demand profile

Accurate electricity demand modeling is critical for assessing the feasibility of HRES, particularly in urban regions where residential energy consumption exhibits seasonal and diurnal variations. This study develops an hourly electricity demand profile for Broadmeadows by combining real-world data and a time-series scaling technique to capture both seasonal and weekly variations. This approach is particularly suited for urban energy modeling where long-term granular demand data may be unavailable but representative weekly profiles exist, as is common in residential load research [62,63].

The demand profile construction is based on hourly electricity consumption data from 209 residential dwellings across four seasons

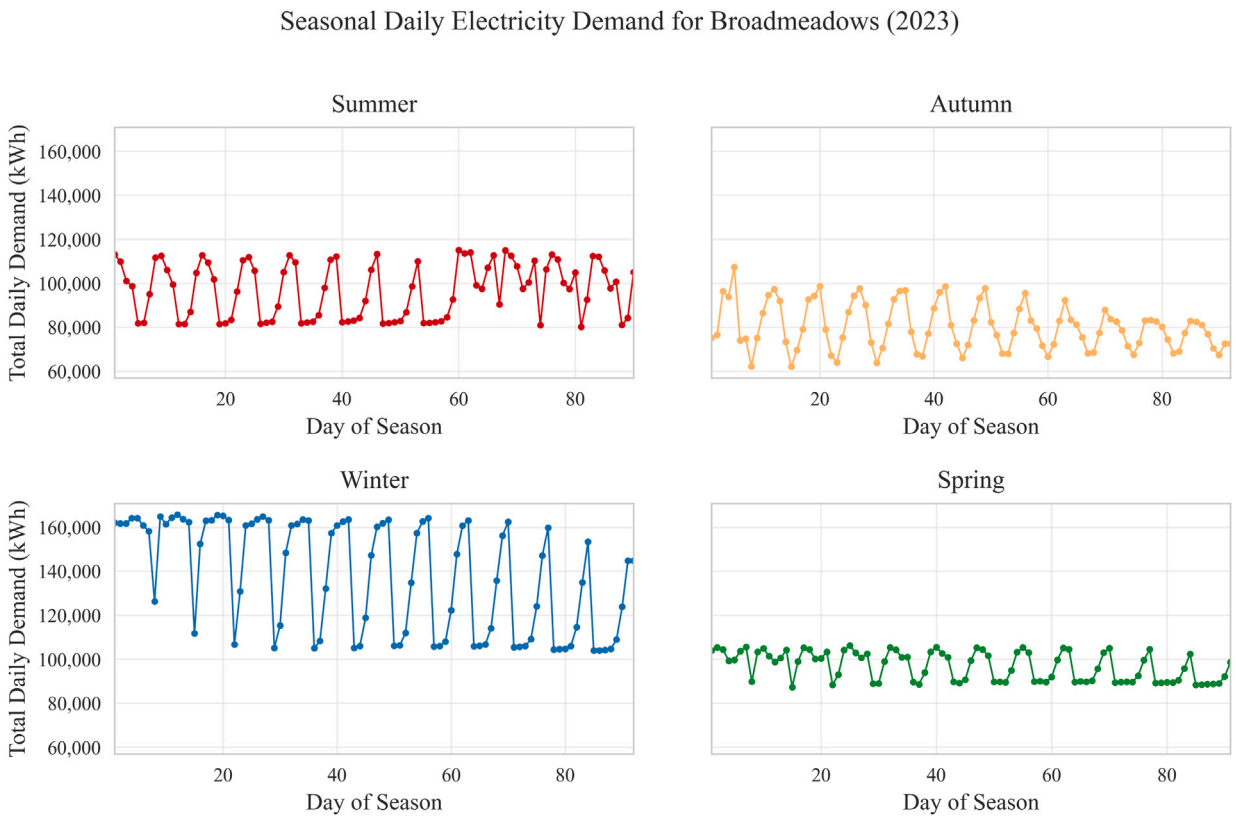

Fig. 1. Monthly Average Electricity Demand with Seasonal Variation in Broadmeadows, Melbourne.

— summer, autumn, winter, and spring — sourced from [64]. Since the dataset contains only one week of hourly demand per season, it was systematically scaled to represent the total residential sector by incorporating Hume City Council's 2021 dwelling records (4617 households) [65]. Since the available dataset contained only one representative week of hourly data per season, it was necessary to extend it to a full year while preserving hourly consumption trends, seasonal variations, and weekly fluctuations.

The residential demand data originate from the Commonwealth Scientific and Industrial Research Organisation (CSIRO) Australian Residential Energy Dataset (2013–2017, 219 households) [64]. Representative one-week samples for each season were concatenated and scaled using temperature-linked load ratios to form a continuous annual demand profile for Broadmeadows. The resulting hourly profile for 2023 was validated against the AEMO (2023) 30-minute residential demand dataset [66] for Victoria, showing strong agreement with only 2%–5% deviation across diurnal and seasonal trends. Minor residual differences mainly reflect increased rooftop-PV uptake and higher household electrification since the CSIRO observations. This deviation introduces limited uncertainty — affecting short-term dispatch timing rather than annual energy totals. Future studies could explore alternative demand scenarios that account for electric-vehicle charging and heat-pump adoption, which are projected to raise residential load by 10%–25% [67,68].

A time-series demand forecasting approach was applied to extend the dataset while ensuring that it retained realistic intra-seasonal demand fluctuations and weekly variations in hourly energy use patterns. The demand for each subsequent week was estimated based on the previous week's hourly demand, modified by a weekly trend factor to introduce gradual variations over the season, using a recursive time-series forecasting formulation inspired by previous synthetic demand modeling studies [69,70], as shown in Eq. (1):

$$D_{i,w} = D_{i,w-1} \times (i + \gamma_w) \tag{1}$$

Where:

- $D_{i,w}$ represents the electricity demand at hour i during week w.
- $D_{i,w-1}$ denotes the demand at the same hour in the previous week.
- γ_w is a weekly variation factor (randomly selected within $[-0.25, 0.25]$), ensuring that demand follows realistic seasonal trends rather than remaining static.

The Eq. (1), ensures that demand dynamics align with real-world electricity consumption behaviors, preventing artificially static profiles. Each season's first week serves as a baseline, with subsequent weeks iteratively forecasted to maintain seasonal consistency. Higher heating loads in winter and increased cooling demand in summer are incorporated, ensuring realistic intra-seasonal variations. Fig. 1 illustrates the monthly average electricity demand trend, highlighting seasonal energy consumption patterns in Broadmeadows. Fig. 2 provides an hourly electricity demand profile for a representative day (24 h only) in each season, capturing diurnal variations. Peak demand periods during summer and winter correspond to increased cooling and heating requirements, whereas spring and autumn display relatively balanced consumption patterns. This structured approach ensures that the extended dataset accurately reflects real-world residential energy consumption dynamics, enabling robust feasibility assessment for hybrid renewable systems.

The synthetic annual demand profile was validated against the AEMO (2023) 30-minute residential demand dataset for Victoria [66]. The comparison showed strong agreement, with a 2%–5% deviation across both diurnal and seasonal trends. This confirms that the extended dataset captures realistic load behavior and annual energy balance. Minor differences arise mainly from evolving rooftop-PV adoption and household electrification intensity between the CSIRO (2013–2017) [64] data and 2023 conditions. The uncertainty from this extrapolation primarily affects hourly dispatch timing rather than total annual demand. Future work will test sensitivity to emerging demand pathways

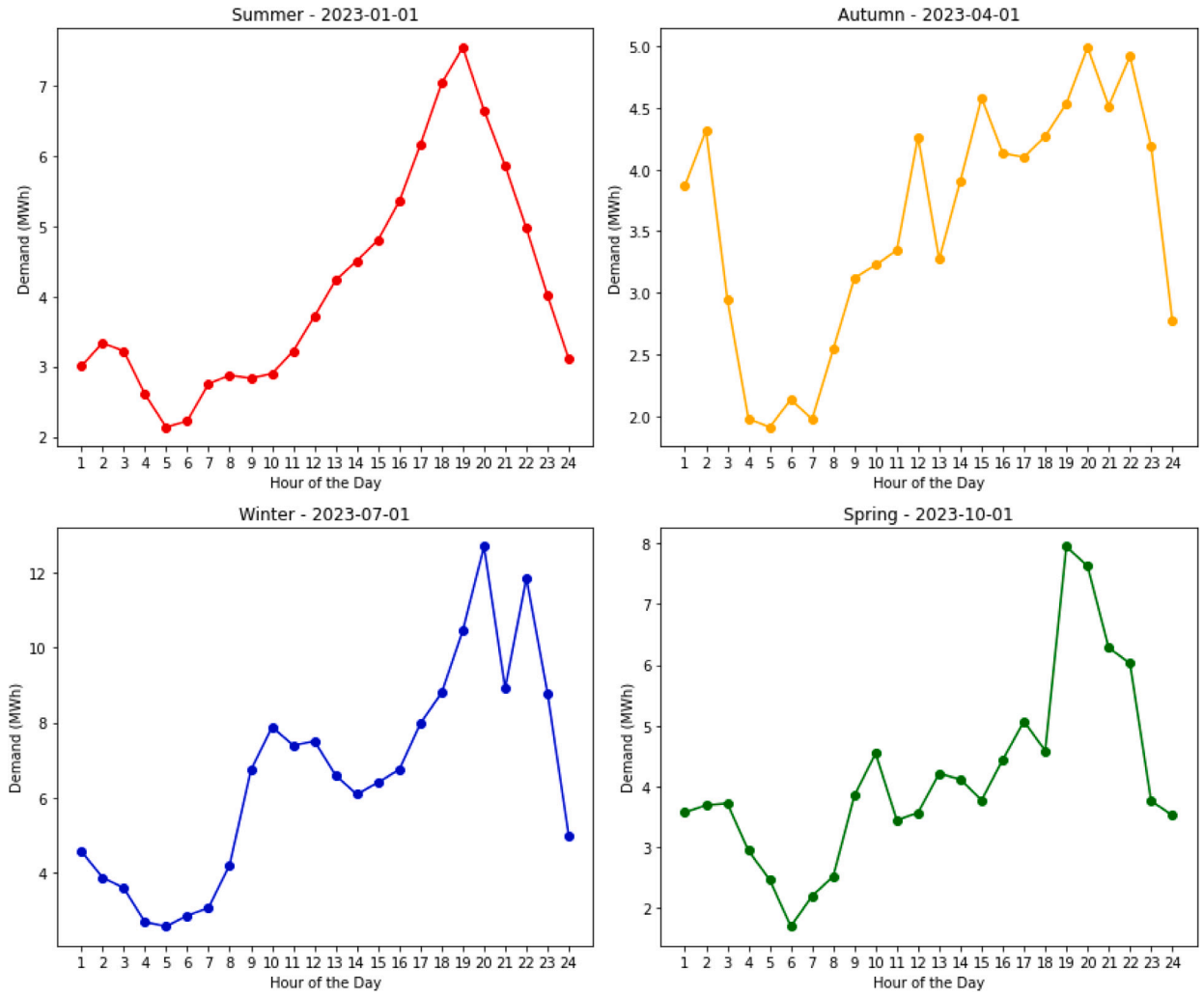

Fig. 2. Hourly electricity demand profiles for a representative day in each season, Broadmeadows, Melbourne.

such as electric-vehicle charging and heat-pump adoption, which are projected to increase residential loads by roughly 10%–25% [67,68].

The residential electricity demand profile used in this study is grounded in the CSIRO Australian Residential Energy Dataset, which monitored 219 Victorian households continuously over a five-year period (2012–2017) [64]. This multi-year observational dataset inherently captures a broad spectrum of operating conditions, including seasonal peak demand associated with heatwaves and winter heating events. The representative weekly profiles adopted here therefore reflect empirically observed household behavior rather than synthetic or idealized load assumptions. When scaled spatially and extended temporally, the resulting annual demand profile preserves realistic peak-to-average demand relationships. Any remaining uncertainty is expected to affect the timing of short-duration peaks rather than the annual energy magnitude, and therefore has a limited influence on system-wide reliability metrics such as fossil-fuel operation hours and storage utilization.

2.2. Wind resource assessment

Assessing wind energy potential in Broadmeadows is essential for accurately evaluating hybrid solar–wind systems, as it directly influences the design, performance, and reliability of energy generation and storage components. In hybrid configurations, especially those with seasonal solar variability, wind energy can provide a complementary resource to maintain supply continuity — particularly during periods of low irradiance, such as winter. High-resolution hourly wind speed data for the period January 1, 2023–December 31, 2023, were sourced from the National Aeronautics and Space Administration Prediction Of Worldwide Energy Resources (NASA POWER) Data Access Viewer [71]. This tool, developed by National Aeronautics and Space Administration (NASA)'s Langley Research Center, provides publicly available satellite-derived meteorological data. The wind speed dataset used in this study originates from the Clouds and the Earth's Radiant Energy System/Modern-Era Retrospective Analysis for Research and Applications (CERES/MERRA-2) database [72], and corresponds to measurements taken at an elevation of 50 m above ground level — consistent with standard methodologies for utility-scale wind resource assessment.

To ensure the accuracy of the wind resource analysis, a suburb-level approach was chosen over a broader regional assessment. Broadmeadows — located within the metropolitan boundary of Melbourne, Victoria — was selected due to its representativeness of urban–suburban energy demand patterns and distinct seasonal climate variations. The NASA POWER tool [72] provides hourly wind speed data for a single geographic coordinate, whereas a larger spatial selection would have resulted in daily averages, insufficient for capturing short-term intermittency. Given the fluctuating nature of wind speeds, high temporal resolution data is crucial for realistic energy generation modeling in hybrid systems.

Fig. 3a shows the monthly wind speed variations, revealing clear seasonal patterns. The highest average wind speed of 6.44 m/s occurs in June, coinciding with winter, whereas the lowest recorded value of

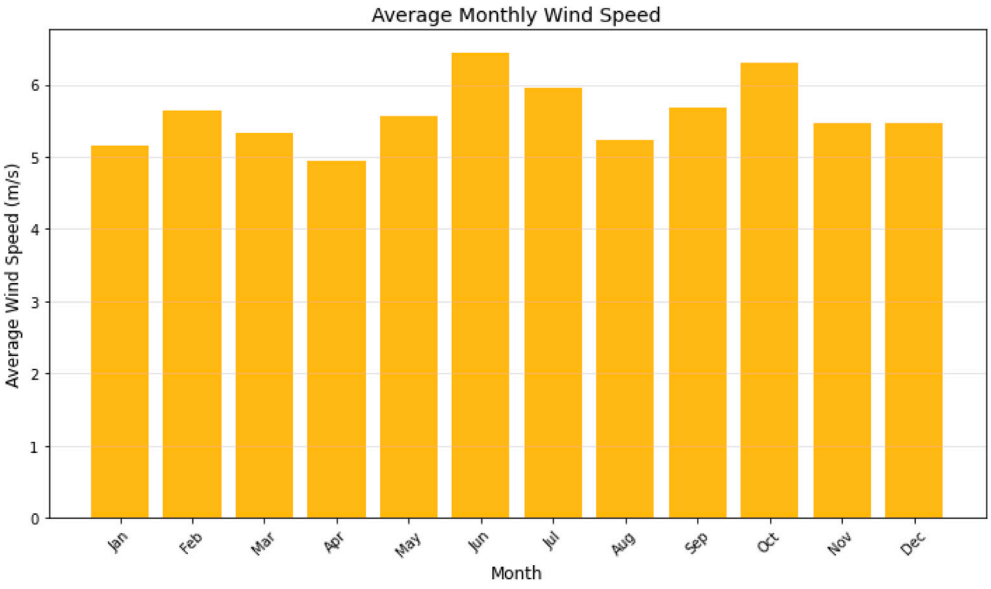

(a) Average Monthly Wind Speed

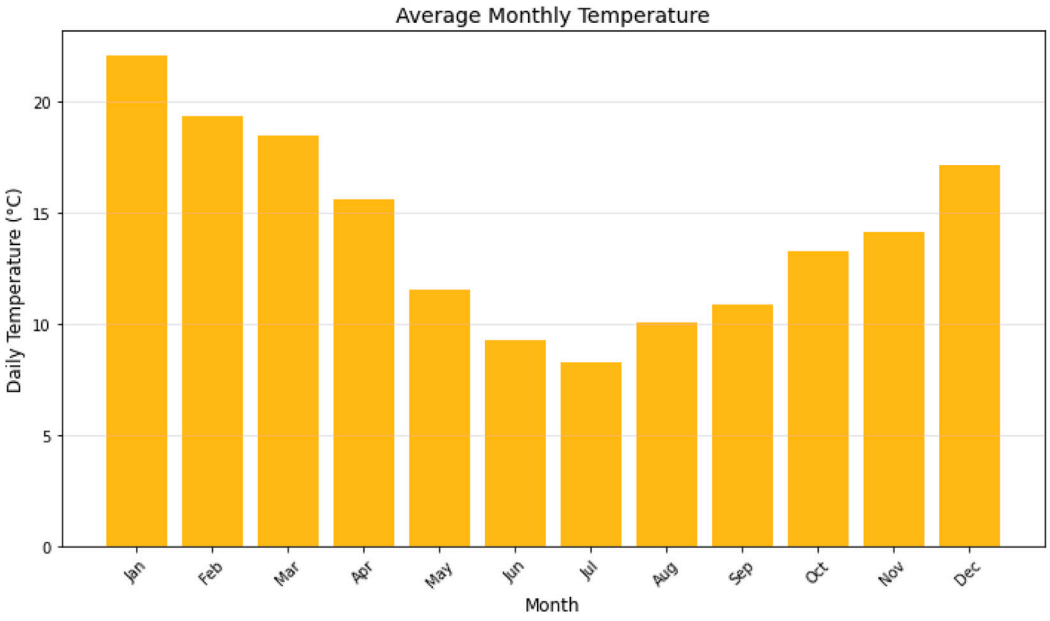

(b) Average Monthly Temperature

Fig. 3. Plot showing the monthly average climate condition of Broadmeadows, between Jan 2023–Dec 2023, (a) wind speed (b) ambient temperature.

4.95 m/s is observed in April, reflecting a temporary dip in wind intensity. This seasonal pattern aligns with broader climatological trends in Victoria, Australia, where winter months generally exhibit higher wind availability. Additionally, recorded wind speeds consistently exceed the typical cut-in speed of 3 m/s required for most commercial Wind turbines (WT), reinforcing the viability of wind energy conversion in the region [24].

These findings are critical for hybrid solar–wind–battery–hydrogen system modeling because accurate characterization of seasonal wind patterns directly affects the reliability of energy generation forecasts, storage design, and system sizing. Without a clear understanding of when wind resources are most abundant — particularly in winter when solar availability is low — models risk underestimating storage needs or over-relying on fossil fuel energy. The observed higher winter wind potential in Broadmeadows suggests that wind energy can play a stabilizing role in hybrid systems by compensating for seasonal solar deficits, thereby enhancing overall energy resilience and reducing reliance on fossil-based backup sources.

2.3. Solar resource assessment

The solar energy potential of Broadmeadows was evaluated using the Photovoltaic Geographical Information System (PVGIS), a high-resolution solar irradiance database developed by the Joint Research Centre (JRC) of the European Commission [73]. PVGIS is a widely recognized tool for assessing PV energy potential, offering geographically precise solar irradiance data essential for renewable energy system modeling. To ensure high temporal resolution, this study retrieved

hourly global solar irradiance data from the Photovoltaic Geographical Information System-fifth-generation European Centre for Medium-Range Weather Forecasts (PVGIS-ERA5) radiation database [74] for the period spanning January 1, 2023–December 31, 2023. This dataset provides a detailed characterization of seasonal solar variability, ensuring accurate estimation of solar energy generation potential.

To optimize PV system performance, the study implemented an optimal tilt (slope) angle of 40° and an azimuth angle of 0°, aligning with the geographical latitude of Broadmeadows. The assessment was conducted at an elevation of 118 m, ensuring that local atmospheric influences such as air mass effects and shading losses were appropriately considered in the analysis.

The seasonal temperature variations in Broadmeadows are illustrated in Fig. 3(b), highlighting significant climatic differences across the year. The highest average temperature of 22.07 °C was recorded in January, coinciding with peak summer conditions, whereas the lowest average temperature of 8.31 °C occurred in July, during winter. While temperature is not a direct indicator of solar irradiance, it plays a crucial role in determining the thermal performance of PV panels. Elevated temperatures are known to reduce PV efficiency due to increased resistive losses and decreased voltage output, emphasizing the importance of seasonal climate considerations in system design. These temperature trends also align with expected climatic patterns in Victoria, where solar irradiance is typically higher in summer and lower in winter due to variations in daylight duration and atmospheric conditions.

The wind speed and solar irradiance distributions in Broadmeadows clearly demonstrate the high potential for PV and wind energy generation at the study site. The consistently favorable wind speeds and substantial solar irradiance levels reinforce the feasibility of a HRES, further supporting the integration of battery and hydrogen storage solutions for enhanced energy reliability and system efficiency.

3. Methodology

3.1. System configuration

The proposed hybrid renewable energy system integrates solar PV, WT, Battery Energy Storage System (BESS), and hydrogen storage to evaluate the feasibility of a sustainable and resilient electricity supply for Broadmeadows. The system architecture and energy flow, as illustrated in Fig. 4, depict the interaction between these components in generation, storage, and consumption, ensuring an optimized and balanced energy supply.

The system consists of two primary RERs:

- PV plant — Converts solar radiation into electricity and operates on the Direct Current (DC) bus.
- WT plant — Generates Alternating Current (AC) and connects to the AC bus, contributing to the overall system's renewable energy supply.

The DC bus facilitates the integration of solar generation, battery storage, and hydrogen electrolysis, ensuring efficient energy conversion and storage before dispatch. The AC bus accommodates wind energy and grid interactions, enabling seamless integration with household electricity demand and fossil fuel energy. A power converter is used to facilitate bidirectional energy exchange between AC and DC buses, ensuring efficient coordination between the components of the wind, solar, battery and hydrogen.

To enhance energy security and stability, the system incorporates two energy storage technologies:

- BESS — Connected to the DC bus via a bidirectional power converter, enabling short-term energy storage and dispatch.
- Hydrogen storage system — Utilizes surplus electricity in a PEM electrolyzer to produce hydrogen (H_2), which is stored in H_2 tanks and later converted back into electricity using a fuel cell for long-term storage.

Additionally, the system integrates distributed rooftop PV installed on individual households. Electricity generated from rooftop PV is prioritized for local consumption, while excess generation is combined with centralized PV plants and WT to meet broader demand. This approach ensures maximum utilization of available solar resources before relying on storage or supplementary energy sources.

When renewable generation and storage are insufficient to meet demand, fossil fuel energy sources (e.g., diesel, coal, or natural gas) serve as a last-resort backup to maintain system reliability.

This hybrid system configuration is analyzed to assess its technical feasibility, evaluating how different renewable energy and storage combinations perform under varying seasonal and operational conditions. The results provide insights into energy sufficiency, backup fossil-fuel use, and economic viability, enabling a comprehensive evaluation of system resilience. Among the nine simulated configurations, the *solar–wind–battery–hydrogen–diesel* system represents the fully integrated setup that achieved near-complete renewable energy coverage and was therefore used to evaluate the overall system efficiency presented in Section 4.7.

3.2. Wind turbine model

The electrical energy output from WT in this study follows the mathematical modeling approach proposed by [41], with modifications to enhance hourly resolution instead of relying on monthly averages. This refinement improves the temporal accuracy of wind power generation integration within the hybrid renewable energy system analysis.

In this study, the Siemens Gamesa SG 2.1-114 WT[75] is selected as a representative commercial unit for modeling purposes. While the study does not prescribe a specific turbine for deployment, this model was chosen based on its compatibility with the moderate wind conditions observed in Broadmeadows and its widespread use in similar-scale installations globally. Its selection facilitates realistic performance and cost estimations, as the turbine's technical and economic characteristics are well-documented, allowing for transparent LCOE analysis and scalability assessment. The turbine has a rated power of 2.1 MW, a rotor diameter of 114 m, and operates within a cut-in speed of 1.5 m/s and cut-out speed of 25 m/s. The power output $P_T(V)$ at various wind speeds follows the manufacturer-provided power curve [75], ensuring an accurate performance representation in energy generation modeling.

3.2.1. Wind turbine plant layout and energy estimation

According to Caravantes et al. [41], WT plant layouts are designed to maximize energy capture while minimizing wake interference. Based on industry standards, turbines are spaced 10 rotor diameters apart along the prevailing wind direction and 5 rotor diameters perpendicular to the wind direction. These estimations follow [76] to minimize turbulence or wake effects, which can reduce energy generation efficiency as wind flows across the turbine blades.

The total energy output from the wind farm is computed by scaling the power output of individual turbines using a land-normalized energy estimation approach. Following the formulation presented by [41], the hourly energy generation $E_{w,h}$ is given by Eq. (2):

$$E_{w,h} = \frac{P_T(V) \times N_T \times f_{\text{avail}}}{10^6 \times A_{wt}} \tag{2}$$

where $P_T(V)$ is the turbine at wind speed V, N_T is the number of turbines, $f_{\text{availability}} = 0.98$ is the availability factor, and $A_{wt} = 0.6498\ \text{km}^2$ is the land area per turbine. This approach ensures spatial scalability and accounts for turbine spacing standards, wake losses, and land-use constraints.

For total energy over a given period T, the cumulative energy output is computed using Eq. (3)

$$E_{w,\text{total}} = \sum_{t=1}^{T} E_{w,h} \tag{3}$$

Where T is the number of hours in the simulation.

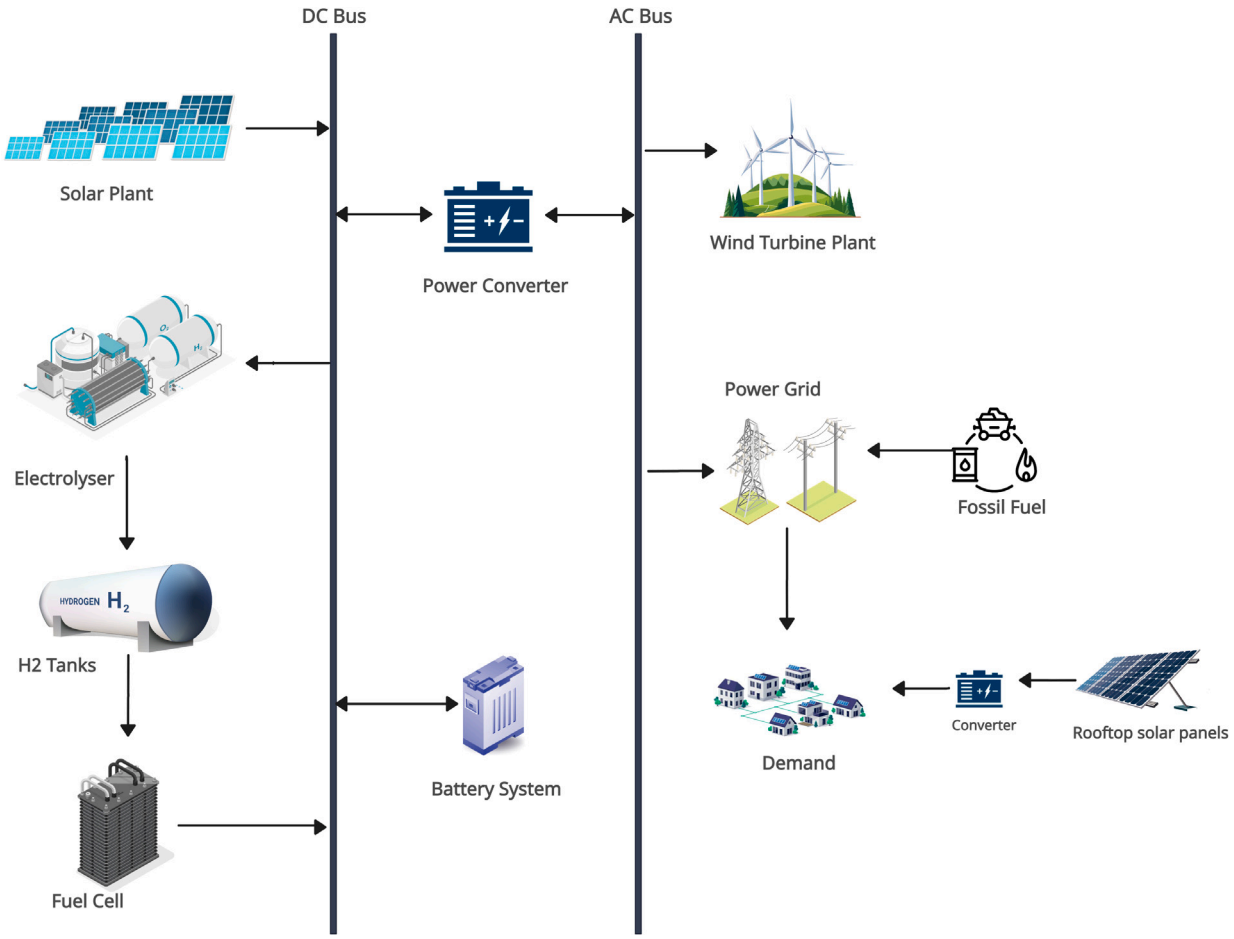

Fig. 4. Schematic layout of the proposed HRES integrating solar PV, WT, battery, hydrogen chain, and diesel backup through a unified AC/DC bus.

3.2.2. Scaling and system integration

In this study, WT plants are modeled as an array of up to five turbines, with variations in turbine count N_T=[1,2,3,4,5] to evaluate the impact of scaling wind energy capacity in the hybrid system. This configuration represents incremental wind energy capacities ranging from 2.1 MW (one turbine) to 10.5 MW (five turbines), allowing for a systematic assessment of how increased wind capacity affects energy availability, storage requirements, and fossil fuel energy use. The lower-capacity configurations reflect limited wind deployment scenarios, whereas higher-capacity configurations simulate larger wind farms that significantly contribute to energy sufficiency and resilience.

While [41] employed a monthly average-based approach to estimate wind farm energy output, this study refines the methodology by applying it at an hourly temporal resolution, using real hourly wind speed data retrieved from NASA POWER. The power output is computed using the manufacturer's turbine-specific power curve [75], ensuring realistic modeling of output variations throughout the year. This enhanced resolution enables more accurate simulation of short-term intermittency, energy dispatch patterns, and the dynamic interaction between wind generation, storage behavior, and fossil fuel energy use within the HRES.

3.3. Photovoltaic model

The PV model in this study estimates the hourly energy output of a single PV panel based on solar irradiance, system efficiency, and panel characteristics. To enhance accuracy, high-resolution hourly solar irradiance data from the PVGIS-ERA5 database was imported and directly mapped to the corresponding simulation timestamps within the PV model. This time-aligned integration ensures that each hour's solar input reflects actual climatic variability, which is then processed through established mathematical formulations to estimate panel-level energy output under varying meteorological conditions. This method allows for dynamic modeling of solar energy generation in response to short-term irradiance and temperature fluctuations. The ESPSC 400 M PERC monocrystalline panel [77] is selected due to its high efficiency (20.17%), stable performance under temperature variations, and reliability in Melbourne's climate. This 400 W panel, with a surface area of 2.1 m^2, maintains efficient operation above 25 °C, making it suitable for the study location.

3.3.1. Solar energy estimation

The solar energy generation methodology follows [78], ensuring accurate energy estimation for PV panels. Instead of using daily averages, this study employs an hourly Peak Solar Hours (PSH) approach, computed using Eq. (4):

$$\mathrm{PSH} = \frac{G(i)}{1000} \quad [\text{hours basis, kWh/m}^2] \tag{4}$$

Where G(i) represents the hourly global irradiance (Wh/m2), representing the actual sunlight availability in Broadmeadows for energy generation analysis. The G(i) on the PV panel is further computed using Eq. (5):

$$\mathrm{G}(i) = \frac{G_b(i) + G_d(i) + G_r(i)}{1000} \tag{5}$$

Where G_b (i) represents the direct beam irradiance, G_d (i) is the diffuse irradiance, and G_r (i) is the reflected irradiance, are collected from the PVGIS tool [79] for Broadmeadows on an hourly basis (Jan

2023–Dec 2023). For hourly electrical energy output of a single PV panel is computed by using the formula in Eq. (6) as define by [78]:

$$E_{panel} = PSH \times P_{peak} \times \eta_{global} \times A_{sp} \quad (6)$$

Where:

- P_{peak} = 0.4 kW (panel's rated peak power)
- A_{sp} = 2.1 m^2 (panel's surface area)
- η_{global} = Overall system efficiency

3.3.2. System efficiency estimation

According to [78], the overall system efficiency η_{global} accounts for various real-world losses and is calculated using Eq. (7):

$$\eta_{global} = FF \times \eta_{temp} \times \eta_{conn} \times \eta_{dirt} \times SF \quad (7)$$

Where Form Factor (FF) quantifies the panel's maximum power output relative to open-circuit voltage and short-circuit current, is calculated using Eq. (8) given by [24]:

$$FF = \frac{P_{max}}{V_{oc} \times I_{sc}} \quad (8)$$

Using ESPSC 400 M PERC panel characteristics [77], the P_{max} = 400 W, V_{vc} = 49.5 V and I_{sc} = 10.1 A. By replacing all these values in Eq. (8), we get FF = 0.798.

The Temperature Correction Factor (η_{temp}) accounts for the effect of temperature on power output and is defined in Eq. (9):

$$\eta_{temp} = 1 + \beta(T_{oper} - 25) \quad (9)$$

The temperature coefficient β is assumed to be −0.574%/°C, with the operating temperature (T_{oper}) of 45 °C, as defined in [77]. Substituting these values in Eq. (9), the temperature-adjusted efficiency is calculated as η_{temp} = 0.885.

Additionally, [77] reports that the grid connection efficiency (η_{conn}) = 0.98 accounts for inverter and wiring losses, the dirt and soiling factor (η_{dirt})=0.97 represents performance degradation due to dust accumulation, and the Safety Factor (SF) = 0.95 incorporates system uncertainties. Substituting these values in Eq. (7), the global efficiency is determined as η_{global}=0.637.

3.3.3. Scaling to rooftop and large-scale photovoltaic systems

For residential rooftop PV systems, each dwelling is assumed to have a 4-kW system. Since each ESPSC 400 M PERC panel has a 400 W capacity (0.4 kW), a 4-kW system consists of 10 panels per household. With 4617 dwellings in Broadmeadows, the total residential rooftop energy ($E_{rooftop}$) output is calculated using Eq. (10):

$$E_{rooftop} = E_{panel} \times 10 \times 4617 \quad (10)$$

This methodology is also extended to simulate energy generation for larger solar plant installations with capacities ranging from 1 MW to 50 MW. The total number of panels required for each plant size (N_{panels}) is determined through Eq. (11):

$$N_{panels} = \frac{C_{plant}}{C_{panel}} \quad (11)$$

Where C_{plant} is the total installed capacity of the solar plant in our simulation, C_{panel} = 0.4 W is the rated power of a single ESPSC 400 M PERC panel.

To ensure a realistic energy estimate, a Performance ratio (PR) of 0.85 is applied, accounting for additional real-world losses such as inverter inefficiencies, dust accumulation, and electrical losses. The final energy output across different system configurations is then estimated according to Eq. (12):

$$E_{plant} = E_{panel} \times N_{panels} \times PR \quad (12)$$

This structured methodology ensures accurate hourly energy estimations for both residential rooftop PV systems and large-scale solar farms, providing a comprehensive assessment of solar energy potential under Melbourne's climatic conditions.

3.4. Energy storage model

3.4.1. Battery energy storage system

The BESS is designed to store excess renewable energy from both solar and wind sources and discharge it when demand exceeds generation, particularly at night (when solar output is zero) and during low renewable generation periods, such as winter months. The system enhances energy dispatch efficiency while optimizing storage capacity to minimize fossil fuel energy use and extend battery lifespan.

For this study, the Hoppecke lead–acid battery [80] was selected due to its deep-cycle capability and high roundtrip efficiency. The battery specifications include a nominal voltage of $V_B = 2V$, nominal capacity of C_{single} = 3000 Ah, roundtrip efficiency of η_B = 0.86, and Depth of Discharge (DoD) of 70%. To determine the required battery storage capacity, a systematic approach is adopted, considering both short-term energy shortfalls and system efficiency constraints.

The first step in estimating the required battery storage is to assess the worst-case nighttime energy shortfall, which represents the maximum cumulative shortfall over a single night. To ensure a reliable energy reserve, a 15% buffer is included to account for demand uncertainties and conversion inefficiencies. The total required storage capacity ($E_{req\_storage}$) is determined using Eq. (13):

$$E_{req\_storage} = E_{shortfall} \times 1.15 \quad (13)$$

Where ($E_{shortfall}$) represents the maximum cumulative shortfall in a single night, and the 15% buffer accounts for demand uncertainties and conversion inefficiencies. Since batteries operate in DC mode, energy losses due to AC–DC conversion must be incorporated to accurately estimate the effective storage requirement. The effective required storage capacity ($E_{eff\_storage}$), which accounts for conversion losses, is calculated using Eq. (14):

$$E_{eff\_storage} = \frac{E_{req\_storage}}{\eta_{conv}} \quad (14)$$

Where η_{conv} = 0.9 represents conversion efficiency as defined in [81].

To finalize the battery sizing process, the energy capacity of a single battery unit is determined in order to calculate the total number of units needed. The energy stored per battery unit ($E_{battery}$) is computed using Eq. (15):

$$E_{battery} = \frac{C_{single} \times V_B}{1000} \quad (15)$$

Here, the division by 1000 converts watt-hours (Wh) to kilowatt-hours (kWh). Using Eqs. (14) and (15), the total number of batteries ($N_{batteries}$) required to meet the storage demand is calculated using Eq. (16):

$$N_{batteries} = \frac{E_{eff\_storage}}{E_{battery} \times DOD \times \eta_B} \quad (16)$$

Where DoD ensures that the battery is not discharged excessively, which can reduce its lifespan.

To enhance battery longevity, a charge–discharge control strategy is implemented. This strategy dynamically regulates State of Charge (SOC), restricting charge levels to a maximum of 90% to avoid overcharging and restricting discharge to 5% to avoid deep cycling [82]. The available charging capacity of the battery (B_{avail_cap}) at any given time step is calculated using Eq. (17):

$$B_{avail\_cap} = E_{eff\_storage} - SOC_{t-1} \quad (17)$$

The Hoppecke lead–acid battery was selected as the reference storage technology to preserve methodological consistency across all modeled configurations. The study emphasizes comparative system-level techno-economic performance rather than component-specific benchmarking; adopting a single, well-characterized battery chemistry prevents variations in efficiency or cost assumptions that could distort the comparative results. Lead–acid systems remain the most widely

deployed and economically accessible option for community-scale hybrid applications in Australia, combining 85%–90% round-trip efficiency with 10–15 years of operational life and a relatively low capital cost [14,83,84]. Advanced chemistries such as lithium-ion [44] and vanadium-redox flow batteries [85] can be integrated within the existing Python-based framework, yet their inclusion is reserved for future research focusing on component optimization and lifecycle evaluation.

Although batteries serve as an effective short-term storage solution, they are typically insufficient during extended periods of low availability of renewable energy, particularly in winter, when solar and wind generation decline simultaneously. As such, this study proposes the integration of long-duration storage solutions, namely hydrogen-based systems, to ensure continuous energy availability and improve the resilience of the year-round system.

3.4.2. Hydrogen energy storage system

The hydrogen energy storage system in this study consists of two main components: hydrogen production through electrolysis and power generation through a PEM fuel cell. These technologies store excess renewable energy in the form of hydrogen, which is later converted back into electricity when needed, ensuring system reliability and reducing dependence on fossil fuel energy use.

3.4.2.1. Electrolyzer hydrogen production. The hydrogen production methodology follows the approach outlined by [41], ensuring a robust estimation of hydrogen generation from surplus renewable energy. Hydrogen is produced using PEM electrolyzer, which operates at 59% efficiency ($\eta_{\text{PEM}} = 0.59$), accounting for conversion losses during electrolysis. The electrolyzer converts surplus renewable energy into hydrogen via water electrolysis, storing it for future electricity generation. The hourly hydrogen production ($P_{H_2,w}$) is computed using Eq. (18) as given by [41]:

$$P_{H_2,w} = \frac{E_{\text{surplus}} \times \eta_{\text{PEM}}}{HHV_{H_2}} \quad \text{[kg/hour]} \tag{18}$$

Where E_{surplus} is the surplus renewable energy available at each hour (kWh/hour), and $HHV_{H_2} = 39$ kWh/kg is the Higher Heating Value of hydrogen [86], used to quantify hydrogen's energy content. The produced hydrogen is stored in a hydrogen storage system, ensuring that energy is available for later use.

Although large-scale hydrogen production assessments such as [41] focus on estimating hydrogen potential based on land availability and regional energy distribution, this study adopts a simulation-driven hourly energy dispatch framework. Instead of using static land use assumptions, hydrogen generation in this study is dynamically modeled based on real-time surplus renewable energy, calculated after sequentially meeting household demand and battery storage thresholds. This hourly energy balance approach ensures that hydrogen is only produced when actual excess energy is available within the simulated system, providing a more realistic and operationally grounded estimate of hydrogen production under hybrid system constraints.

While the battery storage system manages short-term energy imbalances, extended periods of low renewable generation require an alternative energy reserve. Hydrogen storage addresses long-duration energy shortages, ensuring system stability during seasonal variations. The total energy deficit (E_{def}), defined as the energy shortfall after solar, wind, and battery contributions, is computed using Eq. (19):

$$E_{\text{def}} = E_d - (E_{\text{ss}} + E_{\text{ws}} + E_{\text{bss}}) \tag{19}$$

Where E_d represents total energy demand, E_{ss} and E_{ws} are the hourly energy outputs from solar and wind, and E_{bss} is the contribution from battery storage. To ensure that the hydrogen storage system can compensate for the worst-case seasonal shortfall, the largest continuous energy deficit over the year is calculated using Eq. (20):

$$E_{\text{def,max}} = \max\left(\sum_{h=1}^{8760} E_{\text{def}}\right) \tag{20}$$

Where 8760 h represent a full year of simulation. This represents the worst-case scenario, where renewable generation and battery storage are both insufficient for an extended period. The required hydrogen storage capacity (H_2^{str}) to fully compensate for this seasonal energy gap is determined using Eq. (21):

$$H_2^{\text{str}} = \frac{E_{\text{def,max}}}{HHV_{H_2} \times \eta_{\text{FC}}} \tag{21}$$

This ensures that the hydrogen storage system is adequately sized to supply backup energy during prolonged periods of low renewable availability, especially in winter.

3.4.2.2. Fuel cell system. The stored hydrogen is converted back into electricity using a PEM fuel cell, which operates at 59% efficiency ($\eta_{FC} = 0.59$) [87]. The hourly electrical energy output from the fuel cell is calculated using Eq. (22), as defined in [28].

$$E_{\text{FC}} = P_{H_2,w} \times HHV_{H_2} \times \eta_{\text{FC}} \tag{22}$$

To ensure system reliability, the PEM fuel cell is sized using an hourly simulation-based energy dispatch model developed for this study. Within this simulation, residual demand refers to the unmet electricity load after accounting for contributions from solar, wind, and battery storage systems. By identifying the maximum hourly residual demand over the entire simulation year, the required fuel cell power rating (P_{FC}) can be determined. This approach ensures that the fuel cell is capable of meeting peak energy shortfalls without oversizing the system, thereby maintaining reliability while optimizing capital expenditure. The corresponding fuel cell capacity is computed using Eq. (23).

$$P_{\text{FC}} = \frac{E_{\text{def,max}}}{\eta_{\text{FC}}} \tag{23}$$

This ensures that the fuel cell has the capability to meet peak energy deficits, optimizing system performance and cost-effectiveness.

Both the electrolyzer and fuel cell are represented as steady-state energy-conversion modules calibrated to industrially relevant performance. The adopted electrolyzer efficiency (70%–75%) and fuel-cell efficiency (55%–60%) correspond to commercial PEM systems operating at current densities of 1.5–2.0 A cm^{-2} and hydrogen utilization factors of 0.8–0.9 [88,89]. These ranges are consistent with demonstration-scale PEM installations and ensure that simulated hydrogen production and reconversion quantities remain within empirically validated bounds. Transient electrochemical phenomena — such as polarization losses, temperature dynamics, and degradation — are not explicitly modeled, as the present study emphasizes annual energy balance and techno-economic realism rather than cell-scale kinetics. This steady-state representation aligns with prior hybrid renewable-hydrogen studies that favor transparency and reproducibility for long-term simulation frameworks. All efficiency assumptions were benchmarked against published PEM and Solid Oxide Fuel Cell (SOFC) datasets [90], to confirm that conversion yields lie within realistic operating limits.

By integrating PEM electrolysis for hydrogen production and a fuel cell for energy recovery, the hybrid system is structured to address both short-term and long-term storage needs within the dispatch framework. Battery storage is configured to handle rapid, daily fluctuations in renewable generation and demand, whereas hydrogen storage is intended for sustained periods of low generation — particularly during seasonal deficits. This complementary storage architecture enables temporal energy balancing across multiple timescales and is assessed through simulation to evaluate its contribution to energy resilience and reduced fossil fuel energy use under varying seasonal and operational conditions.

In this study, hydrogen is assumed to be stored as compressed gas at 30–35 bar, consistent with small- to medium-scale renewable H_2 systems designed for suburban applications. Gaseous storage was selected due to its technological maturity, safety record, and moderate compression energy demand relative to liquid hydrogen. Liquid

Table 1
Technical specifications and cost parameters for key system components in the hybrid solar–wind–battery–hydrogen energy system.

PV [77,78]	
Parameter	Values
Model	ESP5C 400 M PERC
Efficiency	20%
Capacity	400 W (0.4 kW per panel)
Capital Cost	$980/kW
Replacement Cost	$980/kW
O&M Cost	2% of CAPEX annually
Lifetime	15 years

WT [41,75]	
Parameter	Values
Model	Siemens Gamesa SG 2.1-114
Cut-in Speed	1.5 m/s
Cut-out Speed	25 m/s
Capacity	2.1 MW
Capital Cost	$50,000/kW
Replacement Cost	$50,000/kW
O&M Cost	$1500/year
Lifetime	20 years

Battery Storage [80,81]	
Parameter	Values
Model	Li-Ion Hoppecke lead–acid
Efficiency	86%
Nominal Voltage	2V
Nominal Capacity	3000 Ah
Converter Efficiency	90%
Capital Cost	$1644/unit
O&M Cost	$10/year
Lifetime	10 years

Electrolyzer [37]	
Parameter	Values
Model	PEM
Efficiency	75%
Capacity	1 kW
Capital Cost	$3000/kW
Replacement Cost	$2500/kW
O&M Cost	1% of CAPEX annually
Lifetime	50,000 h

Hydrogen Tank [24,87]	
Parameter	Values
Capital Cost	$500/kg
Replacement Cost	$500/kg
O&M Cost	1% of CAPEX annually
Lifetime	25 years

Fuel Cell [28,87]	
Parameter	Values
Model	PEM
Efficiency	59%
Capacity	1 kW
Capital Cost	$600/kW
Replacement Cost	$300/kW
O&M Cost	1% of CAPEX annually
Lifetime	50,000 h

storage was not considered within the present scope because the liquefaction process entails an energy penalty of approximately 30% of the stored energy and requires cryogenic insulation and boil-off management, which substantially increase system complexity and capital cost [89,91,92]. As the research objective centers on system-level energy resilience and cost evaluation rather than storage-medium optimization, compressed-gas storage provides an appropriate baseline for comparative techno-economic assessment. The Python-based modeling framework remains modular, allowing future integration of liquid or solid-state hydrogen storage modules in extended analyses.

3.5. Economic analysis criteria

The economic viability of the proposed hybrid solar–wind–battery–hydrogen energy system is evaluated using two well-established techno-economic indicators: LCOE and LCOH. These indicators measure the average cost per unit of electricity (AUD/kWh) and hydrogen (AUD/kg H_2) produced over the project's operational lifespan, incorporating Capital Expenditures (CAPEX), replacement costs, Operation and Maintenance (O&M) expenses, and discounting mechanisms to account for financial depreciation [93]. A structured breakdown of financial parameters, including cost elements for solar PV, WT, battery storage, electrolyzers, fuel cells, and hydrogen storage, is presented in Table 1, ensuring a transparent and industry-aligned economic assessment.

The technical specifications and cost parameters for photovoltaic panels, wind turbines, battery systems, electrolyzers, hydrogen storage tanks, and fuel cells used in this study are derived from manufacturer datasheets — such as [75] for WT, [77] for PV modules, and [80] for batteries and are further validated through peer-reviewed literature [24,37,41,77,78,80,81,87,94]. These references ensure realistic techno-economic modeling by reflecting commercially available technologies, operational efficiencies, and cost benchmarks. A structured summary of all parameters is presented in Table 1, providing transparency and consistency in economic assessment.

3.5.1. Levelized cost of energy

The LCOE represents the total cost per kilowatt-hour (AUD/kWh) of electricity generation over the system's lifetime, accounting for capital investment, replacement costs, Operational Expenditures (OPEX), and fossil fuel energy purchases in case of energy shortfalls, as defined by [24]. It is calculated using Eq. (24) as:

$$LCOE = \frac{C_{\text{cap}} + C_{\text{rep}} + C_{O\&M} + C_{\text{grid}}}{\sum_{t=1}^{n} \frac{E_{\text{tot},t}}{(1+r)^t}} \tag{24}$$

Where C_{cap} represents the initial capital cost, which includes the expenses associated with solar PV panels, WT, and battery storage. The term C_{rep} accounts for the discounted replacement cost of system components that require periodic substitution over the 25-year project lifetime. The OPEX, denoted by $C_{\text{O\&M}}$, are assumed as a percentage of the total CAPEX, ensuring continuous system functionality over time. Additionally, grid electricity purchases during energy shortages are represented by C_{grid}, reflecting the cost of external energy dependence. The denominator represents the total energy generated by the system over its lifetime, where $E_{\text{tot},t}$ is the annual energy output (kWh).

To ensure an accurate financial assessment, discounted future cash flows are incorporated using the Present Value Factor (PVF) [95] and is estimated using Eq. (25).

$$PVF = \sum_{t=1}^{n} \frac{1}{(1+r)^t} \tag{25}$$

Where n=25 years is the system lifespan and r=7% represents the discount rate based on [96], reflecting financial depreciation of capital assets.

The denominator of the LCOE equation accounts for the total lifetime energy generation, ensuring a realistic cost comparison with market electricity prices. This approach facilitates a meaningful assessment of economic feasibility, particularly regarding the integration of battery and hydrogen storage technologies into the system.

3.5.2. Levelized cost of hydrogen

The LCOH quantifies the cost of hydrogen production per kilogram (AUD/kg H_2) over the system's lifetime, incorporating electrolyzer operation, hydrogen storage costs, and fuel cell conversion efficiency, as define by [97] . It is estimated using Eq. (26):

$$LCOH = \frac{C_{\text{elec}} + C_{\text{FC}} + C_{\text{H}_2,\text{str}} + C_{\text{H}_2,\text{OM}} + C_{\text{water}}}{\sum_{t=1}^{n} \frac{M_{\text{H}_2,t}}{(1+r)^t}} \quad (26)$$

Where C_{elec} represents the capital and discounted replacement cost of the electrolyzer, while C_{FC} accounts for the fuel cell investment and periodic replacement costs over the system's lifetime. The cost associated with hydrogen storage infrastructure is denoted as $C_{\text{H}_2,\text{str}}$ ensuring that the system maintains sufficient reserves for long-term energy supply during renewable generation shortages. The annual OPEX, expressed as $C_{\text{H}_2,\text{OM}}$, is assumed to be 1% of the total CAPEX [37], reflecting ongoing system maintenance expenses. Additionally, the cost of water required for electrolysis, as defined by the National Renewable Energy Laboratory (NREL) [98], is incorporated as C_{water}, estimated based on a fixed cost of 1 AUD/m^3.

Since hydrogen storage serves as a long-term energy buffer, the denominator accounts for total hydrogen production over the project's lifespan. The term $M_{\text{H}_2,t}$ represents the annual hydrogen production (kg H_2) discounted at $r = 0.07$ over $n = 25$ years [96], ensuring that the economic assessment captures seasonal variations in hydrogen production while maintaining consistency with real-world hydrogen generation patterns.

By incorporating discounted cost structures — such as upfront CAPEX, component replacement costs, and annual O&M cost adjusted over time using a 7% discount rate — this analysis delivers a transparent and structured economic evaluation of the proposed hybrid energy system. Coupled with lifetime energy production metrics, the resulting LCOE and LCOH provide meaningful insights into the long-term financial viability of integrating battery and hydrogen storage solutions into renewable energy configurations.

The results facilitate cost benchmarking with conventional electricity and hydrogen production methods, offering a comprehensive understanding of long-term project feasibility. This analysis highlights the economic trade-offs between battery storage and hydrogen storage, supporting informed decision-making for sustainable and cost-effective energy system deployment in urban and suburban settings.

3.6. Simulation model

This study employs a scenario-driven simulation approach — commonly used in hybrid energy systems research — to assess the feasibility of various renewable energy configurations over a full-year simulation at hourly resolution [99,100]. The model dynamically balances energy generation, storage, and consumption, ensuring an rule based dispatch strategy while minimizing reliance on fossil fuel energy use. Unlike studies that rely on short-term forecasting techniques [28], this approach accounts for seasonal variations and long-term energy supply–demand interactions, providing a comprehensive assessment of system performance under real-world operational conditions.

To facilitate efficient energy allocation, RB-HDA is implemented, prioritizing local renewable energy utilization before engaging storage or fossil fuel energy use. The energy dispatch strategy, structured in Algorithm 1, ensures that available renewable energy is first used to meet demand, followed by the storage of excess energy in the battery for short-term use, and hydrogen production via electrolysis when surplus energy exceeds battery capacity. During energy deficits, stored energy in batteries is discharged first, followed by hydrogen conversion using a fuel cell, while fossil fuel energy is engaged only as a last resort.

To comprehensively analyze system feasibility, the study evaluates nine distinct energy system configurations, categorized into solar-only, wind-only, and hybrid solar–wind systems, as shown in Fig. 5. These configurations illustrate the progressive integration of storage technologies, starting from direct solar or wind utilization to advanced systems incorporating battery and hydrogen storage for enhanced reliability. Solar-only and wind-only systems rely on a single renewable source, either with or without storage, whereas hybrid solar–wind systems leverage the complementary nature of solar and wind energy to improve energy security.

Each configuration is simulated at an hourly resolution for a full year, capturing seasonal fluctuations in renewable generation and demand. The primary objective is to determine whether a given configuration can achieve independence from fossil fuel energy use, maximize renewable energy utilization, and ensure system reliability under varying meteorological conditions. This structured simulation framework enables a holistic assessment of hybrid energy system performance, providing critical insights into the trade-offs between energy sufficiency, storage requirements, and economic feasibility.

Algorithm 1 Renewable Energy Dispatch Strategy

Input: Solar PV Output (P_{solar}), Wind Output (P_{wind}), Demand (P_{demand})
Battery State of Charge (SOC_{battery}), Battery Capacity (C_{battery})
Hydrogen Storage Level (H_2^{storage}), Fuel Cell Efficiency (η_{FC})
Fossil fuel Energy Supply ($P_{\text{nonrenewable}}$)
// **Step 1: Direct utilization of solar and wind energy**
$P_{\text{available}} = P_{\text{solar}} + P_{\text{wind}}$
if $P_{\text{available}} \geq P_{\text{demand}}$ **then**
    Supply energy directly to demand
    $Surplus_{\text{energy}} = P_{\text{available}} - P_{\text{demand}}$
else
    $Energy_{\text{deficit}} = P_{\text{demand}} - P_{\text{available}}$
end if
// **Step 2: Store excess energy in the battery (short-term storage)**
if $Surplus_{\text{energy}} > 0$ **and** $SOC_{\text{battery}} < C_{\text{battery}}$ **then**
    Store $Surplus_{\text{energy}}$ in battery
    $Surplus_{\text{energy}} -= Stored_{\text{energy}}$
end if
// **Step 3: Hydrogen production via electrolysis (long-term storage)**
if $Surplus_{\text{energy}} > 0$ **then**
    Convert $Surplus_{\text{energy}}$ to hydrogen via electrolysis
    Update H_2^{storage}
end if
// **Step 4: Discharging the battery and hydrogen storage during deficits**
if $Energy_{\text{deficit}} > 0$ **then**
    if $SOC_{\text{battery}} > 0$ **then**
        Discharge battery to meet demand
        Update SOC_{battery}
        $Energy_{\text{deficit}} -= Battery_{\text{discharge}}$
    end if
    if $Energy_{\text{deficit}} > 0$ **and** $H_2^{\text{storage}} > 0$ **then**
        Convert hydrogen to electricity using PEM fuel cell
        Update H_2^{storage}
        $Energy_{\text{deficit}} -= Hydrogen_{\text{power output}} \times \eta_{\text{FC}}$
    end if
end if
// **Step 5: Utilize fossil fuel energy as a last resort**
if $Energy_{\text{deficit}} > 0$ **then**
    Use $P_{\text{nonrenewable}}$ to meet remaining demand
    Update total fossil fuel energy consumption
end if

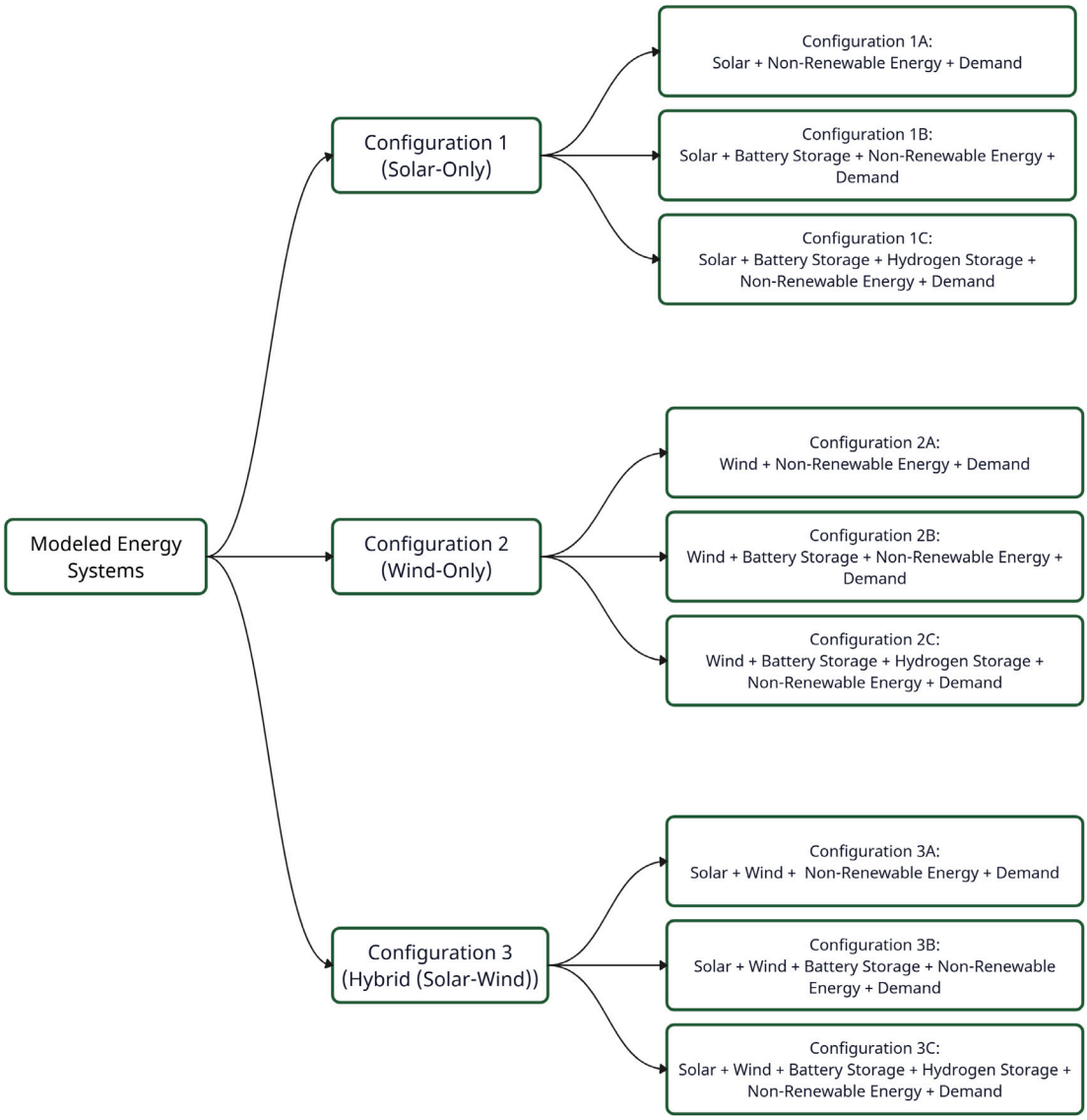

Fig. 5. Classification of the nine modeled hybrid energy configurations by generation source and storage integration.

3.6.1. Computational model and energy dispatch visualization

The simulation model is implemented in Python to perform hourly energy simulations across an entire year. Its structure consists of three main elements: (i) high-resolution meteorological inputs for solar irradiance, wind speed, and temperature, (ii) component models for PV, WT, batteries, and hydrogen systems, and (iii) a dispatch algorithm that balances generation, storage, and demand while engaging fossil backup only when necessary. By linking these components, the model evaluates system feasibility under realistic operating conditions and quantifies the extent to which different configurations reduce fossil fuel energy reliance.

To enhance clarity in energy dispatch logic, Figs. 6 7 and 8 present flowcharts that visualize the structured energy management strategy across different configurations. Each flowchart distinguishes the operational hierarchy of solar, wind, battery, and hydrogen storage using color-coded dashed lines, representing incremental system configurations within solar-only, wind-only, and hybrid solar–wind systems.

Fig. 6 illustrates the solar-only systems, where green dashed lines represent configurations relying solely on solar and fossil fuel energy, red dashed lines indicate the addition of battery storage for short-term energy balancing, and blue dashed lines incorporate hydrogen storage for long-term energy security. Similarly, Fig. 7 follows the same structured approach for wind-only systems, highlighting incremental improvements from standalone wind to battery and hydrogen-integrated setups. Fig. 8 depicts hybrid solar–wind configurations, demonstrating the complementary nature of wind and solar generation, along with storage integration for enhanced reliability.

These flowcharts systematically illustrate the energy dispatch logic applied across the modeled configurations. The process begins by prioritizing real-time utilization of available renewable energy — solar, wind, or both — directly for demand fulfillment. Any surplus is first directed to battery storage for short-term balancing. If battery capacity is full, excess energy is diverted to hydrogen production via electrolysis for long-term storage. During energy deficits, the system discharges stored energy from batteries first, followed by hydrogen reconversion through a fuel cell. Fossil fuel energy sources are only activated as a last resort when all renewable and stored energy resources are exhausted. This hierarchical dispatch strategy ensures maximum renewable energy utilization, optimized storage usage, and minimal dependence on fossil fuel energy use.

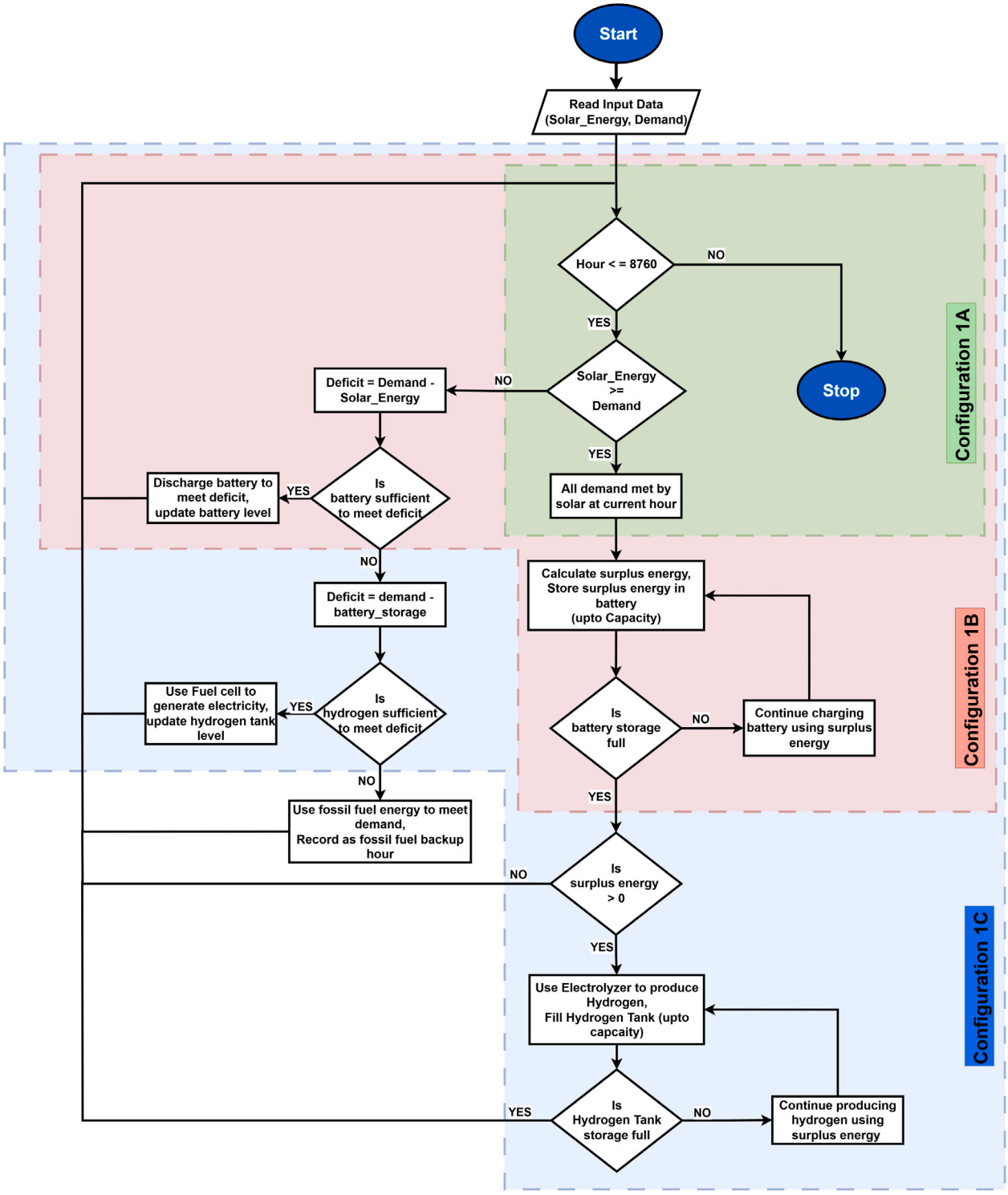

Fig. 6. Energy dispatch decision process for solar-only system scenarios. The flowchart illustrates energy allocation priorities, with dashed lines differentiating solar-only (green), solar + battery (red), and solar + battery + hydrogen (blue) configurations. (For interpretation of the references to color in this figure legend, the reader is referred to the web version of this article.)

This hierarchical dispatch strategy ensures maximum renewable energy utilization, optimized storage usage, and minimal dependence on fossil fuel energy use. To reinforce reproducibility and transparency, the energy management logic was implemented as a deterministic rule-based controller written in Python. The structure follows a fixed operational hierarchy that sequentially allocates available resources according to real-world operating priorities:

$$P_{\text{dispatch}} = \begin{cases} P_{\text{PV}} + P_{\text{WT}} - P_{\text{load}}; & \text{if } P_{\text{PV}} + P_{\text{WT}} \geq P_{\text{load}}, \\ \text{Discharge Battery} \rightarrow \text{Fuel Cell} \rightarrow \text{Diesel backup}, & \text{otherwise.} \end{cases} \tag{27}$$

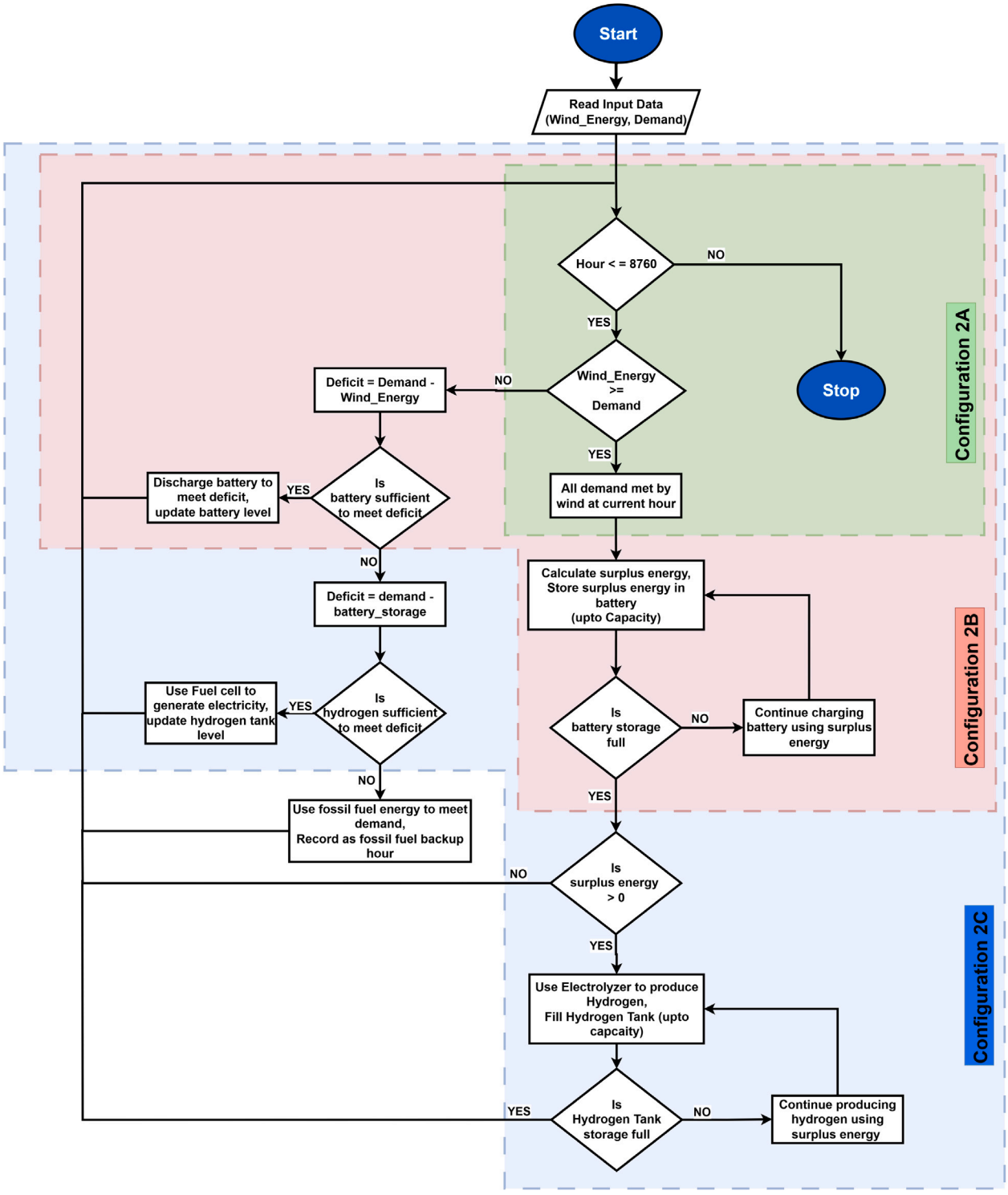

Fig. 7. Energy dispatch decision process for wind-only system scenarios. The flowchart illustrates energy allocation priorities, with dashed lines differentiating wind-only (green), wind + battery (red), and wind + battery + hydrogen (blue) configurations. (For interpretation of the references to color in this figure legend, the reader is referred to the web version of this article.)

Such rule-based schemes are widely adopted in annual techno-economic simulations where long-term energy balancing is of greater interest than short-term dispatch optimization [68,91,101]. This design choice enables full transparency of hourly energy flows while avoiding the computational overhead and data requirements associated with stochastic or model-predictive optimization. Although advanced controllers such as Mixed-integer Linear Programming (MILP) or MPC can enhance sub-hourly scheduling, their impact on aggregated yearly performance and system-level techno-economics is typically marginal. Comparative assessments in recent hybrid-system studies indicate that substituting rule-based dispatch with MILP- or GA-based optimization changes annual LCOE and LCOH by less than 3%–5% [101,102]. Hence, the adopted deterministic hierarchy introduces negligible bias while maintaining interpretability of component

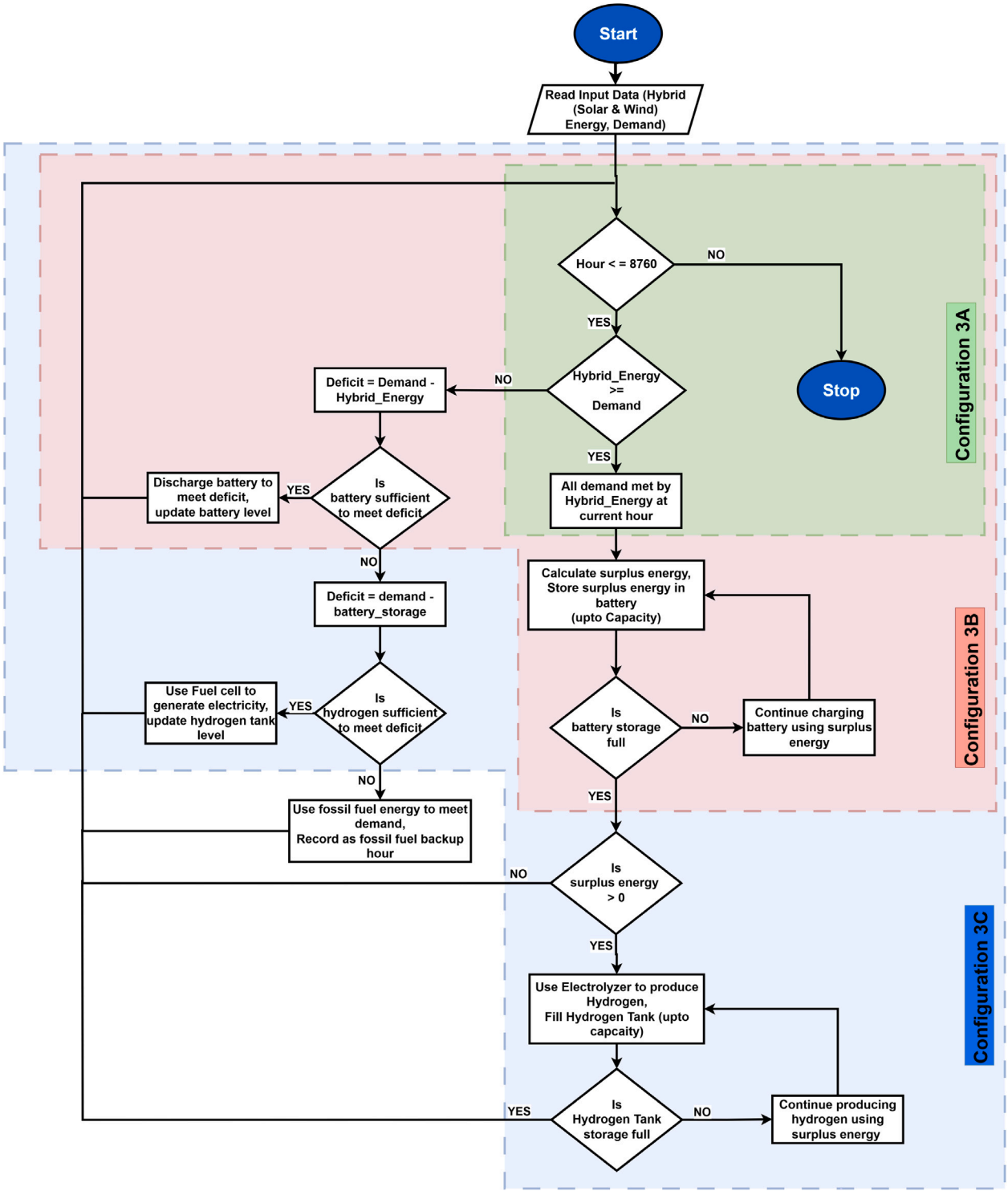

Fig. 8. Energy dispatch decision process for Hybrid (Solar & Wind) system scenarios. The flowchart illustrates energy allocation priorities, with dashed lines differentiating wind + solar (green), wind + solar + battery (red), and wind + solar + battery + hydrogen (blue) configurations. (For interpretation of the references to color in this figure legend, the reader is referred to the web version of this article.)

interactions. The selected approach therefore provides a reproducible and interpretable baseline for policy-oriented assessment of suburban energy resilience.

Furthermore, to address potential conflicting operational priorities, the dispatch controller enforces a deterministic multi-tier hierarchy that ensures mutually exclusive decision paths at each timestep. Renewable generation is first allocated to meet instantaneous demand, and any remaining surplus is routed to battery charging until the upper state-of-charge (SOC) threshold is reached. Only then is the electrolyzer activated for hydrogen production. During deficit periods, the sequence is reversed — battery discharge is prioritized within its permissible SOC window, followed by fuel-cell operation and finally diesel backup.

Because each rule is conditionally executed and bounded by physical thresholds, the controller cannot trigger simultaneous or contradictory actions. This hierarchical sequencing effectively resolves operational conflicts, protects component lifetimes, and guarantees consistent and reproducible outcomes across simulation runs.

The entire hybrid-system framework was developed by the authors in Python 3 using an object-oriented, modular architecture. It was not based on any commercial or third-party simulation software such as Hybrid Optimization of Multiple Energy Resources (HOMER) Pro [103], Transient System Simulation Program (TRNSYS) [104], or MATrix LABoratory (MATLAB) Simulink [105], but rather implemented as an in-house, rule-based computational environment purpose-built for HRES analysis. Each subsystem — including PV generation, WT, battery storage, electrolyzer, fuel cell, and diesel generator — is implemented as an independent class with editable efficiency, degradation, and cost parameters. This structure enables component-level refinement and validation without altering the overall dispatch workflow, offering full transparency and reproducibility. The present formulation reproduces representative efficiency ranges validated against manufacturer and literature data, while its modular design allows seamless substitution with higher-fidelity or experimentally calibrated models in future work. This flexibility ensures that the framework remains both computationally efficient for large-scale techno-economic studies and extensible for future integration with laboratory data or pilot-plant observations, as demonstrated in similar open-source hybrid-energy frameworks [106–108].

4. Results

This section presents a comparative analysis of nine HRES configurations designed for the Broadmeadows region. The comparison is based on four core performance metrics: (i) the percentage of electricity demand met, (ii) reliance on fossil-fuel energy sources, (iii) hours of backup fossil-fuel operation, and (iv) economic feasibility as measured by LCOE and LCOH. A scenario-based structure is adopted, aligning with the system classification introduced in Section 3.6, to evaluate the incremental impact of storage technologies. Specifically, configurations are grouped into three categories: (1) renewable systems without storage, (2) systems with battery integration, and (3) systems with both battery and hydrogen storage. This categorization enables a layered assessment of how progressively complex storage integration influences system reliability, seasonal balancing, and cost-effectiveness under real-world meteorological conditions.

To demonstrate credibility of the component models and the integrated pipeline, we performed three checks. (i) PV, wind, battery, electrolyzer, and fuel-cell blocks reproduce outputs within manufacturer and literature efficiency ranges reported in recent studies [109–112]. In our simulations, PV conversion follows a temperature-corrected performance-ratio formulation [109]; wind power curves match expected cut-in/rated/cut-out behavior for mid-scale machines [110]; battery round-trip efficiency and usable-capacity windows are consistent with contemporary community-scale deployments [111]; and electrolyzer/fuel-cell efficiencies are set to commercial PEM ranges used in recent techno-economic assessments [112]. (ii) Hourly energy-balance closure is maintained across all runs, with configuration-specific capacity factors and storage state trajectories aligning with seasonal resource availability and the validated residential load. The resilience proxy — non-renewable hours — remains $\leq$ 0.01 of annual hours for the PV–WT–battery–H_2 cases, consistent with $\geq$ 99.99% reliability targets discussed in recent hybrid-system evaluations [6,113]. (iii) The resulting cost metrics fall within published ranges: LCOE values for suburban PV–WT with storage and LCOH values for MW-scale PEM integration lie inside bands reported by recent multi-region syntheses and case studies [114–116]. Taken together, these checks indicate that the models are technically sound at component level, conserve energy at system level, and yield techno-economic outcomes aligned with current literature — supporting the credibility of conclusions drawn from the nine configurations.

The nine system configurations modeled in this study — outlined in Section 3.6 and depicted in Fig. 5 — are organized into three categories based on the RERs used and the level of storage integration. The first category includes configurations without any storage component, relying solely on solar energy, wind energy, or their combination, supplemented by fossil fuel energy to address generation shortfalls. These are represented by Configuration 1 A (Solar + fossil fuel Energy + Demand), Configuration 2 A (Wind + fossil fuel Energy + Demand), and Configuration 3 A (Solar + Wind + fossil fuel Energy + Demand). These configurations serve as the baseline for comparison, offering insights into the limitations of standalone renewable systems in meeting hourly electricity demand and managing seasonal variability without storage interventions.

The second category integrates battery storage alongside renewable energy and fossil fuel energy use, enhancing short-term energy balancing and dispatch flexibility. This category includes Configuration 1B (Solar + Battery Storage + fossil fuel Energy + Demand), Configuration 2B (Wind + Battery Storage + fossil fuel Energy + Demand), and Configuration 3B (Solar + Wind + Battery Storage + fossil fuel Energy + Demand). By incorporating BESS, these configurations improve the reliability of energy supply during intraday fluctuations, particularly during nighttime or low-generation hours. However, they remain limited in addressing extended periods of low renewable availability — particularly during winter — highlighting the need for complementary long-term storage solutions.

The third category integrates both battery and hydrogen storage, allowing for extended energy retention and increased system resilience. This includes Configuration 1C (Solar + Battery Storage + Hydrogen Storage + fossil fuel Energy + Demand), Configuration 2C (Wind + Battery Storage + Hydrogen Storage + fossil fuel Energy + Demand), and Configuration 3C (Solar + Wind + Battery Storage + Hydrogen Storage + fossil fuel Energy + Demand). These configurations enable long-term seasonal energy storage, minimizing fossil fuel energy use and ensuring year-round system sustainability.

To evaluate the economic feasibility of each configuration, the study analyzes both the LCOE and the LCOH. LCOE captures the average cost of electricity generation (AUD/kWh) over the system's lifetime, incorporating CAPEX, OPEX, and system efficiency. For configurations with hydrogen integration, LCOH (AUD/kg H_2) is used to assess the cost-effectiveness of long-term energy storage via electrolysis and reconversion. Together, these metrics enable a systematic comparison of battery-based and hydrogen-based storage strategies, highlighting trade-offs between short-term and seasonal storage solutions.

The results presented in the following sections examine renewable energy generation patterns, the impact of battery and hydrogen storage integration, and economic performance across all nine system configurations — beginning with an evaluation of how solar and wind energy align with residential demand under varying seasonal conditions.

4.1. Demand vs renewable energy generation (solar and wind)

Fig. 9 presents a comparative analysis between monthly residential electricity demand and renewable energy generation from wind and solar sources. The upper subplot displays the contribution of wind power across multiple turbine configurations, ranging from 2.1MW (1 turbine) to 10.5MW (5 turbines). The lower subplot illustrates solar generation from centralized PV systems with capacities of 1MW to 50MW, supplemented by 18.5 MW of distributed rooftop PV, representing the total solar potential in Broadmeadows.

The 9 highlights the distinct seasonal variability of solar energy, which peaks in summer and declines sharply in winter due to reduced solar irradiance and shorter daylight hours. Even with the maximum modeled capacity (50 MW + rooftop PV), solar energy alone fails to

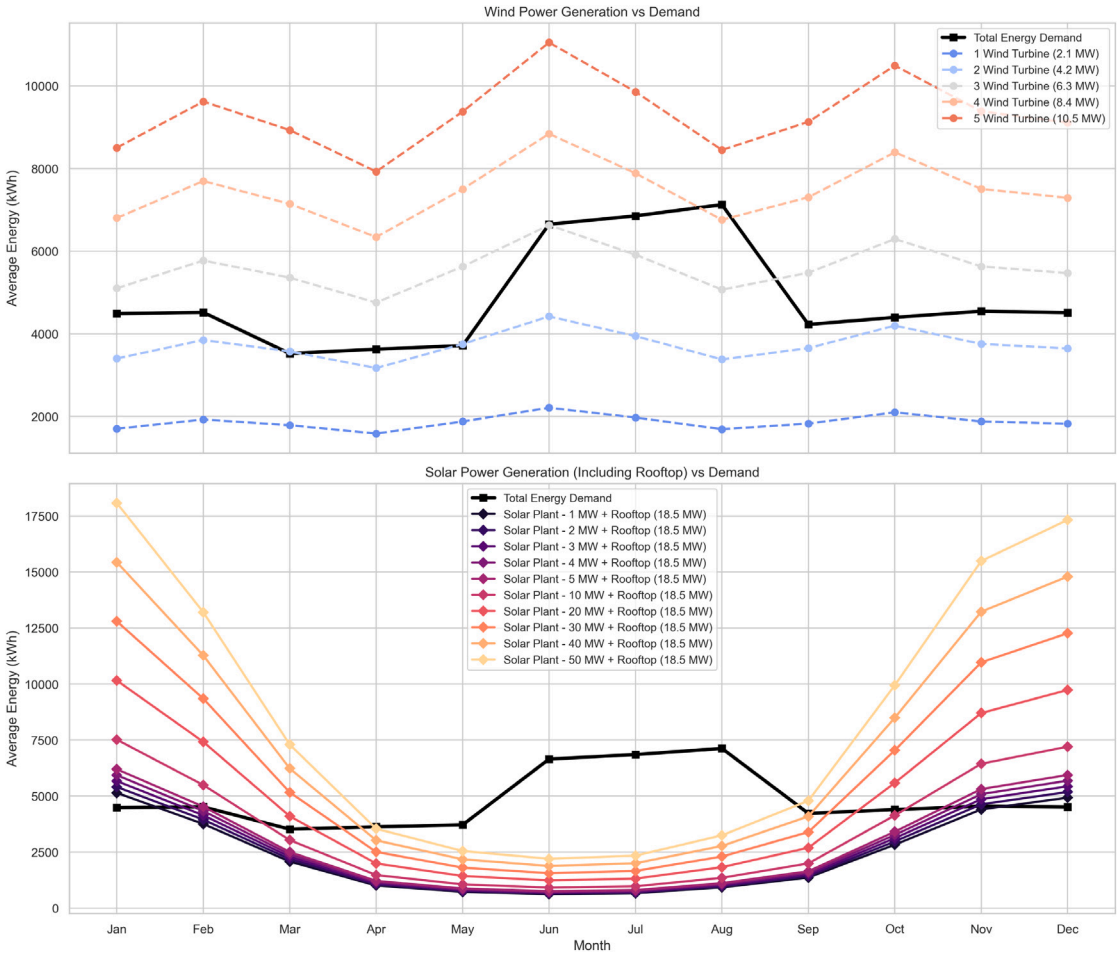

Fig. 9. Monthly comparison of wind and solar power generation against demand in Broadmeadows, Melbourne.

Table 2
Key performance metrics for solar-only, wind-only, and hybrid systems without storage.

RERs	Cases and configuration	Avg. Demand Met (%)	Avg. fossil-fuel energy use (MWh)	Fossil-fuel operation hours	LCOE
Solar	Best (50 MW)	45.71	6.00	1340	0.21
	Average (3 MW)	34.83	7.22	1730	0.25
	Worst (1 MW)	33.59	7.35	1734	0.25
Wind	Best (10.5 MW)	73.95	1.50	493	1.02
	Average (6.3 MW)	52.92	2.56	875	1.01
	Worst (2.1 MW)	3.78	6.62	2043	0.93
Hybrid (Wind + Solar)	Best (Solar 50 MW + Wind 10.5 MW)	85.04	0.83	273	0.66
	Average (Solar 3 MW + Wind 2.1 MW)	33.61	4.35	1403	0.67
	Worst (Solar 1 MW + Wind 2.1 MW)	32.25	4.42	1429	0.70

fully meet winter demand, emphasizing the limitations of solar PV as a standalone solution.

Conversely, wind generation remains comparatively stable across the year, with peak output occurring during winter months — coinciding with higher residential energy demand. In particular, 4-turbine (8.4 MW) and 5-turbine (10.5 MW) systems exhibit generation profiles that closely align with seasonal demand fluctuations, demonstrating their potential to offset fossil fuel energy use during periods of solar underperformance.

These findings highlight the seasonal complementarity between wind and solar generation in Broadmeadows. Solar power shows strong performance in summer due to high irradiance but suffers substantial output reductions in winter. In contrast, wind energy maintains relatively stable generation throughout the year, with a noticeable increase in winter — when demand is highest and solar output is lowest. This inverse seasonal behavior enables wind energy to play a critical stabilizing role by compensating for solar shortfalls, especially in high-capacity wind configurations (e.g., 8.4 MW and 10.5 MW). While solar alone is insufficient to sustain demand year-round, the integration of wind energy into the system enhances energy resilience and reduces fossil fuel energy use. A balanced solar–wind hybrid configuration, supported by battery and hydrogen storage, provides a more robust and seasonally balanced energy supply.

4.2. Performance-based selection and ranking of hybrid energy configurations

To facilitate a robust comparative analysis, this study applies a performance-based selection framework to rank all nine modeled hybrid configurations. The selection is based on four core techno-

economic indicators: (1) renewable energy contribution (% demand met), (2) fossil-fuel operation hours, (3) fossil-fuel energy use (MWh), and (4) economic feasibility (LCOE/LCOH). Each configuration is evaluated across these metrics, normalized using Min–Max scaling (Eq. (29)), and assigned a composite performance score (Eq. (30)). Based on these scores, one best-case, one worst-case, and one average-performing configuration are identified within each system category (solar-only, wind-only, and hybrid). This structured ranking methodology ensures a transparent and consistent basis for case selection and supports a meaningful assessment of technical performance, energy security, and cost-effectiveness.

These metrics are defined as follows: The first metric, the percentage of total demand met by renewable energy, indicates the degree of self-sufficiency, where higher values correspond to reduced reliance on fossil fuel. The second metric, fossil-fuel operation hours, measures system reliability, with fewer hours signifying greater energy security. The third metric, fossil-fuel energy use (MWh), reflects the magnitude of fossil generation required, with lower values indicating greater autonomy and sustainability. The final metric, economic viability, is assessed through both LCOE and LCOH to provide a comprehensive cost-effectiveness evaluation of different storage strategies. Together, these indicators offer a holistic view of system performance under realistic operating conditions.

To systematically rank system performance across multiple criteria, this study adopts a performance-based evaluation framework informed by established Multi-Criteria Decision-Making (MCDM) methodologies commonly used in HRES [117,118]. The approach aims to maximize renewable energy contribution while minimizing fossil-fuel operation hours, fossil-fuel energy use, and economic cost. This objective is mathematically structured as shown in Eq. (28):

$$\max(f_1), \quad \min(f_2, f_3, f_4) \tag{28}$$

Where:

- f_1 represents the percentage of total demand met by renewable energy; higher values indicate greater self-sufficiency and lower fossil-fuel reliance.
- f_2 corresponds to fossil-fuel operation hours, which should be minimized to enhance system reliability.
- f_3 denotes fossil-fuel energy use (MWh), where lower values indicate greater energy autonomy.
- f_4 represents the LCOE and LCOH, which should be minimized to ensure cost-effectiveness and economic viability.

Based on this framework, three representative configurations were selected from each system category, including standalone renewable systems (no storage), battery-integrated systems, and systems combining battery and hydrogen storage. Each group includes a best-performing, worst-performing, and average-performing case, determined by their composite performance scores across four normalized metrics: renewable energy contribution, fossil-fuel operation hours, fossil-fuel energy use (MWh), and economic viability (LCOE/LCOH). This classification results in a total of nine representative configurations, offering a structured basis for comparison both within and across system types. The selected cases highlight the techno-economic trade-offs associated with different storage integration levels under seasonal conditions.

Since the selected techno-economic metrics — namely percentage of demand met, fossil-fuel operation hours, fossil-fuel energy use (MWh), and LCOE/LCOH — operate on different units and optimization directions, Min–Max normalization is applied to bring all metrics onto a common scale. This allows for an unbiased comparison of system configurations. The normalization is calculated using Eq. (29):

$$N_x = \frac{x - x_{\min}}{x_{\max} - x_{\min}} \tag{29}$$

Where N_x is the normalized value for each metric x, and $x_{\min}$ and $x_{\max}$ represent the minimum and maximum values observed across all system configurations. This transformation ensures comparability by aligning metrics with varying magnitudes and optimization goals.

To generate a composite performance score for each configuration, the evaluation maximizes renewable energy contribution while minimizing fossil-fuel operation hours, fossil-fuel energy use (MWh), and economic cost (LCOE/LCOH). The final score is computed using Eq. (30):

$$N_x = \frac{x - x_{\min}}{S_i} = N_{f_1} - N_{f_2} - N_{f_3} - N_{f_4} \tag{30}$$

Where S_i denotes the overall performance score for configuration i, and the normalized terms correspond to each of the four performance metrics. A higher score reflects superior system performance across technical and economic dimensions.

This ranking approach draws on established MCDM methodologies, widely adopted in renewable energy planning to assess hybrid-system viability under conflicting objectives [119]. By applying this structured evaluation framework, the study identifies the most and least effective configurations in terms of energy sufficiency, reliability, and affordability.

The following sections present a detailed evaluation of these representative cases, examining their seasonal energy sufficiency, fossil-fuel operation hours, fossil-fuel energy use (MWh), and overall techno-economic feasibility to identify the most viable hybrid renewable energy system configurations.

4.3. Performance analysis of solar and wind only systems without storage

This section analyzes the performance of solar-only, wind-only, and hybrid solar–wind configurations without energy storage. The analysis covers energy sufficiency, fossil-fuel operation hours, fossil-fuel energy use (MWh), and economic feasibility. Capacities ranging from 1 MW to 50 MW for solar and 2.1 MW and 10.5 MW for wind, enabling comparison across different deployment scales.

A key challenge for systems without storage is their seasonal variability. Which directly affects their ability to maintain a stable energy supply. Solar generation peaks in summer due to higher irradiance, whereas wind generation is typically stronger in winter, tracking regional circulation patterns. These seasonal dynamics indicate that hybrid solar–wind systems can improve overall energy resilience.

4.3.1. Energy sufficiency of solar and wind only systems without storage

The ability of a system to meet energy demand is strongly influenced by fluctuations in solar radiation and wind speeds. Solar PV generation performs well in summer but experiences a substantial decline in winter due to shorter daylight hours and cloud cover.

Table 2 summarizes the average percentage of demand met across system configurations. The best-case solar-only system (50 MW) meets 45.71% of demand, while the worst-case (1 MW) meets only 33.59%, illustrating the limitations of small-scale solar deployments. The average-case (3 MW solar) achieves 34.83%, further highlighting that even medium-scale solar installations cannot ensure year-round sufficiency.

Wind-only systems generally exhibit higher energy sufficiency than solar, particularly in winter. The best-case wind-only system (10.5 MW) meets 73.97% of demand, while the worst-case wind system (2.1 MW) covers only 3.78%, demonstrating that small wind deployments are insufficient for standalone operation. The average-case wind system (6.3 MW) meets 52.92% of demand, reinforcing the advantage of wind energy in maintaining more consistent year-round output.

Hybrid solar–wind systems significantly enhance energy sufficiency, leveraging the complementary seasonal availability of both resources. The best-case hybrid system (50 MW solar + 10.5 MW wind) achieves 85.04% demand met, outperforming standalone solar and wind configurations. Even the worst-case hybrid configuration (1 MW solar + 2.1 MW wind) meets 32.25% of demand, providing improved seasonal stability compared to standalone solar. Fig. 10 (Top-Left Panel) visualizes these trends.

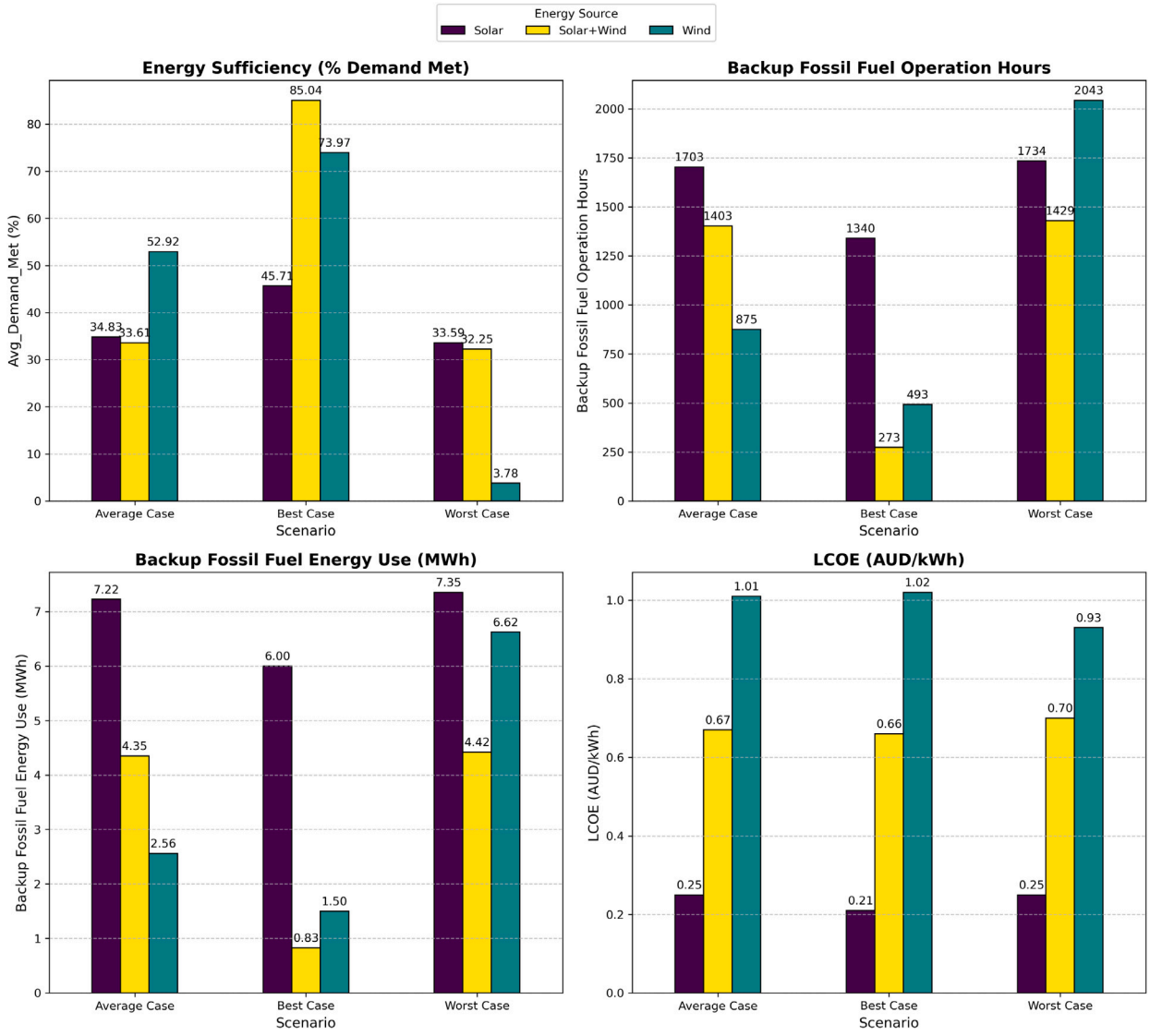

Category	Solar	Wind	Solar+Wind
Best Case	Solar Plant 50MW	Wind Plant 10.5MW	Solar 50MW + Wind 10.5MW
Worst Case	Solar Plant 1MW	Wind Plant 2.1MW	Solar 1MW + Wind 2.1MW
Average Case	Solar Plant 3MW	Wind Plant 6.3MW	Solar 3MW + Wind 2.1MW

Fig. 10. Comparative performance of renewable-only configurations (solar, wind, and hybrid) across best, average, and worst cases.

4.3.2. Fossil fuel energy use (MWh)

Despite their renewable nature, solar-only and wind-only systems remain partially dependent on fossil fuel energy because of intermittency and seasonal variability. Table 2 presents the fossil fuel energy use across different system configurations.

Solar-only systems exhibit the highest usage of fossil fuel energy, particularly in winter. In the worst case (1 MW), fossil fuel energy reaches 7.35 MWh; even the best case (50 MW) still requires 6.00 MWh.

Wind-only systems generally need less fossil fuel energy, aided by stronger winter winds. limits use to 1.50 MWh. By contrast, the worst case (2.1 MW) still draws 6.62 MWh from fossil fuel energy.

Hybrid solar–wind configurations exhibit the lowest fossil fuel energy use, leveraging the seasonal complementarity of both resources. The best-case hybrid system (50 MW solar + 10.5 MW wind) requires only 0.83 MWh of fossil fuel energy, significantly lower than either resource alone. Even in the worst-case hybrid configuration (1 MW solar + 2.1 MW wind), uses 4.42 MWh of fossil fuel energy, still below the standalone systems. Fig. 14 (Bottom-Left Panel) illustrates these trends.

4.3.3. Fossil fuel operation hours analysis

Fossil fuel operation hours indicate the duration when renewable generation is insufficient to meet demand, requiring either storage solutions or fossil fuel energy as backup. Table 2 presents a comparative analysis of fossil fuel operation hours across different system configurations.

Solar-only systems shows frequent fossil fuel operation hours, particularly during winter. The worst-case solar-only configuration (1 MW solar) results in 1734 fossil fuel operation hours per year. while the best-case (50 MW solar) still faces 1340 hours — highlighting the inability of solar PV to ensure continuous supply due to limited winter irradiance and daily variability.

Wind-only systems demonstrate relatively better performance, as shown in Table 2, with the best-case wind system (10.5 MW) reducing fossil fuel energy hours to 493 — nearly three times fewer than the best solar-only case. The average-case wind system (6.3 MW) still limits fossil fuel operation to 875 h, outperforming solar systems of similar capacity. This advantage is primarily due to more consistent wind resources during winter, when solar output drops sharply.

Table 3
Key performance metrics for solar–battery, wind–battery, and hybrid (solar–wind–battery) systems across different scales.

RERs	Cases and configuration	Avg Demand Met (%)	Avg fossil fuel energy use (MWh)	Fossil fuel operation hours	LCOE
Solar + Battery	Best (50 MW)	75.76	3.16	622	0.39
	Average (10 MW)	57.14	5.07	1108	0.68
	Worst (1 MW)	45.39	6.22	1436	0.89
Wind + Battery	Best (10.5 MW)	98.66	0.20	42	1.35
	Average (4.2 MW)	74.35	3.03	875	1.79
	Worst (2.1 MW)	39.94	6.57	1993	2.37
Hybrid (Wind + Solar) + Battery	Best (Solar 50 MW + Wind 10.5 MW)	99.89	0.015	5	2.32
	Average (Solar 3 MW + Wind 2.1 MW)	76.12	3.04	819	6.52
	Worst (Solar 1 MW + Wind 2.1 MW)	75.07	3.14	852	6.77

Hybrid solar–wind systems achieve the lowest fossil fuel operation hours, benefiting from seasonal complementarity. The best-case hybrid system (50 MW solar + 10.5 MW wind) operates on fossil fuel for just 273 hours — a 79% improvement compared to the best solar-only system. Even the worst-case hybrid setup (1 MW solar + 2.1 MW wind) records 1429 h, which is still lower than the standalone solar and wind alternatives. These results are illustrated in Fig. 10 (Top-Right Panel).

4.3.4. Cost analysis (Levelized cost of energy trends)

The LCOE is a central economic indicator, representing the average cost per kilowatt-hour of electricity generated over a system's lifetime. It incorporates CAPEX, O&M expenses, and total energy production. Table 2 summarizes the LCOE results for the solar-only, wind-only, and hybrid solar–wind configurations evaluated in this study.

Among the three system types, solar-only configurations exhibit the lowest LCOE, ranging from 0.21 AUD/kWh in the best case (50 MW solar) to 0.25 AUD/kWh in the worst case (1 MW solar). However, despite favorable cost metrics, these systems suffer from high *fossil fuel operation hours* and elevated *fossil fuel energy use*, especially during winter, which limits their overall viability as standalone solutions.

Wind-only configurations show higher LCOE values, ranging from 1.02 AUD/kWh (best case, 10.5 MW wind) to 0.93 AUD/kWh (worst case, 2.1 MW wind). This cost premium is largely attributed to the higher capital and O&M costs associated with WT infrastructure. Nevertheless, wind systems provide stronger seasonal consistency — particularly in winter — which enhances reliability even in the absence of storage.

Hybrid solar–wind systems demonstrate the most balanced trade-off between cost and performance. The best-case hybrid system (50 MW solar + 10.5 MW wind) achieves a competitive LCOE of 0.66 AUD/kWh, while the worst case (1 MW solar + 2.1 MW wind) reaches 0.70 AUD/kWh. Though these values are slightly higher than standalone solar, the significant reduction in fossil fuel operation hours and fossil fuel energy use is notable. This improvement makes hybrid systems the most economically and operationally resilient renewable-only option.

These trends — summarized in Table 2 and illustrated in Fig. 10 (Bottom-Right Panel) — highlight the economic and operational advantages of hybridization in delivering cost-effective and reliable renewable energy supply under varying seasonal conditions.

The comparative analysis covers solar-only, wind-only, and hybrid solar–wind configurations across best, average, and worst cases. It evaluates energy sufficiency, fossil fuel operation hours, fossil fuel energy use, and LCOE. The figure shows how, without storage, resource composition directly influences system reliability and economic viability at different capacity scales.

4.4. Performance analysis of battery-integrated systems

Integrating battery storage into renewable-based configurations enhances system reliability, reduces fossil fuel operation hours, and limits fossil fuel energy use. In this study, we evaluate solar–battery, wind–battery, and hybrid solar–wind–battery systems at multiple scales, assessing the extent to which short-term storage can improve energy sufficiency and operational stability.

4.4.1. Energy sufficiency of battery-integrated systems

Battery storage increases the proportion of demand met directly using renewable sources by capturing excess generation during peak output periods and discharging it when renewable supply falls short. This mechanism is particularly valuable during night-time or cloudy for solar systems and in periods of reduced wind speed for wind-based systems.

Table 3 summarizes the percentage of demand met across different battery-integrated configurations. solar–battery systems show substantial improvements over standalone solar setups. The best-case solar–battery system (50MW solar + battery) meets 75.76% of demand, while the worst-case (1MW solar + battery) covers 45.39%. The average-case (10MW solar + battery) achieves 57.14%, demonstrating moderate improvements in reliability.

Wind–battery systems generally achieve higher demand coverage than solar–battery systems, especially at larger capacities. The best-case wind–battery system (10.5MW wind + battery) meets 98.66% of demand, indicating near-complete renewable coverage. While the worst-case configuration (2.1MW wind + battery) meets 39.94% of demand, highlighting the dependence on adequate wind resource availability.

Hybrid solar–wind–battery configurations outperform all other setups by leveraging the seasonal complementarity of solar and wind energy. The best-case hybrid system (50MW solar + 10.5MW wind + battery) meets 99.89% of demand. While even the worst-case configuration (1MW solar + 2.1MW wind + battery) achieves 75.07%. Fig. 12 illustrates these results, showing that integrating battery storage with diverse renewable inputs can bring fossil fuel operation hours to negligible levels while simultaneously reducing fossil fuel energy use across the system.

4.4.2. Fossil fuel energy reliance in battery-integrated systems

Battery storage reduces dependence on fossil fuel energy by allowing excess renewable generation to be stored and dispatched during periods of low solar or wind availability. Table 3 summarizes the fossil fuel energy use for different battery-integrated configurations.

Solar–battery systems still require a moderate contribution from fossil fuel sources, with values ranging from 3.16 MWh in the best case (50 MW solar + battery) to 6.22 MWh in the worst case (1 MW solar + battery). These figures reflect the seasonal intermittency of solar power, particularly in winter months when generation is low.

wind–battery systems achieve lower fossil fuel energy use than solar–battery systems, particularly at higher wind capacities. In the best-case configuration (10.5MW wind + battery), fossil fuel input drops to just 0.20 MWh. This improvement is largely attributable to stronger wind resources during winter, which better align with seasonal demand patterns. However, in low-capacity setups (2.1MW), fossil

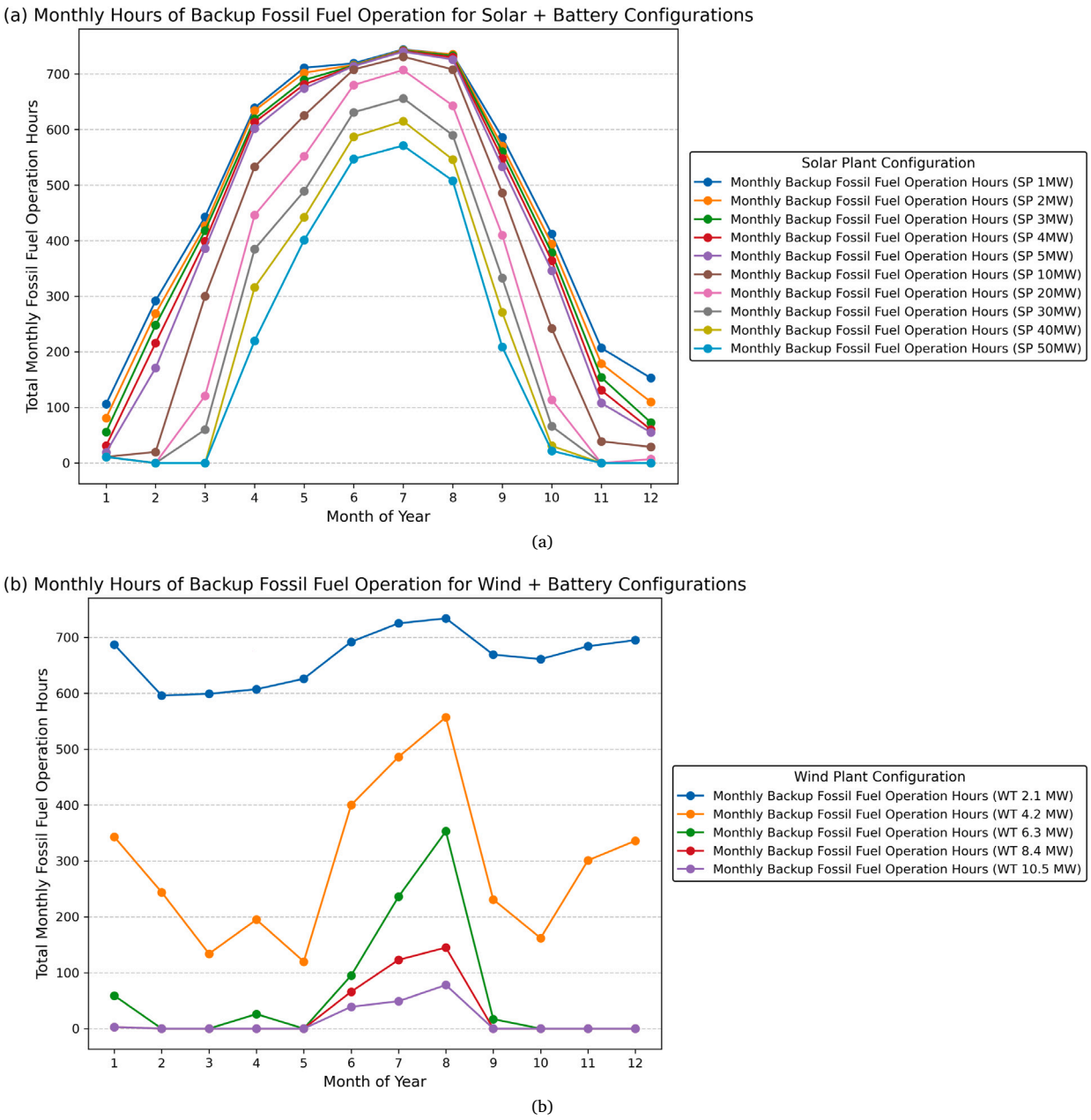

Fig. 11. Monthly fossil-fuel operation hours for (a) solar–battery and (b) wind–battery configurations, showing seasonal variation in fossil-fuel dependence across system capacities.

fuel reliance remains relatively high at 6.57 MWh, underscoring the limitations of undersized wind systems even with battery support.

Hybrid solar–wind–battery configurations achieve the lowest dependence on fossil fuels across all scenarios. The best-case system (50MW solar + 10.5MW wind + battery) requires only 0.015 MWh of fossil fuel energy backup, effectively achieving near-complete energy autonomy. Even in the worst-case (1 MW solar + 2.1 MW wind + battery), usage drops to 3.14 MWh — significantly lower than in solar- or wind-only systems. This outcome highlights the advantage of resource complementarity when combined with short-term storage.

4.4.3. Fossil fuel operation hours analysis of battery-integrated systems

Battery integration reduces fossil fuel operation hours across all system configurations by ensuring stored energy is available during renewable generation shortfalls.

Table 3 presents fossil fuel operation hours for different battery-integrated configurations. solar–battery systems still experience moderate reliance on fossil fuel backup, with the worst-case solar–battery system (1 MW solar + battery) recording 1436 fossil fuel operation hours. In contrast, the best-case configuration (50 MW solar + battery) significantly cuts this figure to 622 h.

wind–battery systems perform better than solar–battery systems in limiting fossil fuel operation hours. The best-case wind–battery system (10.5 MW wind + battery) requires just 42 h of fossil fuel operation annually, reflecting high reliability. However, the worst-case wind–battery configuration (2.1 MW wind + battery) still records 1993 h, indicating that smaller-scale wind–battery setups remain vulnerable to intermittency.

Hybrid solar–wind–battery systems achieve the lowest fossil fuel operation hours, thereby further improving system reliability. The

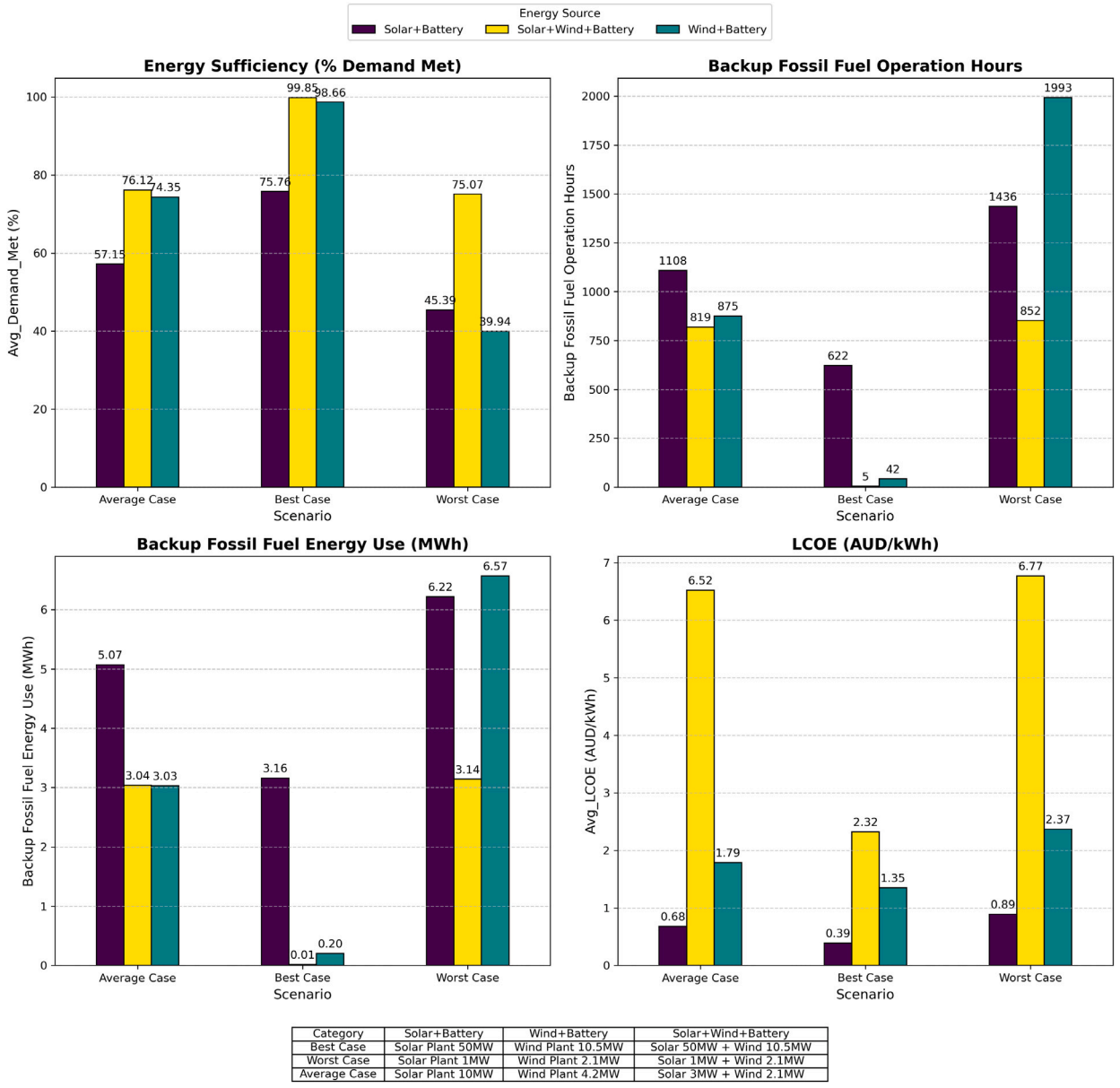

Category	Solar+Battery	Wind+Battery	Solar+Wind+Battery
Best Case	Solar Plant 50MW	Wind Plant 10.5MW	Solar 50MW + Wind 10.5MW
Worst Case	Solar Plant 1MW	Wind Plant 2.1MW	Solar 1MW + Wind 2.1MW
Average Case	Solar Plant 10MW	Wind Plant 4.2MW	Solar 3MW + Wind 2.1MW

Fig. 12. Comparative performance of battery-integrated configurations — solar–battery, wind–battery, and hybrid (solar–wind–battery) — across best, average, and worst cases.

best-case hybrid system (50 MW solar + 10.5 MW wind + battery) reduces fossil fuel operation to only 5 h per year, while the worst-case hybrid system (1 MW solar + 2.1 MW wind + battery) still limits it to 852 h. The distribution of fossil fuel operation hours across different system scales is illustrated in Fig. 11.

4.4.4. Cost analysis of battery-integrated systems

The integration of battery storage leads to an increase in overall LCOE as a result of additional capital investment and operational costs. Nonetheless, this rise in cost is often justified by the significant improvements in fossil fuel operation hour reduction, enhanced energy independence, and greater system reliability. Table 3 summarizes LCOE values for different battery-integrated configurations.

Among the three system types, solar–battery configurations maintain the lowest LCOE values, ranging from 0.39 AUD/kWh in the best-case (50MW solar + battery) to 0.89 AUD/kWh in the worst-case (1MW solar + battery). While these values are higher than those of standalone solar systems. This cost increase is balanced by improved reliability and reduced reliance on fossil fuel energy use.

wind–battery systems generally show higher LCOE values than solar-based systems. The lowest observed is 1.35 AUD/kWh for a 10.5 MW wind plus battery setup, whereas the highest is 2.37 AUD/kWh for a 2.1 MW configuration. This reflects the higher capital and maintenance costs of wind turbines, amplified by the expense of storage integration.

Hybrid solar–wind–battery systems report the highest LCOE values. This is due to the combined infrastructure costs of two renewable sources and large-scale storage. In the best-case hybrid configuration (50MW solar + 10.5MW wind + battery), the LCOE of 2.32 AUD/kWh. while in the worst-case configuration (1MW solar + 2.1MW wind + battery) reaches 6.77 AUD/kWh.

Although integrating batteries increases generation costs, these systems deliver strong operational resilience, meet demand more consistently, and significantly reduce fossil fuel operation hours. Fig. 12

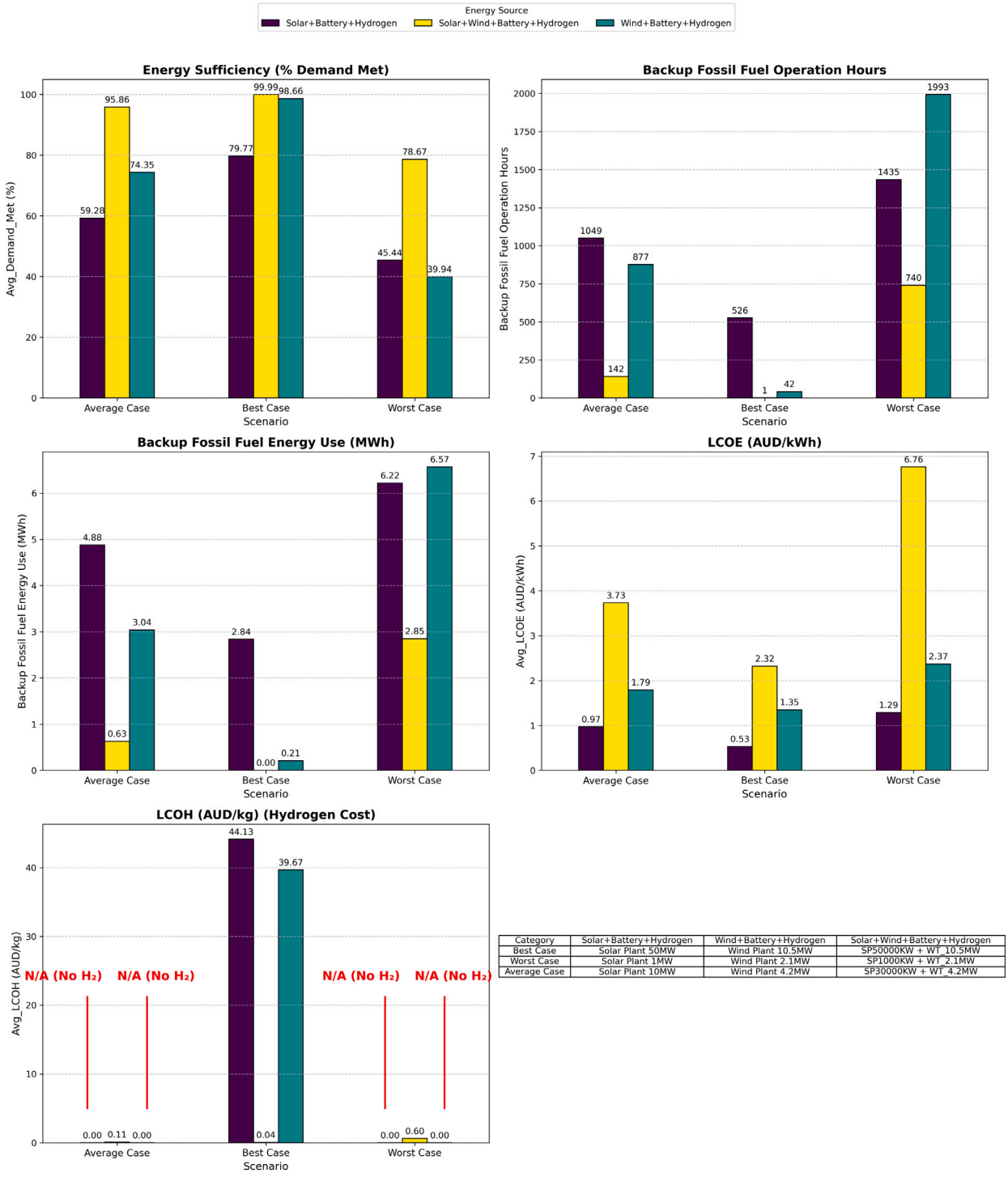

Category	Solar+Battery+Hydrogen	Wind+Battery+Hydrogen	Solar+Wind+Battery+Hydrogen
Best Case	Solar Plant 50MW	Wind Plant 10.5MW	SP50000KW + WT_10.5MW
Worst Case	Solar Plant 1MW	Wind Plant 2.1MW	SP1000KW + WT_2.1MW
Average Case	Solar Plant 10MW	Wind Plant 4.2MW	SP30000KW + WT_4.2MW

Fig. 13. Comparative performance of hydrogen-integrated configurations — solar–battery–hydrogen, wind–battery–hydrogen, and hybrid (solar–wind–battery–hydrogen) — across best, average, and worst cases.

presents the cost–performance trade-off, illustrating how battery storage supports long-term sustainability despite higher initial costs.

4.5. Performance analysis of hydrogen-integrated systems

Incorporating hydrogen storage alongside battery storage within solar, wind, and HRES configurations strengthens system resilience, particularly against seasonal intermittencies. This integration also reduces fossil fuel energy use by enabling surplus renewable generation to be stored and dispatched during periods of low energy production. The following analysis evaluates solar–battery–hydrogen, wind–battery–hydrogen, and hybrid solar–wind–battery–hydrogen configurations across multiple system scales.

4.5.1. Energy sufficiency of hydrogen-integrated systems

Hydrogen storage plays a critical role in enhancing long-term energy sufficiency. Large-scale hybrid systems particularly benefit, as excess renewable energy can be converted to hydrogen, stored for extended periods, and later reconverted to electricity when needed.

Table 4
Key performance metrics for solar–battery–hydrogen, wind–battery–hydrogen, and hybrid (solar–wind–battery–hydrogen) systems across different scales.

RERs	Cases and configuration	Avg Demand Met (%)	Avg fossil fuel energy use (MWh)	Fossil fuel operation Hours	LCOE	LCOH
Solar + Battery + Hydrogen	Best (50 MW)	79.77	2.84	526	0.53	44.13
	Average (10 MW)	59.28	4.88	1049	0.97	∞
	Worst (1 MW)	45.44	6.22	1435	1.29	∞
Wind + Battery + Hydrogen	Best (10.5 MW)	98.66	0.21	42	1.35	39.67
	Average (4.2 MW)	74.35	3.04	877	1.79	∞
	Worst (2.1 MW)	39.94	6.57	1993	2.37	∞
Hybrid (Wind + Solar) + Battery + Hydrogen	Best (Solar 50 MW + Wind 10.5 MW)	99.99	0.0007	1	2.32	0.04
	Average (Solar 3 MW + Wind 2.1 MW)	78.67	0.63	142	3.73	0.11
	Worst (Solar 1 MW + Wind 2.1 MW)	95.86	2.85	740	6.76	0.60

Table 4 presents the percentage of demand met by various hydrogen-integrated configurations. For solar–battery–hydrogen systems, the improvement over battery-only setups is evident but moderate. In the best-case (50 MW solar + battery + hydrogen), 79.77% of demand is met. The worst case (1 MW solar + battery + hydrogen) still covers 45.44% of demand, while the average-case (10 MW solar + battery + hydrogen) achieves 59.28%, indicating incremental gains in energy security with system scale.

Wind–battery–hydrogen systems achieve higher energy sufficiency than solar–hydrogen systems, given the more stable nature of wind energy. The best-case wind–hydrogen system (10.5 MW wind + battery + hydrogen) meets 98.66% of demand, while the worst-case (2.1 MW wind + battery + hydrogen) meets 39.94%. These results underscore the importance of adequate wind capacity for reliable operation.

Hybrid solar–wind–battery–hydrogen systems deliver the highest energy sufficiency, benefiting from the seasonal complementarity of solar and wind resources. The best-case hybrid configuration (50 MW solar + 10.5 MW wind + battery + hydrogen) meets nearly all demand at 99.99%, whereas even the worst case (1 MW solar + 2.1 MW wind + battery + hydrogen) reaches 78.67%. This performance clearly surpasses that of single-source hydrogen-integrated systems. Fig. 13 illustrates these comparative trends.

The relatively higher LCOE observed for hydrogen-integrated configurations arises from two contributing factors. First, the hydrogen chain — including the electrolyzer, compressor, storage tank, and fuel cell — adds capital cost and introduces conversion losses of roughly 40%–45%, reducing net electrical output. Second, the diesel generator retained for reliability support operates during fewer than 0.5% of annual hours. Its fixed standby and maintenance costs are therefore distributed over very limited output, which inflates the levelised cost per kWh even though actual fossil-fuel use remains negligible.

4.5.2. Fossil fuel energy use in hydrogen-integrated systems

Adding hydrogen storage further reduces fossil fuel energy use by enabling seasonal energy shifting and long-term storage.

Table 4 presents the fossil fuel energy use across all system configurations. Solar–hydrogen systems still require partial fossil fuel energy backup, particularly at smaller scales. The worst-case solar–hydrogen system (1 MW solar + battery + hydrogen) requires 6.22 MWh of fossil fuel energy. While the best-case system (50 MW solar + battery + hydrogen) uses only 2.84 MWh.

wind–hydrogen systems perform better than solar–hydrogen systems by reducing reliance on fossil fuel energy. The best-case wind–hydrogen (10.5 MW wind + battery + hydrogen) achieves near-complete renewable sufficiency, using just 0.21 MWh of fossil fuel energy. While the worst-case system (2.1 MW wind + battery + hydrogen) still requires 6.57 MWh.

Hybrid solar–wind–battery–hydrogen systems achieve the lowest fossil fuel energy dependence, strengthening the long-term energy security. The best-case hybrid system (50 MW solar + 10.5 MW wind + battery + hydrogen) uses only 0.0007 MWh, indicating almost complete independence. Even the worst-case hybrid (1 MW solar + 2.1 MW wind + battery + hydrogen) needs just 2.85 MWh, showing a clear improvement over standalone solar or wind systems.

4.5.3. Fossil fuel operation hours analysis in hydrogen-integrated systems

Hydrogen storage plays a critical role in reducing fossil fuel operation hours by ensuring long-term energy availability when solar, wind, and battery reserves are insufficient. Table 4 presents the fossil fuel operation hours recorded across different hydrogen-integrated system configurations.

In solar–hydrogen systems, the reliance on fossil fuel remains significant in smaller-scale deployments. The worst-case (1 MW solar + battery + hydrogen) records 1435 h of fossil fuel operation annually, whereas the best-case (50 MW solar + battery + hydrogen) reduces this to 526 h.

Wind–hydrogen systems demonstrate stronger performance in minimizing fossil fuel use. The best-case wind–hydrogen (10.5 MW wind + battery + hydrogen) requires only 42 fossil fuel operation hours per year, reflecting high reliability, while the worst-case (2.1 MW wind + battery + hydrogen) still accumulates 1993 h.

Hybrid solar–wind–battery–hydrogen systems achieve the lowest fossil fuel operation times, providing the highest level of energy security. The best-case hybrid (50 MW solar + 10.5 MW wind + battery + hydrogen) limits fossil fuel operation to just 1 h annually. Even the worst-case hybrid (1 MW solar + 2.1 MW wind + battery + hydrogen) operates on fossil fuels for 740 hours — still a substantial improvement over single-source hydrogen-based designs. Fig. 13 illustrates the variation in fossil fuel operation hours across system scales.

4.5.4. Cost analysis (levelized cost of energy and hydrogen trends)

The integration of hydrogen storage inevitably increases both capital and operational expenditure, which in turn influences the LCOE and LCOH profiles of the systems. Fig. 13 summarizes the observed cost patterns across the range of configurations assessed.

4.5.4.1. Levelized cost of energy trends. The LCOE of solar–hydrogen systems is the lowest among the analyzed configurations, ranging from 0.53 AUD/kWh for the best-case (50 MW solar + battery + hydrogen) to 1.29 AUD/kWh for the worst-case (1 MW solar + battery + hydrogen). This cost advantage is primarily attributed to the lower capital costs of PV installations. However, seasonal intermittency limits their standalone viability, leading to higher LCOH values in cases with limited surplus energy for hydrogen production.

In comparison, wind–hydrogen systems exhibit higher LCOE values, ranging from 1.35 AUD/kWh in best-case (10.5 MW wind + battery + hydrogen) to 2.37 AUD/kWh in worst case (2.1 MW wind + battery + hydrogen). These higher costs stem from the capital-intensive nature of WT installations and the variability in wind energy availability. Which affects energy storage and conversion efficiency. Despite the cost challenges, wind-based hydrogen production remains more stable throughout the year compared to solar standalone systems.

Hybrid solar–wind–hydrogen systems records the highest LCOE across all configurations, ranging from 2.32 AUD/kWh in the best-case (50 MW solar + 10.5 MW wind + battery + hydrogen) to 6.76 AUD/kWh in the worst-case (1 MW solar + 2.1 MW wind + battery + hydrogen). The increased cost is attributed to the additional infrastructure required for integrating multiple renewable sources and hydrogen storage. However, such systems also deliver the greatest energy sufficiency, with minimal fossil fuel operation hours and negligible fossil fuel energy use. Which reinforces their suitability for long-term, low-carbon energy security despite the higher capital investment.

4.5.4.2. Levelized cost of hydrogen trends. Standalone solar and wind–hydrogen systems exhibit high LCOH values (44.13 AUD/kg for solar–hydrogen, 39.67 AUD/kg for wind–hydrogen), making them economically less viable. These high costs arise from inconsistent hydrogen generation and limited surplus energy.

Hybrid solar–wind–hydrogen systems achieve the lowest LCOH values, ranging from 0.04 AUD/kg (best case) to 0.60 AUD/kg (worst case), demonstrating superior cost-effectiveness. These configurations maximize hydrogen production through a more balanced renewable energy supply, ensuring lower hydrogen production costs and better long-term feasibility.

For configurations where no hydrogen is produced, LCOH is not applicable (N/A) since hydrogen production is zero. As LCOH is calculated as the total cost divided by the annual hydrogen production, when no hydrogen is generated, the denominator becomes zero, making the cost per unit of hydrogen undefined. This underscores the necessity of maintaining sufficient surplus renewable energy to sustain electrolysis and ensure economic feasibility.

4.6. Sensitivity analysis

A detailed sensitivity analysis was conducted to evaluate how component sizing influences the techno-economic performance of the HRES. Variations in solar PV capacity, WT number, battery storage, and hydrogen storage were analyzed under identical meteorological and demand conditions. Each configuration was simulated through the integrated dispatch model, and two primary economic indicators were assessed: the LCOE and the LCOH. This analysis identifies the cost-optimal balance between generation and storage capacities for each subsystem combination.

4.6.1. Hybrid solar–wind–battery–hydrogen system

The hybrid configuration integrating solar, wind, battery, and hydrogen subsystems was analyzed to quantify the sensitivity of the overall techno-economic performance to generation scaling. A total of fifty distinct scenarios (C_1–C_{50}) were simulated by varying the solar-farm capacity from 1 MW to 50 MW and the number of WTs from one to five, while maintaining constant battery and hydrogen storage parameters. The results reveal a consistent downward trend in both LCOE and LCOH as renewable generation capacity increases, demonstrating the system's strong dependence on combined resource scaling.

At smaller capacities (1–5 MW solar with 1–2 WTs), the system experiences frequent shortfalls and high energy costs, with LCOE values exceeding 4 AUD kWh^{-1}. This behavior reflects the heavy reliance on the hydrogen pathway and limited renewable surplus available for electrolyzer operation during periods of low generation. As solar capacity increases to 20–30 MW and the turbine count exceeds three, renewable utilization improves significantly, resulting in stable electrolyzer operation, reduced curtailment, and lower battery cycling stress. Within this mid-range regime, the combined cost metrics converge toward LCOE = 2.35 AUD kWh^{-1} and LCOH = 0.048 AUD $kg_{H_2}^{-1}$, highlighting the emergence of a cost-saturation zone where further capacity additions yield minimal marginal benefits.

Fig. 14 illustrates the sensitivity of LCOE and LCOH to solar-farm capacity. A sharp decline is observed up to approximately 30 MW, beyond which both curves flatten, indicating diminishing economic returns. Similarly, Fig. 15 highlights the role of wind scaling, where increasing the turbine count from one to five reduces LCOE by nearly 65% and produces a corresponding decline in hydrogen cost. This trend arises from the complementary temporal characteristics of the two renewable sources: daytime solar generation stabilizes daytime demand, while wind provides nocturnal supply continuity. Together, these effects enhance electrolyzer utilization and reduce the system's dependence on stored hydrogen and diesel backup.

Seasonal simulation results further confirm the robustness of the hybrid configuration. The system maintains a demand–satisfaction ratio above 99% across all seasons, with minor shortfalls confined to winter months. Battery storage supports intra-day balancing, while hydrogen storage ensures inter-seasonal continuity. Overall, the hybrid solar–wind–battery–hydrogen system demonstrates superior cost performance, energy resilience, and operational stability compared with single-source variants. The configuration comprising a 30 MW solar farm and five wind turbines emerges as the optimal techno-economic solution for the Broadmeadows case study, achieving a balanced trade-off between capital cost, reliability, and renewable energy penetration.

4.6.2. Solar–battery–hydrogen system

The solar–battery–hydrogen configuration was evaluated to assess how variations in PV generation capacity affect the system's techno-economic performance. Table 5 summarizes ten configurations (S_1–S_{10}) with solar-farm capacities ranging from 1 MW to 50 MW, while maintaining constant storage capacities and demand conditions. The results indicate a strong inverse relationship between solar capacity and cost, with both LCOE and LCOH declining as PV generation increases.

At the smallest capacity (S_1), hydrogen production was not achieved due to insufficient renewable surplus to sustain electrolyzer operation; therefore, LCOH is undefined and reported as "N/A" in Table 5. For graphical continuity in Fig. 16, this point is plotted as zero. Once the system scales beyond 2 MW, hydrogen generation commences, initially at very high cost levels (e.g., 87,373 AUD $kg_{H_2}^{-1}$ for S_2) due to low electrolyzer utilization and intermittent operation. As solar capacity increases further, the system transitions into a surplus-driven regime, significantly lowering both LCOE and LCOH. Beyond 30 MW, both metrics stabilize, indicating a cost-saturation region where additional PV expansion yields minimal marginal benefit.

Fig. 16 clearly illustrates this behavior. The LCOE curve shows a steep decline up to around 10 MW, reflecting the rapid improvement in system efficiency as solar availability increases. Beyond this point, the curve flattens, marking diminishing returns. The LCOH profile exhibits an exponential decay from extreme initial values to approximately 44 AUD $kg_{H_2}^{-1}$ at 50 MW, indicating enhanced electrolyzer utilization and stable hydrogen production. Overall, the solar–battery–hydrogen configuration demonstrates strong economies of scale, with the techno-economic optimum achieved at higher solar capacities where both cost and reliability converge.

4.6.3. Wind–battery–hydrogen system

The sensitivity of the wind–battery–hydrogen configuration was evaluated by varying the number of WTs from one to five while maintaining fixed battery and hydrogen storage capacities. Table 6 summarizes the techno-economic results for configurations W_1–W_5. A clear downward trend is observed in LCOE with increasing wind capacity, illustrating the cost benefit of greater renewable generation.

For configurations W_1 and W_2, hydrogen production was not initiated due to insufficient renewable surplus to activate the electrolyzer; consequently, LCOH is undefined and reported as "N/A" in Table 6. To preserve graphical continuity in Fig. 17, these cases are shown with a nominal value of zero. Once the system reaches three or more turbines, hydrogen generation becomes feasible, and LCOH declines sharply from approximately 269 AUD $kg_{H_2}^{-1}$ at W_3 to around 40 AUD $kg_{H_2}^{-1}$ at W_5. In

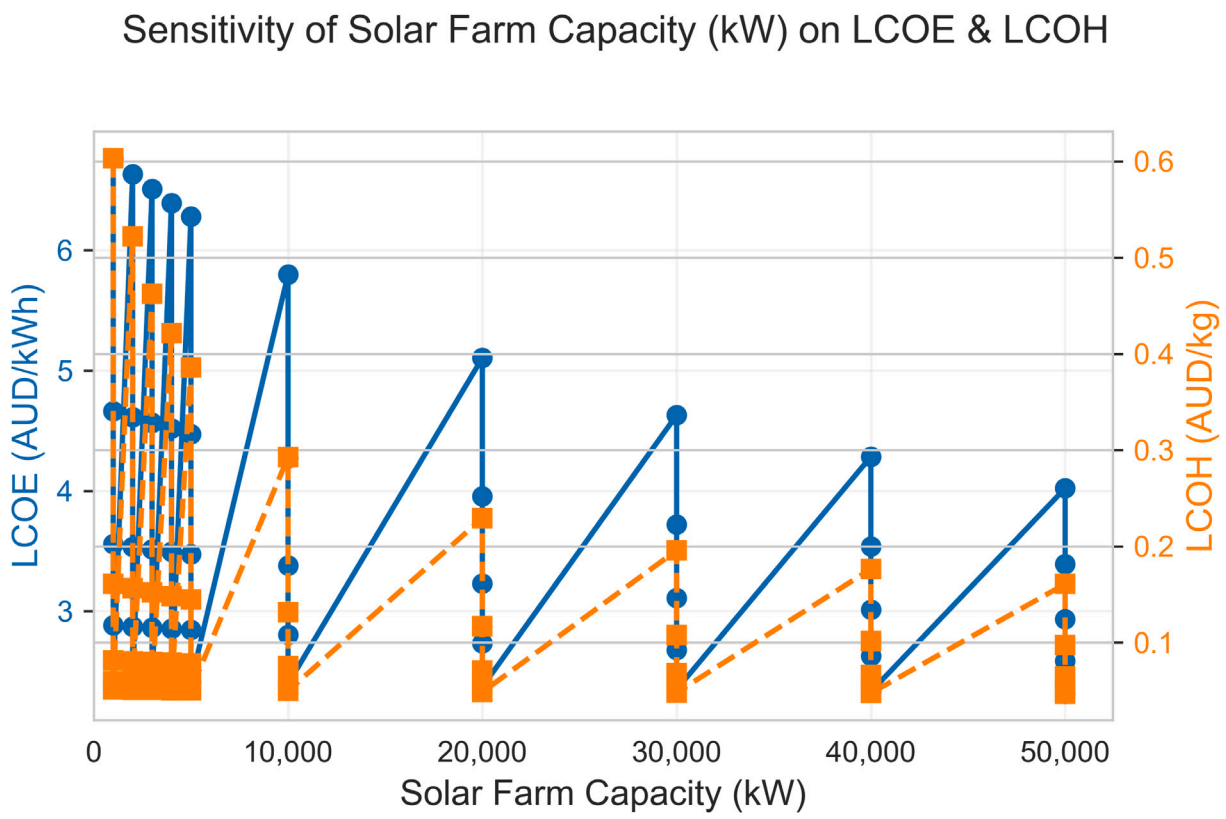

Fig. 14. Sensitivity of solar-farm capacity on LCOE and LCOH for the hybrid solar–wind–battery–hydrogen configuration. Cost reduction saturates beyond 30 MW of PV capacity, indicating diminishing marginal benefits.

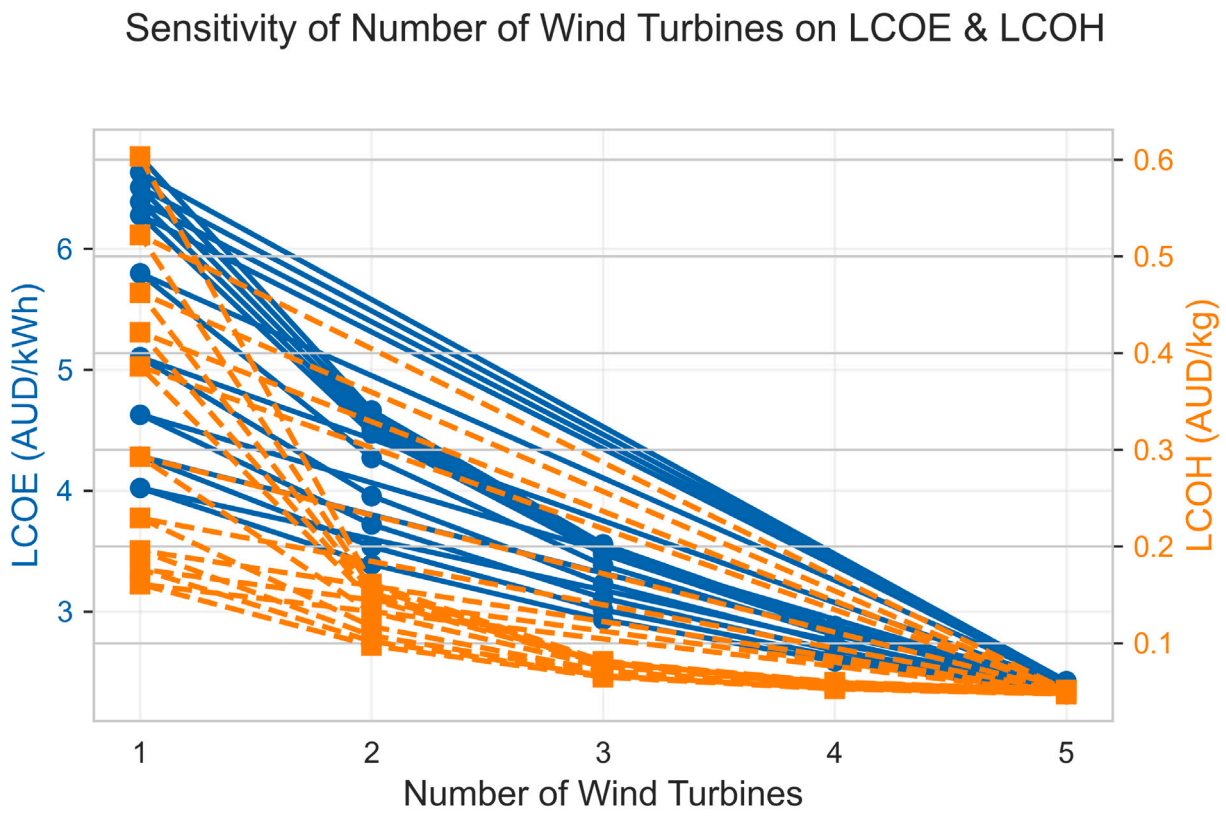

Fig. 15. Sensitivity of wind-turbine number on LCOE and LCOH for the hybrid solar–wind–battery–hydrogen configuration. Increasing turbine count from one to five substantially improves cost performance through enhanced nocturnal generation.

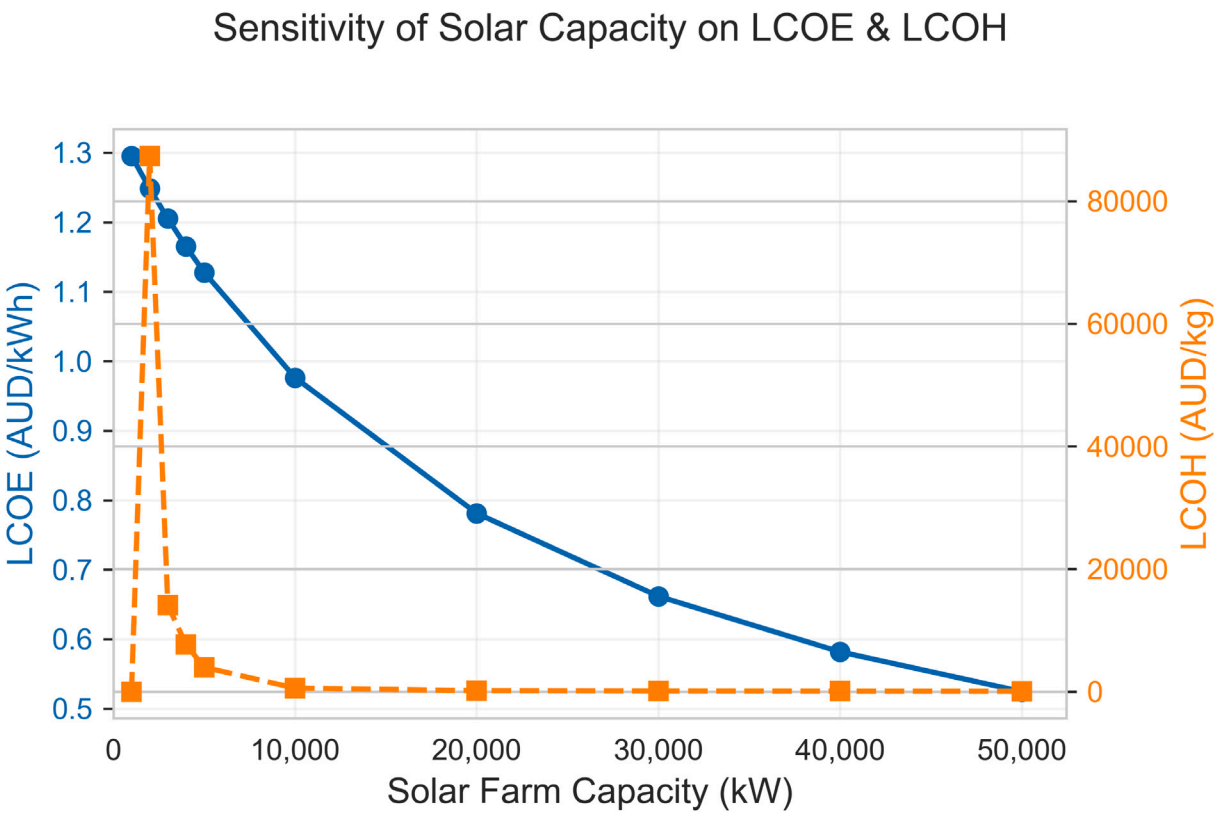

Fig. 16. Effect of solar-farm capacity on LCOE and LCOH for the solar–battery–hydrogen configuration.

Table 5
Performance metrics for the solar–battery–hydrogen system across different solar-farm capacities.

Capacity range	Representative configuration	LCOE (AUD/kWh)	LCOH (AUD/kg)
Low-Capacity Range (1–3 MW)	S1 (1000 kW)	1.296	N/A
	S2 (2000 kW)	1.249	87,373.81
	S3 (3000 kW)	1.205	14,095.77
Medium-Capacity Range (4–10 MW)	S4 (4000 kW)	1.165	7681.90
	S5 (5000 kW)	1.128	3973.23
	S6 (10,000 kW)	0.976	561.53
High-Capacity Range (20–50 MW)	S7 (20,000 kW)	0.781	157.87
	S8 (30,000 kW)	0.662	85.90
	S9 (40,000 kW)	0.582	58.50
	S10 (50,000 kW)	0.525	44.13

parallel, LCOE decreases from 2.37 to 1.35 AUD kWh^{-1}, highlighting improved renewable utilization and reduced reliance on non-renewable backup sources.

Fig. 17 shows that the steep initial drop in LCOE reflects the system's high sensitivity to generation adequacy at low wind capacities, while the flattening trend beyond four turbines indicates diminishing marginal benefits. The observed convergence of both cost metrics confirms that moderate turbine scaling achieves an optimal techno-economic balance without excessive capital addition. Overall, the wind–battery–hydrogen configuration demonstrates substantial improvements in cost efficiency and hydrogen viability with increasing wind penetration, reinforcing its significance within an integrated hybrid renewable framework.

4.7. Overall efficiency of the fully integrated hybrid renewable energy system

To evaluate the conversion effectiveness of the *fully integrated configuration* — comprising solar photovoltaics, wind turbines, battery storage, hydrogen production and reconversion, and diesel backup — the overall system efficiency was defined as the ratio between the total electrical energy supplied to demand and the total renewable electricity generated before storage and conversion losses. This configuration corresponds to the scenario that achieved nearly 100% renewable supply coverage, representing the most comprehensive and operationally autonomous design evaluated in this study:

$$\eta_{\text{system}} = \frac{E_{\text{delivered, load}}}{E_{\text{input, renewables}}} \times 100. \tag{31}$$

For the best-performing Broadmeadows-scale system, the simulated overall efficiency reached approximately 40%, indicating that about two-fifths of the renewable electricity produced was ultimately delivered to end-users after accounting for all conversion and curtailment losses. Across all battery–hydrogen hybrid configurations, system-level efficiency ranged between 27.5% and 83.9% (median 47.6%), depending on capacity sizing and curtailment intensity. Higher efficiencies were observed at smaller scales with limited curtailment, while larger

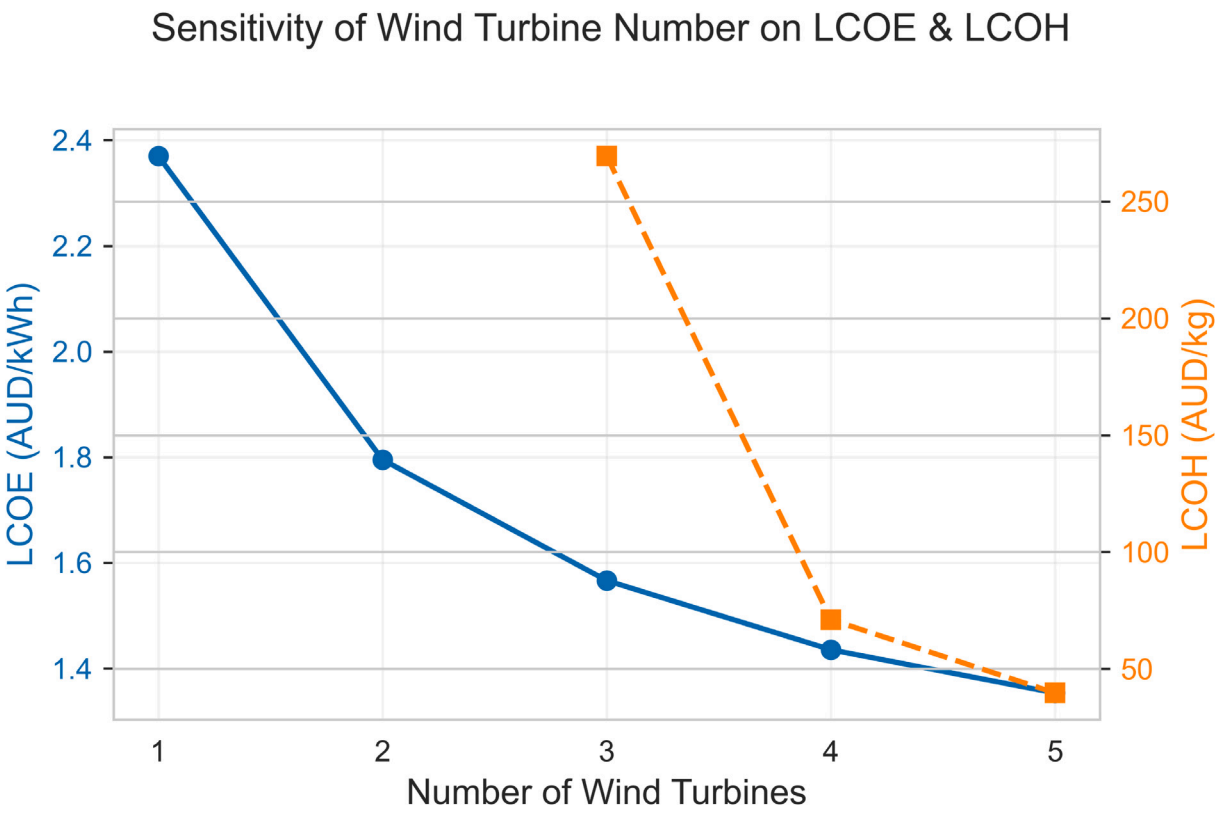

Fig. 17. Effect of wind-turbine number on LCOE and LCOH for the wind–battery–hydrogen configuration.

Table 6
Performance metrics for the wind–battery–hydrogen system across different numbers of wind turbines.

Capacity range	Representative configuration	LCOE (AUD/kWh)	LCOH (AUD/kg)
Low-Capacity Range (1–2 turbines)	W1 (1 WT)	2.370	N/A
	W2 (2 WTs)	1.795	N/A
High-Capacity Range (3–5 turbines)	W3 (3 WTs)	1.567	269.50
	W4 (4 WTs)	1.436	71.07
	W5 (5 WTs)	1.354	39.68

systems exhibited lower energetic efficiency but greater resilience and near-complete renewable autonomy.

This relationship underscores the intrinsic trade-off between energy autonomy and conversion efficiency, a characteristic observed in other high-penetration hybrid renewable-hydrogen systems [91,107,120]. Although multi-stage storage introduces unavoidable losses, the integrated configuration achieves almost total fossil-fuel displacement and represents the optimal balance between renewable utilization and reliability.

4.8. Cost and energy contribution breakdown

To complement the techno-economic comparison, the annual energy contribution of each subsystem was aligned with its relative cost share for the optimal configuration ($PV + WT + Battery + H_2 + Diesel$). Hourly dispatch data from the hybrid simulation were integrated over the year to quantify the proportion of total demand met by each component. PV and wind generation together supplied approximately 78% of the total electricity demand, while the battery contributed about 9% through short-term energy balancing. Hydrogen reconversion via the fuel-cell system provided roughly 10% of the annual supply during extended renewable deficits, and diesel backup covered the remaining 3%. These operational contributions were compared with the corresponding cost composition derived from the techno-economic model, summarized in Table 7. The results reveal that although hydrogen storage contributes only about 10% of annual delivered energy, its capital-intensive subsystem (electrolyzer, tank, and fuel cell) represents nearly 17% of total investment. In contrast, the PV and wind components dominate both energy supply and cost, accounting for 60% of total CAPEX and nearly 80% of generation. Battery storage, while modest in cost (14%), plays a crucial reliability role by reducing renewable curtailment and minimizing diesel operation. This parallel assessment demonstrates that cost allocation within the hybrid system aligns closely with energy utilization priorities, consistent with previous large-scale HRES techno-economic studies [101,108,120].

Table 7
Alignment of subsystem cost and energy contribution shares for the optimal hybrid configuration.

Subsystem	Energy contribution (%)	Cost share (%)
PV + WT	78	60
Battery Storage System	9	14
Hydrogen Storage System	10	17
Diesel Backup	3	8
Total	**100**	**100**

4.9. Hydrogen production potential in battery and hydrogen-integrated solar, wind, and hybrid systems

Hydrogen production potential varies significantly across different system scales. Hybrid solar–wind–hydrogen configurations achieving the highest generation levels. They maintain continuous hydrogen production by taking advantage of the complementary seasonal availability of solar and wind resources. Fig. 18 shows a comparative view of hydrogen production trends across all configurations.

Standalone solar–hydrogen systems produce limited amounts of hydrogen. The best-case (50 MW solar + battery) producing 150,885 kg annually. While smaller-scale fail to generate any hydrogen due to insufficient surplus energy for electrolysis. Wind–hydrogen systems achieve higher hydrogen production potential. The best-case (10.5 MW wind + battery) producing 156,292 kg annually, benefiting from wind energy's greater year-round consistency compared to solar.

Among all configurations, hybrid solar–wind–hydrogen systems demonstrate the highest hydrogen production efficiency. The best-case system (50 MW solar + 10.5 MW wind + battery + hydrogen) achieves an annual hydrogen production of 101.2 million kg, far surpassing standalone solar or wind-based hydrogen generation. The reported hydrogen yield of approximately $1.012\times10^{8}\,\mathrm{kg\,yr^{-1}}$ represents a *theoretical upper-bound potential* derived from complete utilization of surplus renewable electricity under idealized, continuous-operation conditions. When converted to energy units, this quantity corresponds to roughly $3.4\,\mathrm{TWh\,yr^{-1}}$ (LHV) — equivalent to about four to five times the annual electrical demand of the Broadmeadows catchment. It therefore denotes the system-level conversion capacity achievable if all excess solar and wind generation were channeled to electrolysis, rather than a physically deployed plant output. In practical implementation, real hydrogen production would be considerably lower once seasonal curtailment, maintenance downtime, and spatial constraints are accounted for, consistent with observations from large-scale feasibility studies [89,107,120]. The inclusion of this theoretical figure serves to illustrate the magnitude of renewable-to-hydrogen conversion potential under full decarbonization conditions, supporting comparative evaluation of energy resilience and cost pathways rather than representing a specific production target. Even the worst-case hybrid configuration (1 MW solar + 2.1 MW wind + battery + hydrogen) maintains significant hydrogen output.

These results confirm that large-scale hybrid hydrogen systems are the most effective option for sustainable hydrogen supply. They maximize renewable energy utilization while reducing dependence on fossil fuel operation hours.

5. Discussion

The integration of solar and wind resources has long been identified as a promising approach to reduce dependence on fossil fuels and enhance energy resilience. When their complementary generation patterns are harnessed, these resources can smooth variability and deliver more reliable supply throughout the year. Numerous studies have demonstrated that hybridizing RERs, especially solar and wind, improves generation consistency and significantly reduces carbon emissions associated with fossil-based electricity generation [14,28,33,121,122]. Yet, both resources share a common limitation: intermittency. Without sufficient storage capacity, this intermittency leads to hourly and seasonal gaps between supply and demand. Shortfalls can persist even in well-sized systems.

To overcome these reliability issues, recent research has turned to storage integration. Batteries are highly efficient for short-duration buffering, managing day-to-day fluctuations with minimal losses. In contrast, hydrogen storage provides long-duration and seasonal energy retention, making it a natural fit for systems aiming for high renewable penetration [24,123].

This study builds on that foundation. We perform a high-resolution, year-long simulation of hybrid solar–wind systems with both battery and hydrogen storage, designed for the specific meteorological and demand profile of Broadmeadows. Nine configurations are examined in detail. System performance is evaluated using these key metrics: renewable energy contribution, fossil fuel energy use, fossil fuel operation hours, and levelized costs (LCOE and LCOH).

The following discussion interprets these results in the context of our three research questions (RQ1–RQ3). It links the findings to the broader literature while outlining implications for technology design, policy priorities, and long-term energy planning.

5.1. Fossil fuel dependence & energy resilience in solar–wind systems (RQ1)

Hybridizing solar and wind generation is a proven strategy for reducing variability in renewable energy supply. This is particularly relevant in temperate regions such as Victoria, where seasonal shifts in solar irradiance and wind speed are pronounced. Studies including [14,28] show that solar–wind complementarity can improve energy availability and lower fossil fuel energy use. However, much of the existing research relies on idealized resource profiles or short-term simulations, overlooking operational variability, realistic storage constraints, and localized climatic effects. For example, [33] evaluated hybrid system behavior using uniform seasonal demand. While [121] stressed that resilience is difficult to achieve without long-duration storage.

This study builds on these insights through a high-resolution, region-specific techno-economic analysis that integrates hourly meteorological data and realistic storage limits. This approach closes a key gap in spatial and temporal modeling of hybrid renewable systems.

The results indicate that standalone solar and wind systems are constrained by seasonal intermittency. In Broadmeadows, wind-only systems outperform solar-only ones in winter. The best-case wind configuration (10.5 MW) met 73.97% of annual demand, while the best-case solar configuration (50 MW) achieved 45.71%. Despite these capacities, both required substantial fossil fuel energy use in the worst-case conditions. That is, 7.35 MWh for solar and 6.62 MWh for wind, underscoring their inability to operate independently year-round. These findings align with [122], which also identified weak energy resilience in single-source renewable systems without storage.

Hybrid solar–wind configurations exhibit significantly improved energy resilience. The best-case hybrid system (50 MW solar + 10.5 MW wind) met 85.04% of demand while cutting fossil fuel energy use to 0.83 MWh. Even in the worst-case hybrid configuration, the demand met (32.25%) was comparable to solar-only, but with better seasonal stability. This shows that hybridization not only boosts annual reliability, but also improves performance in critical low-resource months.

However, hybridization alone does not eliminate fossil fuel operation hours. The top-performing hybrid still required 273 h of fossil fuel operation annually, mostly during prolonged low-generation periods. This limitation mirrors [28]'s observation that hybrid systems, without storage, cannot bridge extended deficits.

In summary, solar–wind hybridization improves resilience and reduces dependence on fossil fuel energy. However, even under optimal sizing, the absence of storage leaves residual vulnerability, particularly during seasonal lows. By explicitly modeling real-world temporal variability, this study provides a more complete picture of hybrid system behavior than previous works limited to idealized or short-duration analyses [14,33,121].

5.2. Impact of battery & hydrogen storage on seasonal deficits & fossil fuel reliance (RQ2)

Addressing seasonal energy deficits is a major challenge in HRES design, particularly in climates with strong seasonal variation in solar

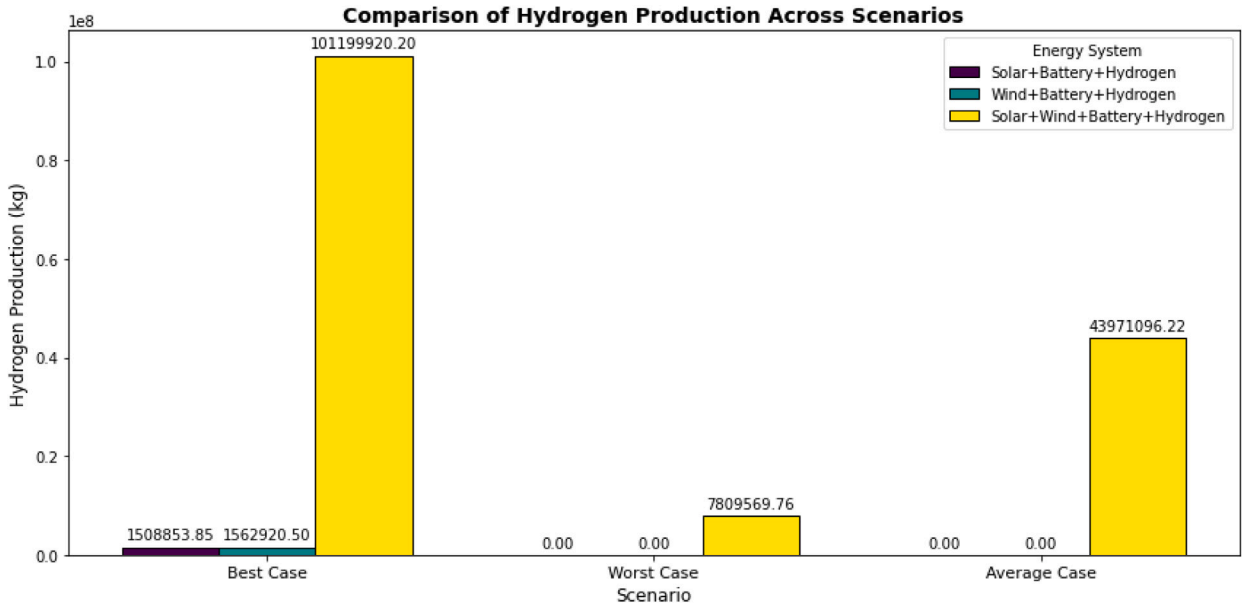

Fig. 18. Hydrogen production across best, average, and worst hydrogen-integrated configurations — solar–battery–hydrogen, wind–battery–hydrogen, and hybrid (solar–wind–battery–hydrogen).

irradiance and wind speeds. While previous studies have examined storage integration in hybrid systems, most focus on short-term fluctuations or single-season reliability. Scale effects and year-round system dynamics are often overlooked [28,33]. Our study extends this understanding by evaluating how battery and hydrogen storage influence performance across multiple seasonal and capacity configurations. This approach offers a more granular view of energy resilience under realistic operating constraints.

Battery storage is found to be highly effective in mitigating short-term energy imbalances. In solar–battery configuration, the percentage of demand met increase from 45.71% (solar-only) to 75.76%, while hours requiring fossil fuel backup fell from 1340 to 622 in the best case scenario. wind–battery configurations performed even better: with the best-performing system meeting 98.66% of demand, with only 42 h of fossil fuel use per year. These results are consistent with [33], which observed similar reliability gains from battery integration when dispatch strategies are tuned for daily variability.

However, batteries alone cannot address seasonal deficits. Energy from high-yield months (e.g., summer) cannot be stored long enough to cover winter peaks, especially in smaller solar–battery configuration. This limitation aligns with [14], where battery-only designs failed to deliver year-round autonomy, particularly in cold seasons.

Hydrogen storage provides a long-duration buffer that can bridge seasonal gaps. In our results, solar–hydrogen configurations met 79.77% of demand, while wind–hydrogen configurations reached 98.66%. Hybrid solar–wind–battery–hydrogen configurations achieved near-complete coverage — up to 99.999% in the best case — with fossil fuel use limited to a single hour annually. These findings support [28], which highlighted hydrogen's low self-discharge and scalability for large-scale seasonal balancing.

However, hydrogen storage effectiveness is highly scale-dependent. In smaller configurations, such as 1 MW solar + 2.1 MW wind + battery + hydrogen, still required fossil fuel backup for up to 740 h per year. The main cause is insufficient surplus renewable output for electrolysis. Similar scale-sensitivity was reported by [121], which stressed that hydrogen capacity must be matched to overall generation.

Overall, battery storage enhances daily operational stability, while hydrogen is essential for seasonal balancing. Systems that integrate both offer the most resilient performance, combining fast response with long-term autonomy. These results align with [14] in advocating smart grid control and predictive dispatch to improve storage utilization and reduce supply–demand mismatches. Such diversity in storage technologies, combined with intelligent energy management, is a key pathway for deploying robust hybrid systems in regions with high seasonal variability.

5.3. *Cost trade-offs across hybrid configurations (levelized cost of energy & hydrogen analysis) (RQ3)*

Economic feasibility remains a critical factor influencing the scalability and real-world implementation of HRES. In this context, the LCOE and LCOH serve as key indicators for evaluating the long-term financial sustainability of different system configurations. Our analysis highlights a complex interplay between reliability, energy independence, and infrastructure costs. This underscores the need for tailored investment strategies that reflect system design and scale.

The concept of *economic viability* in this study is not intended to imply direct parity with prevailing residential electricity tariffs. Instead, it is used to characterize the long-term feasibility of achieving high levels of energy autonomy, supply reliability, and deep decarbonization under realistic suburban operating conditions. The LCOE is therefore interpreted as a system-level indicator that internalizes infrastructure investment, storage redundancy, and reliability provision, rather than as a direct substitute for retail grid electricity prices. From this perspective, HRES are assessed against resilience-oriented benchmarks, such as diesel-assisted microgrids or outage-prone grid dependency, where avoided fossil fuel operation, emissions reduction, and enhanced supply security represent quantifiable economic value beyond unit energy cost alone.

Among battery-integrated systems, solar–battery configurations are the most cost-effective. Their LCOE values range from 0.39 to 0.89 AUD/kWh, aligning with earlier economic evaluations of distributed solar-plus-storage configurations in urban and peri-urban contexts [33,122]. These systems can reduce fossil fuel energy dependency, making them a pragmatic option for mid-scale deployments. However, as noted by [87], limited storage duration constrains their ability to address extended generation deficits, particularly in winter.

wind–battery systems achieve higher energy sufficiency, especially in the Broadmeadows region where wind availability peaks in colder months. However, their higher LCOE values (1.35–2.37 AUD/kWh)

reflect the greater CAPEX and O&M costs of WT and larger-scale storage [14,28]. This cost difference between solar and wind configurations is consistent with International Renewable Energy Agency (IRENA) reports, which point to variations in component lifespans, maintenance needs, and intermittency profiles [87].

Hybrid solar–wind–battery configurations deliver the highest reliability but also the highest LCOE range (2.31–6.77 AUD/kWh). The elevated costs stem from the infrastructure-intensive integration of multiple generation and storage sources. Such systems highlight the economic challenges of full energy autonomy and the importance of targeted policy measures. Such as, capital subsidies, carbon pricing, or capacity payments, to close the gap between technical capability and financial feasibility.

For hydrogen-integrated configurations, economic viability is highly dependent on system scale and the availability of surplus renewable energy. Standalone solar–hydrogen (44.13 AUD/kg) and wind–hydrogen (39.67 AUD/kg) systems remain economically unfeasible due to inconsistent excess energy for electrolysis. These findings match earlier studies that show high hydrogen costs under low utilization conditions [14,24]. In contrast, hybrid solar–wind–battery–hydrogen configurations can achieve remarkably low LCOH value. The best-performing configuration in this study reached 0.04 AUD/kg, enabled by continuous renewable input and high electrolyzer utilization.

Economic performance drops sharply for smaller hybrid systems. Limited surplus energy results in low hydrogen production and disproportionately high unit costs. This confirms that cost-effective hydrogen deployment is achievable mainly at large scales, particularly where complementary resources allow sustained electrolyzer operation across seasons [24].

At the Broadmeadows site, the hybrid solar–wind–battery–hydrogen configuration remains economically viable despite its higher apparent LCOE. The system achieves near-zero fossil-fuel operation and a low levelised cost of hydrogen (0.04 AUD kWh^{-1}) while maintaining full year-round energy autonomy. When compared with local grid tariffs (0.28–0.32 AUD kWh^{-1}) [124] and considering projected reductions in electrolyzer costs by 2030 (>=15%–20% and potentially 50%) [125], the configuration is expected to approach grid-competitive parity and deliver long-term energy resilience for suburban deployment [126].

Although hydrogen integration increases capital costs and marginally raises the overall LCOE, its contribution to energy resilience is both practical and environmentally justified. The improvement from 99.4% to 99.99% reliability — equivalent to roughly 50 h of avoided outages per year — meets Victoria's critical-load reliability benchmark and ensures full autonomy during extended low-renewable periods. This performance cannot be achieved by batteries alone. Moreover, fossil-fuel operation remains below 0.5% of annual hours, producing a > 95% reduction in CO_2 emissions relative to diesel-assisted systems. Hence, even though the percentage gain in reliability appears small, hydrogen integration is economically and environmentally defensible when measured against its avoided-outage value, long-term security benefits, and contribution to deep decarbonization.

In broader context, the techno-economic outcomes of this study are consistent with the emerging literature on hybrid renewable-hydrogen systems, while also revealing distinct regional characteristics. Most international investigations have reported LCOE values ranging between 0.14 and 0.30 USD kWh^{-1} and LCOH values between 4 and 7 USD $kg_{H_2}^{-1}$ for high-yield desert or coastal environments [91,127,128]. In comparison, the present suburban Broadmeadows configuration — subject to moderate solar irradiance and higher urban infrastructure costs — achieves LCOE values of approximately 0.43–0.46 USD kWh^{-1} and LCOH values of 0.026–0.39 USD $kg_{H_2}^{-1}$ for the best-performing large-scale hybrid scenarios, while sustaining a reliability of nearly 99.999% (1 fossil-fuel hour per year). These values correspond to 0.65–0.70 AUD kWh^{-1} and 0.04–0.60 AUD $kg_{H_2}^{-1}$, aligning with the lowest-cost outcomes reported in Sections 4.7 and 4.5.4. They are also comparable to regional hybrid–hydrogen analyses in Australia and other temperate suburban contexts [108,120,129].

In summary, battery storage remains the most financially viable option for near-term reliability gains, particularly at the household or district scale. Hydrogen storage, while less cost-effective on its own, becomes viable under large-scale, surplus-rich conditions. Combining both storage types offers the best technical performance but requires substantial financial incentives to overcome capital cost barriers. These findings not only confirm earlier evidence but also provide region-specific, scale-sensitive insights for shaping energy policy, grid planning, and investment strategies in areas with similar climatic and infrastructural profiles. While the numerical results are specific to Broadmeadows, the modeling framework can be adapted to other regions by updating local weather, cost, and policy inputs, making it broadly applicable to diverse real-world settings

5.4. Land-use implications and practical context

The simulated hybrid configurations represent a theoretical energy-balance framework that evaluates whether the Broadmeadows suburb could, in principle, meet its residential electricity demand entirely from renewable sources. Translating these configurations into physical deployment requires assessing land availability and technology power densities. Based on representative benchmarks from [130,131], the estimated land requirement is approximately 1 km^2 for a 22.36 MW solar photovoltaic array and about 0.4 km^2 for four mid-size wind turbines. These values correspond to typical suburban-scale installations and serve as indicative upper bounds rather than precise siting requirements.

In practice, PV generation would likely be distributed across residential rooftops, commercial buildings, and under-utilized brownfield sites, substantially reducing the need for dedicated open land. Wind turbines could be installed in nearby industrial or open tracts where planning regulations permit moderate hub heights. Hydrogen infrastructure — including electrolysers, compression units, and storage tanks — could be co-located within existing industrial estates or along repurposed gas-pipeline corridors. Such integration is consistent with spatial strategies proposed in the *Victorian Renewable Hydrogen Industry Development Plan* (2021) [132–135].

Accordingly, the current study quantifies the technical and economic potential of complete renewable supply rather than the physical land-allocation feasibility. These estimates provide a first-order spatial reference for assessing urban-scale renewable-hydrogen integration and support future planning analyses that combine energy modeling with geospatial land-use evaluation.

5.5. Challenges of integrating hybrid renewable energy systems

HRES that combine solar, wind, battery, and hydrogen storage are increasingly promoted as a route toward sustainable, resilient, and decarbonized energy systems. They can strengthen grid reliability, cut greenhouse gas emissions, and reduce fossil fuel energy use. Yet, the path to large-scale adoption is far from straightforward. High upfront capital requirements remain a major obstacle. In many cases, design practices fail to optimize component sizing or dispatch, leading to underperformance. Existing grid infrastructure also imposes physical and operational limits that can restrict integration. While these issues have been explored extensively in the literature, most studies treat them in isolation rather than as interconnected barriers [93,136]. The present study extends this discourse by demonstrating how these factors interact in real-world hybrid configurations and influence techno-economic performance under variable operating and environmental conditions.

5.5.1. High capital costs and economic barriers

Despite their long-term environmental and operational advantages, HRES demand substantial upfront capital. This is particularly true for high-cost components such as battery banks, electrolyzers, hydrogen storage tanks, and fuel cells. Our results show that hybrid configurations enhance energy sufficiency and reduce fossil fuel energy use, yet these benefits often come with a higher LCOE — in some hybrid solar–wind–battery systems, reaching 6.77 AUD/kWh. For hydrogen-based setups, the LCOH remains prohibitively high in small-scale deployments, exceeding 39 AUD/kg. This is largely due to the inconsistent availability of surplus electricity for electrolysis.

These trends align with earlier economic analyses, including [136], which highlight the sensitivity of hydrogen costs to system scale and utilization. Reviews by [87,93] similarly identify capital expenditure as the dominant cost driver in hybrid systems, especially in early stages of market adoption. Without targeted policy mechanisms — tax incentives, capital subsidies, and renewable financing frameworks — cost parity with fossil fuel alternatives will remain elusive. Large-scale public–private partnerships, such as the Australia's Hydrogen Energy Supply Chain (HESC) project [137], demonstrate how coordinated investment and supportive regulation can accelerate both deployment and cost reduction.

5.5.2. System optimization and power management

The efficiency of HRES depends on optimal component selection, accurate system sizing, and effective real-time energy dispatch. Our simulations show that without well-calibrated hydrogen and battery capacities, even multi-source systems can experience seasonal energy deficits and an increased reliance on fossil fuel energy use. These challenges reflect broader findings in the literature, where suboptimal configurations cause renewable curtailment, underutilized storage, and higher dependence on backup generation [67].

Recent studies have highlighted the potential of advanced optimization approaches — such as AI-based dispatch control, predictive energy management, and real-time load forecasting to significantly improve the performance of HRES [122]. Integrating these technologies within microgrid architectures can boost local energy autonomy, support demand-side flexibility, and reduce pressure on the broader grid [138]. Although this study adopts a rule-based dispatch approach, future work should explore dynamic, real-time control strategies capable of minimizing energy losses and increasing renewable utilization, particularly under conditions of high demand variability or extreme weather events.

5.5.3. Grid infrastructure and renewable integration barriers

Large-scale deployment of hybrid renewable systems depends on a modern grid. The infrastructure must handle variable renewable inputs and connect with decentralized storage. Without smart grid capabilities, fluctuating generation from solar, wind, or hydrogen fuel cells can cause instability. It can also trigger energy curtailment and inefficient dispatch, lowering overall performance.

This study supports these concerns that even well-configured hybrid systems require efficient grid connectivity to fully utilize their generation potential. Smart grid investments, real-time energy monitoring, and automated demand response technologies can improve system flexibility and grid resilience [121]. Policy frameworks such as Australia's Renewable Energy Zones (REZ) initiative [94] highlight how regional grid upgrades can facilitate higher penetration of hybrid renewable systems. Strengthening transmission networks and decentralizing energy distribution will be critical for seamless integration of hydrogen-based storage solutions into national grids.

5.6. Limitations of the study

This study provides a detailed, high-resolution techno-economic assessment of hybrid solar–wind–battery–hydrogen systems. However, several limitations must be acknowledged. These help to place the results in context and point toward areas for future work. Most limitations arise from modeling assumptions. Some operational processes were simplified, and the dispatch logic does not capture all real-world behaviors. Certain grid and market dynamics were also excluded. These factors could influence system performance and economic outcomes in practice.

5.6.1. Model assumptions and data constraints

This study uses a simulation-based approach with high-resolution NASA-derived wind and solar datasets, combined with industry-standard efficiency assumptions. These inputs allow for a robust initial assessment. However, real-world system performance can vary due to microclimatic effects, unexpected energy losses, and long-term component degradation. For PV systems, a fixed performance ratio (PR = 0.85) is applied. This does not account for gradual output decline, soiling, or site-specific installation impacts. While these assumptions offer clarity in modeling, they simplify reality. Pilot-scale demonstrations and stochastic modeling could better capture dynamic behaviors under varying operational conditions.

5.6.2. Lack of real-time optimization

The dispatch logic follows a fixed hierarchy — solar and wind are used first, followed by battery, hydrogen, and finally fossil fuel backup. This rule-based strategy works under deterministic scenarios. However, it cannot adapt to rapid shifts in system state, market prices, or weather patterns. Real-time control approaches, such as MILP, heuristic methods, or Artificial Intelligence (AI)-based predictive dispatch, could deliver higher efficiency. They would also allow the system to respond more flexibly to operational challenges.

5.6.3. Grid integration and demand-side flexibility

In this study, the grid serves only as a notional backup source used to quantify residual non-renewable hours and does not participate in wholesale energy trading or export profit calculations. The dispatch framework therefore represents an autonomous suburban microgrid rather than a grid-interactive system.

The analysis assumes unlimited grid access for imports and exports. It does not consider transmission bottlenecks, demand-response participation, or congestion effects. In practice, these factors can reduce the economic viability of hybrid systems. They can also force curtailment during periods of high generation. Including grid power-flow constraints, demand flexibility, and coordinated regional storage in future modeling would provide a closer match to real-world grid operations.

Although the present analysis treats the grid as a notional backup, suburban networks often impose feeder-level export caps and import limitations. If a ±20% capacity cap were applied, renewable curtailment would rise slightly due to restricted export during high-generation hours, increasing the calculated LCOE by roughly 3%–5% and lowering the renewable-energy fraction by 1%–2% [139]. Similar suburban-microgrid studies for Victoria and New South Wales report comparable effects under feeder constraints [101,140]. These modest deviations suggest that while constrained-grid operation may marginally reduce utilization efficiency, it does not alter the broader feasibility or decarbonization conclusions of this study.

5.6.4. Limited scope of renewable energy resources

This study focuses on solar and wind energy as the primary renewable inputs, due to their widespread availability and scalability in the target region. However, other dispatchable renewable resources — such as hydropower, geothermal, and bioenergy — were not considered. Including such sources could further improve energy security, reduce storage requirements, and support base-load generation. A broader assessment incorporating these technologies would provide a more holistic view of HRES design for future work.

Addressing these limitations is key to moving from feasibility studies to deployable system designs. Such work must be able to withstand the technical, economic, and policy complexities of large-scale renewable integration.

While the present study employs steady-state component equations for annual techno-economic evaluation, the underlying Python framework has been purposefully designed for future experimental integration and refinement. Subsequent research will focus on incorporating empirical data from component-level testing and pilot-scale hybrid demonstrations to calibrate efficiency, degradation, and dynamic response characteristics. This progression will extend the current simulation toward a validated digital-twin environment, enhancing predictive reliability and enabling adaptive optimization under real operating conditions [141,142].

6. Conclusion

This study presented a comprehensive techno-economic feasibility assessment of hybrid solar–wind–battery–hydrogen energy configurations for the Broadmeadows region of Melbourne. The results show that standalone solar and wind configurations contribute significantly to renewable generation but cannot provide a stable year-round supply. Seasonal and hourly intermittency limits their reliability, and even large-scale deployments without storage cannot achieve full energy autonomy.

Hybrid solar–wind configurations improved performance compared to standalone options. They supplied 85.04% of annual electricity demand and reduced fossil fuel use to 0.83 MWh per year in the best case. However, they still required 273 h of fossil fuel backup, confirming that hybridization alone cannot deliver full reliability. Adding battery storage strengthened short-term balancing and reduced fossil fuel reliance to only five hours annually, but it could not address seasonal deficits. Hydrogen storage proved essential in large-scale configurations, enabling 99.99% demand coverage with just one fossil fuel backup hour per year. Its feasibility, however, was highly scale dependent.

The techno-economic analysis revealed clear trade-offs. Solar–battery configurations achieved the lowest costs, with LCOE values between 0.39 and 0.89 AUD/kWh, making them suitable for small- to medium-scale applications. Their limited ability to manage seasonal variability, however, restricted their autonomy. Wind–battery configurations provided higher reliability but required greater investment, with LCOE values of 1.35–2.37 AUD/kWh. Hybrid solar–wind–battery configurations offered the highest resilience but showed high costs, with LCOE values of 2.31–6.77 AUD/kWh, highlighting the need for policy support and incentives to enable adoption. Hydrogen-integrated configurations displayed the strongest scale effects. Standalone solar–hydrogen and wind–hydrogen options were not viable, recording LCOH values of 44.13 and 39.67 AUD/kg. In contrast, large-scale solar–wind–hydrogen configurations achieved a feasible best case of 0.04 AUD/kg. This result confirms that cost-effective hydrogen storage is feasible only in large-scale systems with substantial renewable overcapacity and consistent surplus generation.

While the results confirm the technical feasibility of achieving near-complete renewable coverage for the Broadmeadows case, they should be interpreted within the context of the site's specific meteorological and demand characteristics. Variations in solar irradiance, wind resource quality, and infrastructure costs across regions can substantially influence system performance. Comparative assessments across Australian climates have reported LCOE variations of 5%–10% and hydrogen cost shifts of 10%–20% depending on local resource availability and utilization rates [69,84,114]. Consequently, the conclusions presented here represent an upper-bound potential under idealized suburban conditions rather than a universal benchmark. Introducing probabilistic weather ensembles or stochastic cost modeling in future analyses would provide formal uncertainty bounds for LCOE, LCOH, and resilience outcomes, thereby strengthening the robustness of regional policy interpretation.

These findings confirm earlier evidence and provide region-specific insights for shaping energy policy, grid planning, and investment strategies in areas with similar climatic and infrastructural profiles, rather than representing a uniform outcome applicable to all contexts.

6.1. Future work

Future studies on HRES should build on this work by exploring advanced operational strategies that improve both efficiency and flexibility. Real-time optimization and AI-driven dispatch could reduce system losses and better align renewable generation with variable demand. Machine learning-based forecasting would allow more accurate planning under uncertainty, while adaptive energy management could support dynamic switching between batteries and hydrogen storage within hybrid configurations.

Economic modeling of HRES also requires greater attention. Lifecycle cost assessments, including component degradation, replacement, and maintenance, are essential for refining long-term feasibility estimates. At the system level, research on grid integration will be critical. Demand-side flexibility, decentralized control, and smart metering should be investigated to enable large-scale adoption of hydrogen-integrated HRES. Stronger links between technical models and policy frameworks will also help bridge the gap between feasibility studies and practical deployment.

CRediT authorship contribution statement

Waqar Ali Khan: Writing – original draft, Visualization, Validation, Software, Methodology, Investigation, Formal analysis, Conceptualization. **Ashkan Pakseresht:** Writing – review & editing, Supervision, Conceptualization. **Caslon Chua:** Supervision. **Ali Yavari:** Writing – review & editing, Supervision, Resources, Methodology, Investigation, Funding acquisition, Conceptualization.

Declaration of competing interest

The authors declare that they have no known competing financial interests or personal relationships that could have appeared to influence the work reported in this paper.

Acknowledgments

This work has been supported by the Future Energy Exports Cooperative Research Centre (FEnEx CRC), whose activities are funded by the Australian Government's Cooperative Research Centre Program

Acronyms

AC	Alternating Current
AI	Artificial Intelligence
BESS	Battery Energy Storage System
CAPEX	Capital Expenditures
CBD	Melbourne's Central Business District
CERES/MERRA-2	Clouds and the Earth's Radiant Energy System/Modern-Era Retrospective Analysis for Research and Applications
CSIRO	Commonwealth Scientific and Industrial Research Organisation
DC	Direct Current
DoD	Depth of Discharge
FF	Form Factor
GHG	Greenhouse Gas

HESC	Australia's Hydrogen Energy Supply Chain
HOMER	Hybrid Optimization of Multiple Energy Resources
HRES	Hybrid Renewable Energy Systems
IRENA	International Renewable Energy Agency
JRC	Joint Research Centre
LCOE	Levelized Cost of Energy
LCOH	Levelized Cost of Hydrogen
MATLAB	MATrix LABoratory
MCDM	Multi-Criteria Decision-Making
MILP	Mixed-integer Linear Programming
ML	Machine Learning
MPC	Model Predictive Control
NASA	National Aeronautics and Space Administration
NASA POWER	National Aeronautics and Space Administration Prediction Of Worldwide Energy Resources
NREL	National Renewable Energy Laboratory
O&M	Operation and Maintenance
OPEX	Operational Expenditures
PEM	Proton Exchange Membrane
PR	Performance ratio
PSH	Peak Solar Hours
PV	Photovoltaic
PVF	Present Value Factor
PVGIS	Photovoltaic Geographical Information System
PVGIS-ERA5	Photovoltaic Geographical Information System-fifth-generation European Centre for Medium-Range Weather Forecasts
RB-HDA	Rule-Based Heuristic Dispatch Algorithm
RERs	Renewable Energy Resources
REZ	Australia's Renewable Energy Zones
SF	Safety Factor
SOC	State of Charge
SOFC	Solid Oxide Fuel Cell
TRNSYS	Transient System Simulation Program
WT	Wind turbines

References

[1] Raimi D, Zhu Y, Newell RG, Prest BC. Global energy outlook 2024: Peaks or plateaus, Resources for the future.

[2] Diesendorf M, Taylor R. Transitioning the energy system. In: The path to a sustainable civilisation: technological, socioeconomic and political change. Springer; 2023, p. 53–88.

[3] Duraiswami RA. Global carbon capture and storage efforts: Challenges and opportunities. J Geol Soc India 2025;101(2):143–8.

[4] Al-Rawashdeh H, Al-Khashman OA, Al Bdour JT, Gomaa MR, Rezk H, Marashli A, Arrfou LM, Louzazni M. Performance analysis of a hybrid renewable-energy system for green buildings to improve efficiency and reduce GHG emissions with multiple scenarios. Sustainability 2023;15(9):7529.

[5] Aboumahboub T, Brecha RJ, Shrestha HB, Fuentes U, Geiges A, Hare W, Schaeffer M, Welder L, Gidden MJ. Decarbonization of Australia's energy system: Integrated modeling of the transformation of electricity, transportation, and industrial sectors. Energies 2020;13(15):3805.

[6] Tripathi S, Shrivastava A, Jana K. An efficient energy management system for a micro-grid system considering the volatility of hybrid renewable energy. Int J Hydrog Energy 2025;101:673–91.

[7] Holder DM, Yavari A. Port energy models alignment with real port activities, their coverage of hydrogen technologies, and as tools for decarbonisation. Int J Hydrog Energy 2025;165:150202. http://dx.doi.org/10.1016/j.ijhydene.2025.150202, URL https://www.sciencedirect.com/science/article/pii/S0360319925032008.

[8] Noyan OF, Hasan MM, Pala N. A global review of the hydrogen energy eco-system. Energies 2023;16(3):1484.

[9] Hashmi R, Liu H, Yavari A. Digital twins for enhancing efficiency and assuring safety in renewable energy systems: A systematic literature review. Energies 17(11). http://dx.doi.org/10.3390/en17112456, URL https://www.mdpi.com/1996-1073/17/11/2456.

[10] Change C. Mitigating climate change. In: Working Group III contribution to the sixth assessment report of the intergovernmental panel on climate change.

[11] Blakers A, Stocks M, Lu B, Cheng C. The observed cost of high penetration solar and wind electricity. Energy 2021;233:121150.

[12] Saleh A, Antar RK, Ali AJ. Design and simulation of hybrid renewable energy system for on-grid applications. In: IMDC-IST proceedings of 2nd international multi-disciplinary conference theme: integrated sciences and technologies. 2022, p. 339–40.

[13] Slama AH, Toumi S, Saidi M, Saidi L. Hres systems state of the art: Topologies, sizing approaches, and evaluation criteria. In: 2023 international conference on control, automation and diagnosis. IEEE; 2023, p. 1–6.

[14] Abdin Z, Al Khafaf N, McGrath B. Feasibility of hydrogen hybrid energy systems for sustainable on-and off-grid integration: An Australian rezs case study. Int J Hydrog Energy 2024;57:1197–207.

[15] Hannan M, Abu SM, Al-Shetwi AQ, Mansor M, Ansari M, Muttaqi KM, Dong Z. Hydrogen energy storage integrated battery and supercapacitor based hybrid power system: A statistical analysis towards future research directions. Int J Hydrog Energy 2022;47(93):39523–48.

[16] Yavari A, Harrison CJ, Gorji SA, Shafiei M. Hydrogen 4.0: A cyber–physical system for renewable hydrogen energy plants. Sensors 24(10). http://dx.doi.org/10.3390/s24103239, URL https://www.mdpi.com/1424-8220/24/10/3239.

[17] Agajie TF, Ali A, Fopah-Lele A, Amoussou I, Khan B, Velasco CLR, Tanyi E. A comprehensive review on techno-economic analysis and optimal sizing of hybrid renewable energy sources with energy storage systems. Energies 2023;16(2):642.

[18] Mullanu S, Chua C, Molnar A, Yavari A. Artificial intelligence for hydrogen-enabled integrated energy systems: A systematic review. Int J Hydrog Energy 2025;141:283–303. http://dx.doi.org/10.1016/j.ijhydene.2024.08.013, URL https://www.sciencedirect.com/science/article/pii/S0360319924031628.

[19] Mulumba AN, Farzaneh H. Techno-economic analysis and dynamic power simulation of a hybrid solar-wind-battery-flywheel system for off-grid power supply in remote areas in Kenya. Energy Convers Manag: X 2023;18:100381.

[20] Affi S, Cherif H, Belhadj J. Smart system management and techno-environmental optimal sizing of a desalination plant powered by renewables with energy storage. Int J Energy Res 2021;45(5):7501–20.

[21] Giedraityte A, Rimkevicius S, Marciukaitis M, Radziukynas V, Bakas R. Hybrid renewable energy systems—a review of optimization approaches and future challenges. Appl Sci 2025;15(4):1–30.

[22] Arsad AZ, Hannan M, Al-Shetwi AQ, Mansur M, Muttaqi K, Dong Z, Blaabjerg F. Hydrogen energy storage integrated hybrid renewable energy systems: A review analysis for future research directions. Int J Hydrog Energy 2022;47(39):17285–312.

[23] Khan WA, Pakseresht A, Chua C, Yavari A. Digital twin role for sustainable and resilient renewable power plants: A systematic literature review. Sustain Energy Technol Assess 2025;75:104197. http://dx.doi.org/10.1016/j.seta.2025.104197, URL https://www.sciencedirect.com/science/article/pii/S2213138825000281.

[24] Hussam WK, Barhoumi EM, Abdul-Niby M, Sheard GJ. Techno-economic analysis and optimization of hydrogen production from renewable hybrid energy systems: Shagaya renewable power plant-Kuwait. Int J Hydrog Energy 2024;58:56–68. http://dx.doi.org/10.1016/j.ijhydene.2024.01.153, URL https://www.sciencedirect.com/science/article/pii/S0360319924001757.

[25] Chen W-B. Assessing global land-based solar–wind complementarity using high-resolution climate reanalysis for hybrid renewable energy design. Energy Convers Manage 2025;343:120267.

[26] Zhuang Y, Xu K, Bin L, Ma C, Zhang J, Lian J. Assessing China's wind-solar energy potential and complementarity under climate change: An environmental adaptability perspective. J Clean Prod 2025;528:146778.

[27] Zhang X, Zhang H, Zhang L, Du L, Wang Q, Zhou D. Optimization of a wind-pv-hydrogen production coupling system considering economy, environment, and reliability. Int J Hydrog Energy 2025;105:441–57.

[28] Chamout MW, Perl A, Hengeveld EJ, Aué J-j. Simulation and analysis of hybrid hydrogen-battery renewable energy storage for off-electric-grid Dutch household system. Int J Hydrog Energy 2024;70:170–82.

[29] ALAhmad AK, Verayiah R, Shareef H. Long-term optimal planning for renewable based distributed generators and battery energy storage systems toward enhancement of green energy penetration. J Energy Storage 2024;90:111868.

[30] Wang B, Zhaoxiang B. Hydrogen energy storage: Mitigating variability in wind and solar power for grid stability in Australia. Int J Hydrog Energy 2025;97:1249–60.

[31] Malik FH, Hussain GA, Alsmadi YM, Haider ZM, Mansoor W, Lehtonen M. Integrating energy storage technologies with renewable energy sources: a pathway toward sustainable power grids. Sustainability 2025;17(9):4097.

[32] Kwon K, Lee H-B, Kim N, Park S, Joshua SR. Integrated battery and hydrogen energy storage for enhanced grid power savings and green hydrogen utilization. Appl Sci 2024;14(17):7631.

[33] Kim DK, Rho KH, Na Y, Kim M. Evaluation of energy storage technologies for efficient usage of wind power in the far-eastern region: A techno-economic analysis. J Energy Storage 2021;39:102595.

[34] Kim SH, Shin Y-J. Optimize the operating range for improving the cycle life of battery energy storage systems under uncertainty by managing the depth of discharge. J Energy Storage 2023;73:109144.

[35] Rayit NS, Chowdhury JI, Balta-Ozkan N. Techno-economic optimisation of battery storage for grid-level energy services using curtailed energy from wind. J Energy Storage 2021;39:102641.
[36] Bhandari R. Standalone electricity supply system with solar hydrogen and fuel cell: Possible to get rid of storage batteries? Int J Hydrog Energy 2025;104:599–610.
[37] Basu S, John A, Kumar A, et al. Design and feasibility analysis of hydrogen based hybrid energy system: a case study. Int J Hydrog Energy 2021;46(70):34574–86.
[38] Park J, Kang S, Kim S, Kim H, Cho H-S, Lee JH. Comparative techno-economic evaluation of alkaline and proton exchange membrane electrolysis for hydrogen production amidst renewable energy source volatility. Energy Convers Manage 2025;325:119423.
[39] Araújo HF, Gómez JA, Santos DM. Proton-exchange membrane electrolysis for green hydrogen production: Fundamentals, cost breakdown, and strategies to minimize platinum-group metal content in hydrogen evolution reaction electrocatalysts. Catalysts 2024;14(12):845.
[40] Al-Ghussain L, Ahmad AD, Abubaker AM, Hassan MA. Exploring the feasibility of green hydrogen production using excess energy from a country-scale 100% solar-wind renewable energy system. Int J Hydrog Energy 2022;47(51):21613–33.
[41] Caravantes D, Carbajal J, Celis C, Marcelo-Aldana D. Estimation of hydrogen production potential from renewable resources in Northern Peru. Int J Hydrog Energy 2024;50:186–98.
[42] De León CM, Ríos C, Molina P, Brey J. Levelized cost of storage (lcos) for a hydrogen system. Int J Hydrog Energy 2024;52:1274–84.
[43] Curcio E. Techno-economic analysis of hydrogen production: Costs, policies, and scalability in the transition to net-zero. Int J Hydrog Energy 2025;128:473–87.
[44] Li L, Wang B, Jiao K, Ni M, Du Q, Liu Y, Li B, Ling G, Wang C. Comparative techno-economic analysis of large-scale renewable energy storage technologies. Energy AI 2023;14:100282.
[45] Liu T, Yang Z, Duan Y, Hu S. Techno-economic assessment of hydrogen integrated into electrical/thermal energy storage in PV+ wind system devoting to high reliability. Energy Convers Manage 2022;268:116067.
[46] Herc L, Pfeifer A, Duić N. Optimization of the possible pathways for gradual energy system decarbonization. Renew Energy 2022;193:617–33.
[47] Guerra OJ, Dalvi S, Thatte A, Cowiestoll B, Jorgenson J, Hodge B-M. Towards robust and scalable dispatch modeling of long-duration energy storage. Renew Sustain Energy Rev 2025;207:114940.
[48] Koholé YW, Ngouleu CAW, Fohagui FCV, Tchuen G. A comprehensive comparison of battery, hydrogen, pumped-hydro and thermal energy storage technologies for hybrid renewable energy systems integration. J Energy Storage 2024;93:112299.
[49] Hassan MA, El-Amary NH. Economic and technical analysis of hydrogen production and transport: a case study of Egypt. Sci Rep 2025;15(1):9002.
[50] Heidarykiany R, Ababei C. Advanced day-ahead scheduling of hvac demand response control using novel strategy of q-learning, model predictive control, and input convex neural networks. Energy AI 2025;20:100509.
[51] Mylonas A, Macià-Cid J, Péan TQ, Grigoropoulos N, Christou IT, Pascual J, Salom J. Optimizing energy efficiency with a cloud-based model predictive control: A case study of a multi-family building. Energies 2024;17(20):5113.
[52] Farrag M, Lai CS, Darwish M, Taylor G. Improving the efficiency of electric vehicles: Advancements in hybrid energy storage systems. Vehicles 2024;6(3):1089–113.
[53] Schleifer AH, Harrison-Atlas D, Cole WJ, Murphy CA. Hybrid renewable energy systems: the value of storage as a function of PV-wind variability. Front Energy Res 2023;11:1036183.
[54] Raza MS, Abid MI, Akmal M, Munir HM, Haider ZM, Khan MO, Alamri B, Alqarni M. A comprehensive assessment of storage elements in hybrid energy systems to optimize energy reserves. Sustainability 2024;16(20):8730.
[55] Sun W, Tian C, Jin Y. Cost and reliability analysis of a hybrid renewable energy systems-a case study on an administration building. MIST Int J Sci Technol 2022;10:29–35.
[56] Modu B, Abdullah MP, Bukar AL, Hamza MF. A systematic review of hybrid renewable energy systems with hydrogen storage: Sizing, optimization, and energy management strategy. Int J Hydrog Energy 2023;48(97):38354–73.
[57] Wimalaratna YP, Afrouzi HN, Mehranzamir K, Siddique MB M, Liew SC, Ahmed J. Analysing wind power penetration in hybrid energy systems based on techno-economic assessments. Sustain Energy Technol Assess 2022;53:102538.
[58] Rogeau A, Vieubled J, de Coatpont M, Nobrega PA, Erbs G, Girard R. Techno-economic evaluation and resource assessment of hydrogen production through offshore wind farms: A European perspective. Renew Sustain Energy Rev 2023;187:113699.
[59] Prina MG, Dallapiccola M, Moser D, Sparber W. Machine learning as a surrogate model for energyplan: Speeding up energy system optimization at the country level. Energy 2024;307:132735.
[60] Vincent SA, Tahiru A, Lawal RO, Aralu CE, Okikiola AQ. Hybrid renewable energy systems for rural electrification in developing countries: Assessing feasibility, efficiency, and socioeconomic impact. World J Adv Res Rev 2024;24:2190–204.
[61] Al-Ghussain L, Ahmad AD, Abubaker AM, Mohamed MA. An integrated photovoltaic/wind/biomass and hybrid energy storage systems towards 100% renewable energy microgrids in university campuses. Sustain Energy Technol Assess 2021;46:101273.
[62] Shao L, Wan C, Xu C, Xu Y. A hybrid interval optimization method for urban integrated energy system operation. In: 2022 IEEE/IAS industrial and commercial power system Asia. IEEE; 2022, p. 1422–8.
[63] Haleema K, Juluri SK, Sree SP, Karnekota P, Murugaperumal K. Sustainable designing of hybrid renewable electrification system for urban residential community load. In: 2023 4th international conference for emerging technology. IEEE; 2023, p. 1–7.
[64] Ambrose M. Rbee house averages [online]. 2019, URL https://public.tableau.com/app/profile/michael.ambrose/viz/Dahboards_AVGonly_Lastversionofdata-21082019_15664551425010/Dashboardbyenduse. [Accessed 22 2019].
[65] HUME. Broadmeadows population and dwellings [online]. 2021, URL https://profile.id.com.au/hume/population?WebID=110#:~:text=Broadmeadows&text=The%20Census%20usual%20resident%20population,average%20household%20size%20of%202.92. [Accessed: [Accessed Date]].
[66] Colelough BC. Australian energy market operator national electricity market network optimal power flow modelling, arXiv preprint arXiv:2403.18851.
[67] Hassan Q, Algburi S, Sameen AZ, Salman HM, Jaszczur M. A review of hybrid renewable energy systems: Solar and wind-powered solutions: Challenges, opportunities, and policy implications. Results Eng 2023;20:101621.
[68] Ikram AI, Shafiullah M, Islam MR, Rocky MK. Techno-economic assessment and environmental impact analysis of hybrid storage system integrated microgrid. Arab J Sci Eng 2024;49(12):15917–34.
[69] Wang Z, Wang H. Identifying the relationship between seasonal variation in residential load and socioeconomic characteristics. In: Proceedings of the 8th ACM international conference on systems for energy-efficient buildings, cities, and transportation. 2021, p. 160–3.
[70] Zhuang X, Yu Y, Chen A. A combined forecasting method for intermittent demand using the automotive aftermarket data. Data Sci Manag 2022;5(2):43–56.
[71] Stackhouse PW, Macpherson B, Broddle M, McNeil C, Barnett AJ, Mikovitz C, Zhang T. Introduction to the prediction of worldwide energy resources (power) project: Nasa applied sciences week 2021. In: 2021 NASA applied sciences week. 2021.
[72] NASA. Modern-era retrospective analysis for research and applications, version 2 [online]. 2024, URL https://gmao.gsfc.nasa.gov/reanalysis/merra-2/data_access/. [Accessed 2024].
[73] Gassar AAA, Cha SH. Review of geographic information systems-based rooftop solar photovoltaic potential estimation approaches at urban scales. Appl Energy 2021;291:116817.
[74] EUSCIENCE. Photovoltaic geographical information system (pvgis) [online]. 2024, URL https://joint-research-centre.ec.europa.eu/index_en. [Accessed 2024].
[75] SIEMENS. Siemens gamesa renewable energy. sg 2021:2.1e114. 2021, URL https://www.siemensgamesa.com/es-es/-/media/siemensgamesa/downloads/es/products-and-services/onshore/brochures/siemens-gamesa-onshore-wind-turbinesg-2-1-114-es.pdf. [Accessed 2021].
[76] Posso F, Zambrano J. Estimation of electrolytic hydrogen production potential in venezuela from renewable energies. Int J Hydrog Energy 2014;39(23):11846–53.
[77] ZHEJIANG. Espsc 380w-400w [online]. 2019, URL https://www.enfsolar.com/pv/panel-datasheet/crystalline/44454. [Accessed 02 2025].
[78] Pitarch Ripollés M. Dimensionado y diseño de un parque solar fotovoltaico de conexión a red para el suministro colectivo de la localidad de la mata.
[79] Zorer R, Volschenk C, Hunter J, et al. Pvgis: a free online solar photovoltaic calculator tool to optimise light harvesting in viticulture. In: Enoforum 2017, Vicenza, 16-18 maggio 2017. 2017.
[80] HOPPECKE. Installation, commissioning and operating instructions for valve-regulated stationary lead-acid batteries [online]. 2023, URL https://www.hoppecke.com/fileadmin/Redakteur/Hoppecke-Main/Products-Import/vrl_manual_en.pdf. [Accessed 03 February 2025].
[81] Clark C, Harris B. Valve regulated lead–acid battery degredation model for industry applications. In: World congress on engineering asset management. Springer; 2023, p. 203–14.
[82] Kostopoulos ED, Spyropoulos GC, Kaldellis JK. Real-world study for the optimal charging of electric vehicles. Energy Rep 2020;6:418–26.
[83] Al-Hanahi B, Wen J, Habibi D, Aziz A. Techno-economic analysis of hybrid hydrogen fuel-cell/pv/wind turbine/battery/diesel energy system for rural coastal community in western Australia. In: 2023 international conference on sustainable technology and engineering. IEEE; 2023, p. 1–6.
[84] Rahimi I, Nikoo MR, Gandomi AH. Techno-economic analysis for using hybrid wind and solar energies in Australia. Energy Strat Rev 2023;47:101092.
[85] Poli N, Bonaldo C, Moretto M, Guarnieri M. Techno-economic assessment of future vanadium flow batteries based on real device/market parameters. Appl Energy 2024;362:122954.
[86] Neb SE. Overview of the pem silyzer family.

[87] IRENA GHCR. Scaling up electrolysers to meet the 1.5 c climate goal. Abu Dhabi: International Renewable Energy Agency.
[88] Iribarren Á, Barrios EL, Rivera M, Wheeler P, Sanchis P, Ursúa A. On the impact of high-power grid-connected thyristor rectifiers on the efficiency of hydrogen electrolyzers. In: 2024 international conference on renewable energies and smart technologies. IEEE; 2024, p. 1–5.
[89] Acar C, Dincer I, Mujumdar A. A comprehensive review of recent advances in renewable-based drying technologies for a sustainable future. Dry Technol 2022;40(6):1029–50.
[90] Padinjarethil AK, Pollok S, Hagen A. Degradation studies using machine learning on novel solid oxide cell database. Fuel Cells 2021;21(6):566–76.
[91] Al Makky A, Kanjo HA, Farag MM, Hamid A-K, Hussein M, Salameh T. Techno-economic feasibility of green hydrogen production using hybrid solar-wind energy systems in oman. Int J Thermofluids 2025;101302.
[92] Zabanova Y. The eu in the global hydrogen race. 2023.
[93] Citaristi I. Economics and finance. In: The Europa directory of international organizations 2022. Routledge; 2022, p. 800–6.
[94] Simshauser P. Renewable energy zones in Australia's national electricity market. Energy Econ 2021;101:105446.
[95] Chauhan A, Saini R. Techno-economic optimization based approach for energy management of a stand-alone integrated renewable energy system for remote areas of India. Energy 2016;94:138–56.
[96] Citaristi I. International energy agency—IEA. In: The Europa directory of international organizations 2022. Routledge; 2022, p. 701–2.
[97] Chen Q, Gu Y, Tang Z, Wang D, Wu Q. Optimal design and techno-economic assessment of low-carbon hydrogen supply pathways for a refueling station located in Shanghai. Energy 2021;237:121584.
[98] Karim S, Faissal A, et al. National renewable energy laboratory. In: Handbook of algal biofuels. Elsevier; 2022, p. 599–613.
[99] Rasool MH, Perwez U, Qadir Z, Ali SMH. Scenario-based techno-reliability optimization of an off-grid hybrid renewable energy system: A multi-city study framework. Sustain Energy Technol Assess 2022;53:102411.
[100] Morcillo JD, Angulo F, Franco CJ. Simulation and analysis of renewable and nonrenewable capacity scenarios under hybrid modeling: A case study. Mathematics 2021;9(13):1560.
[101] Danish M, Kanwal S, Perwez U, Iftikhar SH, Ahmed BA, Hakeem AS, Askar K. A comprehensive review of green hydrogen-based hybrid energy systems: Technologies, evaluation, and process safety. Energy Rev 2025;100154.
[102] Mazibuko T, Moloi K, Akindeji K. Techno-economic design and optimization of hybrid energy systems. Energies 2024;17(16):4176.
[103] Ross-Hopley D, Ugwu L, Ibrahim H. Review of techno-economic analysis studies using homer pro software. Eng Proc 2024;76(1):94.
[104] Rana A, Gróf G. Assessment of prosumer-based energy system for rural areas by using trnsys software. Clean Energy Syst 2024;8:100110.
[105] Saitov E, Sodiqov T. Modeling an autonomous photovoltaic system in the matlab simulink software environment. In: AIP conference proceedings, vol. 2432, AIP Publishing LLC; 2022, 020022.
[106] Abbass A. Hybrid renewable energy microgrid optimization: an analysis of system performance and cost-efficiency using python-generated custom code for diesel-wind-solar configurations. Energy Storage Sav.
[107] Al-Rbaihat R. Sensitivity analysis of a hybrid pv-wt hydrogen production system via an electrolyzer and fuel cell using trnsys in coastal regions: A case study in Perth, Australia. Energies 2025;18(12):3108.
[108] Alkhafa A, Kadhim MG, Saad A, et al. Performance analysis of hybrid renewable energy systems under variable operating conditions. Sol Compass 2025;100134.
[109] Jed MEH, Logerais P-O, Malye C, Riou O, Delaleux F, El Bah M. Analysis of the performance of the photovoltaic power plant of Sourdun (France). Int J Sustain Eng 2021;14(6):1756–68.
[110] Megaptche CAM, Waita S, Kim H, Musau PM, Aduda BO. Multi-dimensional analysis in optimal sizing of hybrid renewable energy systems for green energy growth in garoua, cameroon: From techno-economic and social models to policies. Energy Convers Manage 2024;315:118804.
[111] Rahman MA, Kim J-H, Hossain S. Recent advances of energy storage technologies for grid: A comprehensive review. Energy Storage 2022;4(6):e322.
[112] Al-Douri A, Groth KM. Hydrogen production via electrolysis: State-of-the-art and research needs in risk and reliability analysis. Int J Hydrog Energy 2024;63:775–85.
[113] Nallainathan S, Arefi A, Lund C, Mehrizi-Sani A. Microgrid reliability incorporating uncertainty in weather and equipment failure. Energies 2025;18(8):2077.
[114] Marzouk OA. Expectations for the role of hydrogen and its derivatives in different sectors through analysis of the four energy scenarios: Iea-steps, iea-nze, irena-pes, and irena-1.5 c. Energies 2024;17(3):646.
[115] Vatankhah Ghadim H, Haas J, Breyer C, Gils HC, Odonkor P, Read EG, Xiao M, Peer R. Clean technology cost projections: investment and levelized costs of solar, wind, battery, and hydrogen. Sci Data 2025;12(1):1670.
[116] Mobayen S, Assareh E, Dezhdar A, Hoseinzadeh S, Garcia DA. Dynamic analysis and multi-objective optimization of an integrated solar energy system for zero-energy residential complexes. Energy Convers Manage 2025;341:119924.
[117] Zhou G, Gu Y, Yuan H, Gong Y, Wu Y. Selecting sustainable technologies for disposal of municipal sewage sludge using a multi-criterion decision-making method: A case study from China. Resour Conserv Recycl 2020;161:104881.
[118] Hosseini Dehshiri SJ, Mostafaeipour A, Le T, Sabagh AR. Evaluation of sustainable hydrogen production technologies on an industrial scale using comparative analysis of decision-making methods. Environ Sci Pollut Res 2024;1–17.
[119] Yuan J, Li Y, Luo X, Zhang Z, Ruan Y, Zhou Q. A new hybrid multi-criteria decision-making approach for developing integrated energy systems in industrial parks. J Clean Prod 2020;270:122119.
[120] Al-Ghussain L, Lu Z, Alrbai M, Al-Dahidi S, He X, Elgowainy A, Wang M. Global techno-economic and life cycle greenhouse gas emissions assessment of solar and wind based renewable hydrogen production. Appl Energy 2025;401:126595.
[121] Papadis E, Tsatsaronis G. Challenges in the decarbonization of the energy sector. Energy 2020;205:118025.
[122] Srivastava S. Generation of hybrid energy system (solar-wind) supported with battery energy storage. Int J Res Appl Sci Eng Technol 2022;10(9):1439–46.
[123] Holder D, Percy SD, Yavari A. A review of port decarbonisation options: Identified opportunities for deploying hydrogen technologies. Sustainability 16(8). http://dx.doi.org/10.3390/su16083299, URL https://www.mdpi.com/2071-1050/16/8/3299.
[124] Yin X, Wu B, Shen Y, Li H. The formation and development of australia's electricity financial market and implications for China's electricity market development. In: 4th energy conversion and economics annual forum, Vol. 2024, IET; 2024, p. 67–71.
[125] Shahabuddin M, Rhamdhani MA, Brooks GA. Technoeconomic analysis for green hydrogen in terms of production, compression, transportation and storage considering the australian perspective. Processes 2023;11(7):2196.
[126] Marzouk OA. 2030 ambitions for hydrogen, clean hydrogen, and green hydrogen. Eng Proc 2023;56(1):14.
[127] Paliwal H, Dave V. Optimisation tools and techniques for hybrid renewable energy sources: a review. Int J Renew Energy Technol 2022;13(2):114–43.
[128] Li R, Jin X, Yang P, Sun X, Zhu G, Zheng Y, Zheng M, Wang L, Zhu M, Qi Y, et al. Techno-economic analysis of a wind-photovoltaic-electrolysis-battery hybrid energy system for power and hydrogen generation. Energy Convers Manage 2023;281:116854.
[129] Nasser M, Megahed TF, Ookawara S, Hassan H. Techno-economic assessment of clean hydrogen production and storage using hybrid renewable energy system of pv/wind under different climatic conditions. Sustain Energy Technol Assess 2022;52:102195.
[130] Agupugo CP, Ajayi AO, Salihu OS, Barrie I. Large scale utility solar installation in the USA: Environmental impact and job. Glob J Eng Technol Adv 2024;21(02):023–34.
[131] Wachs E, Engel B. Land use for United States power generation: A critical review of existing metrics with suggestions for going forward. Renew Sustain Energy Rev 2021;143:110911.
[132] Kar SK, Sinha AS K, Bansal R, Shabani B, Harichandan S. Overview of hydrogen economy in Australia. Wiley Interdiscip Rev: Energy Environ 2023;12(1):e457.
[133] Ocenic E. Trends in hydrogen production projects for energy and climate purposes–a descriptive analysis of the iea database. In: ERAZ 2023/9-Knowledge-Based Sustainable Development-CONFERENCE PROCEEDINGS, Udruženje ekonomista i menadžera Balkana. p. 475–80.
[134] Fay M, Hallegatte S, Vogt-Schilb A, Rozenberg J, Narloch U, Kerr T. Decarbonizing development: Three steps to a zero-carbon future. World Bank Publications; 2015.
[135] Sharpe O, Raman K. The Australian hydrogen centre–feasibility studies for achieving 10 and 100% renewable hydrogen in South Australia and Victoria. Aust Energy Prod J 2024;64(2):S191–6.
[136] Glenk G, Reichelstein S. Economics of converting renewable power to hydrogen. Nat Energy 2019;4(3):216–22.
[137] Longden T. Analysis of the Australian hydrogen strategy. In: Periscope–occasional analysis brief series 2.
[138] Correia AF, Lopes JM, Coimbra AP, Moura P, De Almeida AT. Architecture and control simulation for improved system resiliency of a building microgrid. In: 2023 IEEE/IAS 59th industrial and commercial power systems technical conference. IEEE; 2023, p. 1–8.
[139] Wright S, Frost M, Wong A, Parton KA. Australian renewable-energy microgrids: A humble past, a turbulent present, a propitious future. Sustainability 2022;14(5):2585.
[140] Dosa A, Olanrewaju OA, Mora-Camino F. A comprehensive review of hybrid renewable microgrids: Key design parameters, optimization techniques, and the role of demand response in enhancing system flexibility. Energies 2025;18(19):5154.
[141] Khalifa F, Marzouk M. Integrated blockchain and digital twin framework for sustainable building energy management. J Ind Inf Integr 2025;43:100747.
[142] Khan WA, Pakseresht A, Chua C, Yavari A. Digital twin role for sustainable and resilient renewable power plants: A systematic literature review. Sustain Energy Technol Assess 2025;75:104197.